ABSTRACT

Title of Document: BIOLOGICAL NANOFACTORIES: ALTERING CELLULAR RESPONSE VIA LOCALIZED SYNTHESIS AND DELIVERY

Rohan Fernandes, Doctor of Philosophy, 2008

Directed By: Professor William E. Bentley, Fischell Department of Bioengineering

Conventional research in targeted delivery of molecules-of-interest involves either packaging of the molecules-of-interest within a delivery mechanism or pre-synthesis of an inactive prodrug that is converted to the molecule-of-interest in the vicinity of the targeted area. Biological nanofactories provide an alternative approach to targeted delivery by locally synthesizing and delivering the molecules-of-interest at surface of the targeted cells. The machinery for synthesis and delivery is derived from the targeted cells themselves. Biological nanofactories are nano-dimensioned and are comprised of multiple functional modules. At the most basic level, a biological nanofactory consists of a cell targeting module and a synthesis module. When deployed, a biological nanofactory binds to the targeted cell surface and locally synthesizes and delivers molecules-of-interest thus altering the response of the targeted cells.

In this dissertation, biological nanofactories for the localized synthesis and delivery of the 'universal' quorum sensing signaling molecule autoinducer-2 are demonstrated. Quorum sensing is process by which bacterial co-ordinate their activities at a population level through the production, release, sensing and uptake of signaling

autoinducers and plays a role in diverse bacterial phenomena such as bacterial pathogenicity, biofilm formation and bioluminescence. Two types of biological nanofactories; magnetic nanofactories and antibody nanofactories are presented in this dissertation as demonstrations of the biological nanofactory approach to targeted delivery. Magnetic nanofactories consist of the AI-2 biosynthesis enzymes attached to functionalized chitosan-mag nanoparticles. Assembly of these nanofactories involves synthesis of the chitosan-mag nanoparticles and subsequent assembly of the AI-2 pathway enzymes onto the particles. Antibody nanofactories consist of the AI-2 biosynthesis enzymes self assembled onto the targeting antibody. Assembly of these nanofactories involves creation of a fusion protein that attaches to the targeting antibody. When added to cultures of quorum sensing bacteria, the nanofactories bind to the surface of the targeted cells via the targeting module and locally synthesize and deliver AI-2 there via the synthesis module. The cells sense and uptake the AI-2 and alter their natural response. Prospects of using biological nanofactories to alter the native response of targeted cells to a 'desired' state, especially with respect to down-regulating undesirable co-ordinated bacterial response, are envisioned.

BIOLOGICAL NANOFACTORIES: ALTERING CELLULAR RESPONSE VIA LOCALIZED SYNTHESIS AND DELIVERY

By

Rohan Fernandes

Dissertation submitted to the Faculty of the Graduate School of the
University of Maryland, College Park, in partial fulfillment
of the requirements for the degree of
Doctor of Philosophy
2008

Advisory Committee:
Professor William E. Bentley, Chair
Professor Gregory F. Payne
Associate Professor John P. Fisher
Associate Professor Sheryl Ehrman
Professor Lourdes G. Salamanca-Riba

Dedication

For My Parents Lionel and Lorna,

Siblings Siddharth and Priyanka,

and for Varnika

Acknowledgements

I would like to thank my advisor Dr. William E. Bentley for giving me an opportunity to work in his lab and for overseeing my intellectual journey from the time I entered the University of Maryland as a new graduate student until the completion of my Ph.D. The discussions and conversations we have had, both work-related and unrelated, have been simultaneously stimulating, challenging and most importantly, enjoyable! A special thank you to my colleagues (now friends), both past and present, at the Bentley lab for making the day to day life in the lab something to look forward to and for offering support and intellectual input during the lean phases. I would also like to acknowledge people with whom I have collaborated with during the course of my research especially Xiaolong Luo, Matthew Dowling, Dr. Gregory F. Payne, Dr. Gary W. Rubloff, Dr. Reza Ghodssi and Dr. Srinivasa Raghavan. I would like to acknowledge my dissertation committee members Dr. Gregory F. Payne, Dr. John P. Fisher, Dr. Sheryl Ehrman and Dr. Lourdes G. Salamanca-Riba. Finally, I would like to acknowledge the facilities provided by the Center for Biosystems Research, University of Maryland Biotechnology Institute and Fischell Department of Bioengineering, University of Maryland and the funding sources, without which, this research would not have been possible.

Table of Contents

List of Tables

List of Figures

List of Abbreviations

AB = autoinducer bioassay

Ab-NF = antibody nanofactory

AHL = acylated homoserine lactone

AI-2 = autoinducer-2

Amino-fluorescein = ((4'-aminoacetamido) methyl) fluorescein

BioMEMS = biological microelectromechanical systems

BSA = bovine serum albumin

DPD = 4,5-dihydroxy-2,3-pentanedione

DTNB = 5,5'-Dithiobis (2-nitrobenzoic acid)

GFP = green fluorescent protein

HG_3LPT = $(His)_6$-Protein G_3-LuxS-Pfs-$(Tyr)_5$

HGLPT = $(His)_6$-Protein G-LuxS-Pfs-$(Tyr)_5$

HLPT = $(His)_6$-LuxS-Pfs-$(Tyr)_5$

IMAC = immobilized metal ion affinity chromatography

IPTG = isopropyl β-D-thiogalactopyranoside (IPTG)

LB = Luria Bertani

Lsr = LuxS responsive

LuxS = S-ribosylhomocysteinase

MEMS = microelectromechanical systems

MNF = magnetic nanofactory

MNF-HFLPT = magnetic nanofactory containing immobilized HLPT

NHS-fluorescein = 5- (and 6)-carboxyfluorescein succinimidyl ester

ONPG = o-nitrophenyl-β-D-galactopyranoside

PB = phosphate buffer

PB6 = phosphate buffer, pH 6

PBS = phosphate buffered saline

PDMS = polydimethylsiloxane

Pfs = S-adenosylhomocysteine nucleosidase

PQS = *Pseudomonas* quinolone signal

QS = quorum sensing

RFU = relative fluorescence units

R-THMF = (2R, 4S)-2-methyl-2,3,3,4-tetrahydroxytetrahydrofuran

SAH = S-(5'-deoxyadenosin-5')-L-homocysteine

SAM = S-adenosylmethionine

SRH = S-ribosylhomocysteine

TNB = 5-thio-2-nitrobenzoic acid

Chapter 1: Introduction to Biological Nanofactories

1.1 Targeted Delivery

Targeted delivery has been employed and is currently being studied in a diverse range of biological applications. There is a large body of peer-reviewed literature available on the subject: a search conducted using the words 'targeted delivery' in the database Pubmed (www.pubmed.gov) returns 7138 hits as of October 2008. Targeted delivery has been investigated in a variety of therapies such as treatment of HIV [1, 2], cancer [3, 4], diabetes [5, 6], pulmonary diseases [7, 8], endothelial diseases [9, 10], to name a few, and in applications such as gene delivery [11, 12], imaging [13, 14] etc. Selective targeting is effected using wide ranging delivery mechanisms such as quantum dots [15, 16], viral vectors [17, 18], nanoparticles [19, 20] and nanotubes [21, 22], liposomes [23, 24], polymeric systems [25, 26] etc. The rationale behind using targeted delivery is to facilitate or increase the effect of the delivered cargo to the targeted area (cells, vasculature, tissues or organs) and to reduce unwanted and non-specific effects of it in the surrounding area. The ultimate goal of all these applications is to alter the response in the targeted area to a 'desired state' which is different from the 'original state'.

There are two main approaches to targeted delivery. In the first approach, the molecule-of-interest which could be a synthetic molecule [27, 28], a growth factor [29, 30], a signal molecule [31, 32] etc is synthesized, packaged within a delivery mechanism and then delivered to the targeted area thus altering the response there. Recent examples of the same in literature include delivery of therapeutic agents to cancer cells [19, 33] and delivery of genes [12, 34] to targeted cells. The second approach involves using prodrugs. Prodrugs

are inactive or significantly less active molecules which are first synthesized, administered to the target area and then activated or converted to an active state there. Prodrugs have been used to in applications such as cancer therapy [35, 36], ocular therapy [37, 38], Parkinson's disease therapy [39, 40] and overcoming bacterial resistance [41, 42].

In this dissertation, a third and fundamentally different approach to creating an altered response within the targeted area is presented. It involves taking cues from the targeted area (for e.g. cells, tissue etc) itself to modulate or alter response in the targeted area. Specifically, an intrinsic synthesis pathway that produces the molecule-of- interest within the targeted area is taken and reconstructed *in vitro*. The reconstructed pathway is then locally delivered to the target cells using delivery mechanisms that will be covered later. The pathway locally synthesizes and delivers the molecule-of-interest in the targeted area. The interaction of the molecule-of-interest with the targeted area produces an altered response. This approach differs from the previous two approaches in that the native machinery from the target area itself is utilized to confer an altered response in the targeted area. Figure 1-1 compares the three approaches. This novel generic approach to targeted delivery is applied in the field of bacterial communication. The motivation for undertaking this work, global hypothesis, specific aims and outlines of the studies conducted are described in the subsequent sections of this chapter.

Figure 1-1. Different approaches to targeted delivery. a. Packaging the molecule-of-interest within a delivery mechanism. The delivery mechanism releases the molecule in the vicinity of the target area. b. Presynthesis and delivery of a prodrug that is activated in the targeted area. c. In vitro reconstruction of a synthesis pathway that is delivered to the target area where it locally synthesizes and delivers the molecule-of-interest.

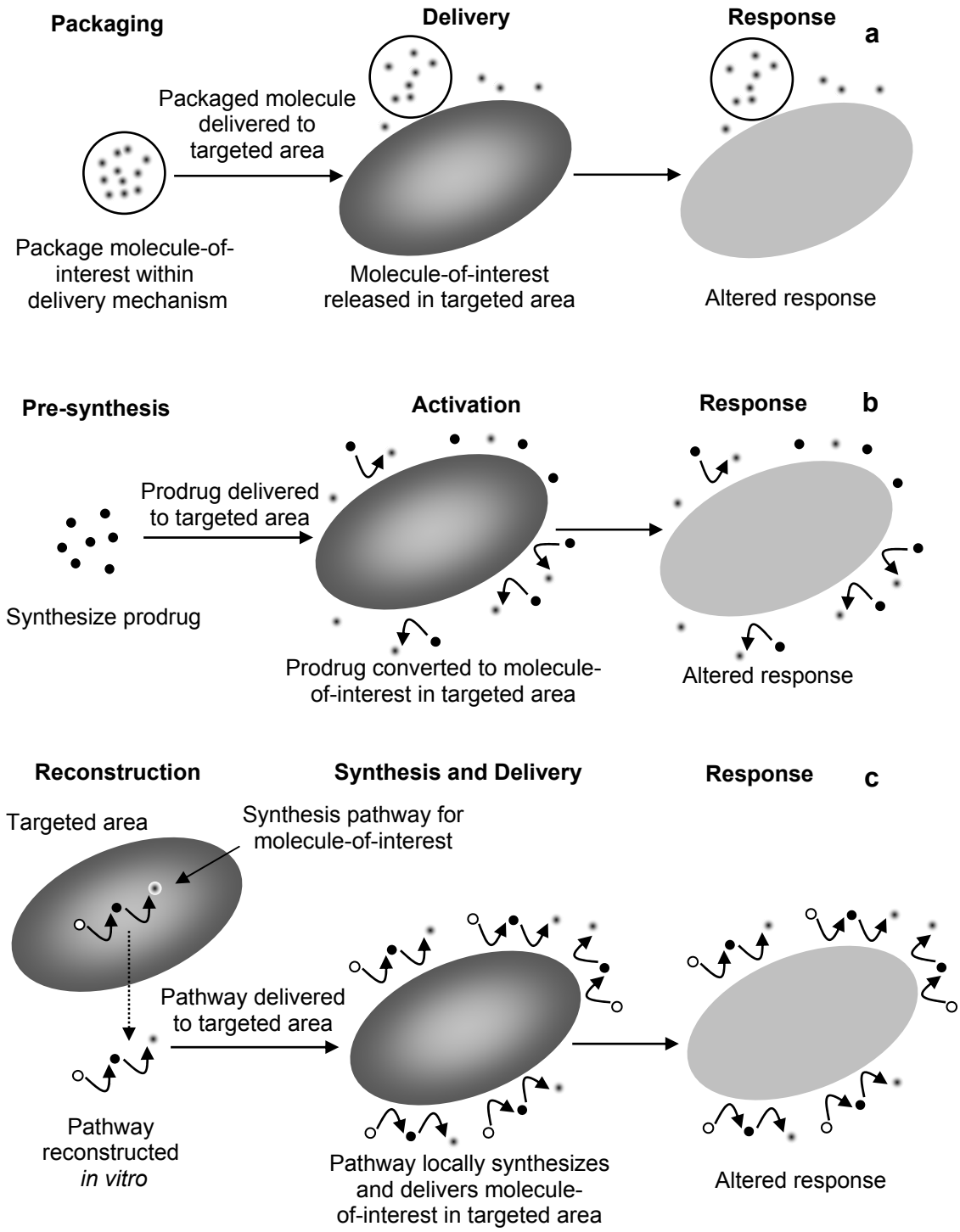

1.2 Bacterial Communication

Bacteria have long been regarded as independent unicellular organisms. However bacteria cannot be viewed as isolated entities as they are capable of coordinating their activities and producing a multi-cellular response. The phenomenon whereby bacteria exchange small chemical molecules, monitor their population density and co-ordinate gene expression in a population dependent manner is termed as quorum sensing (QS) [43]. Bacterial communication occurs within a species (intra-species), with other species (inter-species) as well as with other organisms (inter-kingdom) [44, 45]. Examples of intra-species bacterial communication include single species bacterial infections such as cholera (caused by *Vibrio cholerae*) [46, 47] and chronic lung infections in cystic fibrosis (caused by *Pseudomonas aeruginosa*) [48, 49]. Inter-species bacterial communication has been observed between the numerous species of bacteria in the gut [50, 51] and in oral flora [52]. Inter-kingdom bacterial communication includes interactions of bacteria of the genus *Rhizobium* [53] with leguminous roots of plants for nitrogen fixing and interactions between marine bacteria of the genus *Vibrio* and marine squids resulting in bioluminescence [54, 55].

Previously bacteria were thought to communicate through two distinct classes of molecules: acylated homoserine lactones used by Gram-negative bacteria and oligopeptides used by Gram-positive bacteria. However bacterial communication is not limited to these two classes of molecules and is observed to occur through other signaling molecules such as autoinducer-2 (AI-2), pseudomonas quinolone signal (PQS) and bradyoxetin and other molecules to a lesser extent [44]. Figure 1-2 shows the major classes of signaling (QS) molecules.

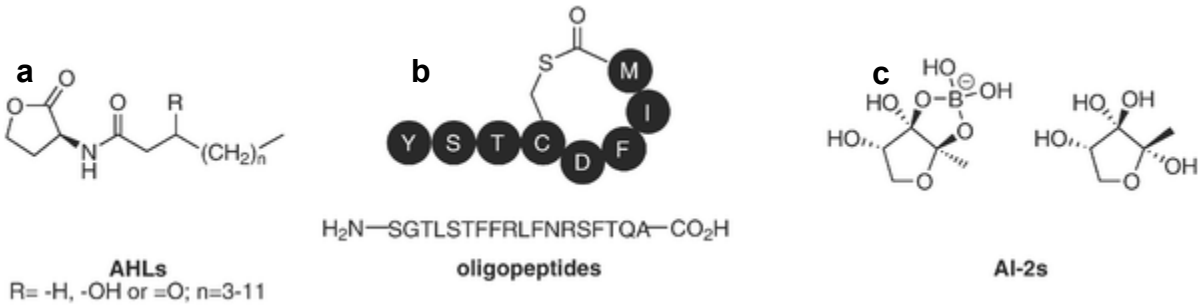

Figure 1-2. Chemical structures of the various classes of molecules used in quorum sensing based (QS) communication. a. Acylated homoserine lactones (AHL). b. Oligopeptides. c. Autoinducer-2 (AI-2). Adapted from Lowery *et al.* [44].

QS in bacteria has been found to play a role in a wide array of multi-cellular bacterial responses such as bioluminescence [56, 57], biofilm formation [58, 59], toxin production and virulence [46, 60], sporulation [61] and swarming motility [62]. Many of these multi-cellular responses are undesirable. For example, the formation of biofilms is a major source of infections in the human body. According to a National Institutes of Health estimate, over 80% of microbial infections in the body are caused by formation of biofilms [63]. In addition to impacting human health, multi-cellular bacterial responses impact numerous industrial and engineering applications as well. Bacterial fouling of process engineering equipment such as heat exchangers greatly reduces their performance and increases costs [64]. Formation of bacterial biofilms can either accelerate or decelerate corrosion based on the conditions prevalent within the film [65]. Clearly, understanding bacterial communication and the outcomes of bacterial communication (particularly multi-cellular response) is important.

Of the various classes of QS molecules, AI-2 is particularly interesting as both Gram-positive and Gram-negative bacteria communicate via AI-2. The enzyme that

synthesizes 4,5-dihydroxy-2,3-pentanedione (DPD), the precursor to AI-2, has been found in over 70 bacterial species [44]. These include bacteria such as *Escherichia coli* [66] and *Salmonella typhimurium* [67] that are the common causes of food contamination, pathogenic bacteria such as *Listeria monocytogenes* [68] and *Bacillus anthracis* [69] and oral bacteria such as *Actinomyces naelundii* [52] and *Streptococcus oralis* [52]. In addition, there exist species of bacteria that do not possess their own AI-2 synthesis machinery but are capable of transducing the AI-2 signal (as it is indicative of the presence of other bacteria) [70]. On account of the relative ubiquity of AI-2 and AI-2 based QS in bacteria, AI-2 has been dubbed as the universal signaling molecule [71]. The work in this dissertation involves AI-2 and AI-2 based QS in two bacteria *Escherichia coli* and *Salmonella typhimurium*, details of which follow subsequently.

1.3 Quorum Sensing in *E. coli* and *S. typhimurium*

In *E. coli* and *S. typhimurium*, DPD is a product of the activated methyl cycle, the main donor of methyl in many archaebacterial, eubacterial and eukaryotic cells (Figure 1-3) [44]. As part of the cycle, the metabolite S-adenosylmethionine (SAM) is converted to the toxic intermediate S-adenosylhomocysteine (SAH) via methyl transferases. SAH is converted to S-ribosylhomocysteine (SRH) and adenine via the enzyme S-adenosylhomocysteine nucleosidase (Pfs). The enzyme S-ribosylhomocysteinase (LuxS) then acts on S-ribosyl homocysteine and converts it to DPD and homocysteine. Homocysteine is recycled to produce methionine [44].

DPD undergoes rapid intra-molecular cyclization to form a family of cyclic molecules (Figure 1-4) known as the AI-2 family of molecules. Thus AI-2 should not be

regarded as a single structure but a group of molecules capable of inducing signaling in bacteria. Different bacteria are capable of transducing different forms of the AI-2 molecule. In *S. typhimurium*, the form of AI-2 that produces signaling was determined to be (2R, 4S)-2-methyl-2,3,3,4-tetrahydroxytetrahydrofuran (R-THMF) [72]. In *E. coli*, the exact structure of the signal molecule has not yet been determined and is currently under investigation.

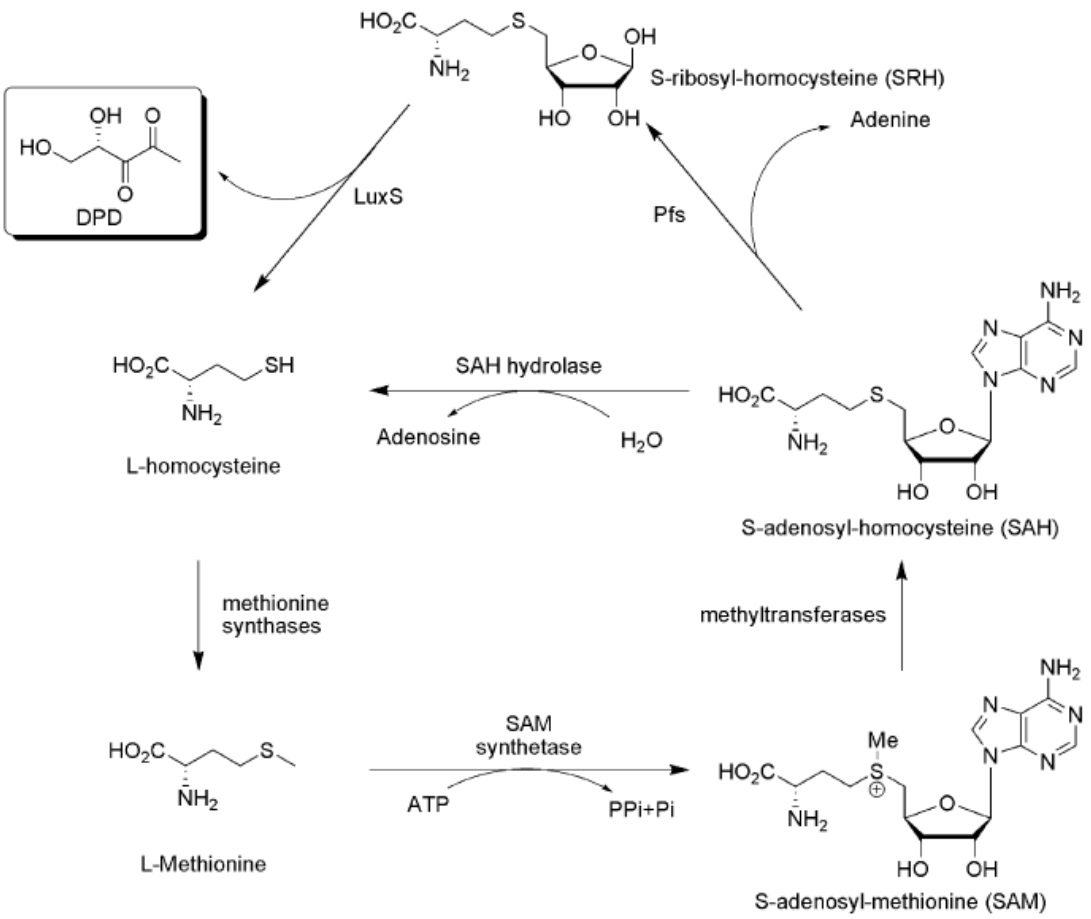

Figure 1-3. Activated methyl cycle in bacteria. Metabolite SAM is converted to toxic intermediate SAH. The enzyme Pfs converts SAH to SRH and adenine and the enzyme LuxS converts SRH to DPD, the precursor to AI-2, and homocysteine. Homocysteine is recycled to form methionine. Adapted from Lowery *et al.* [44].

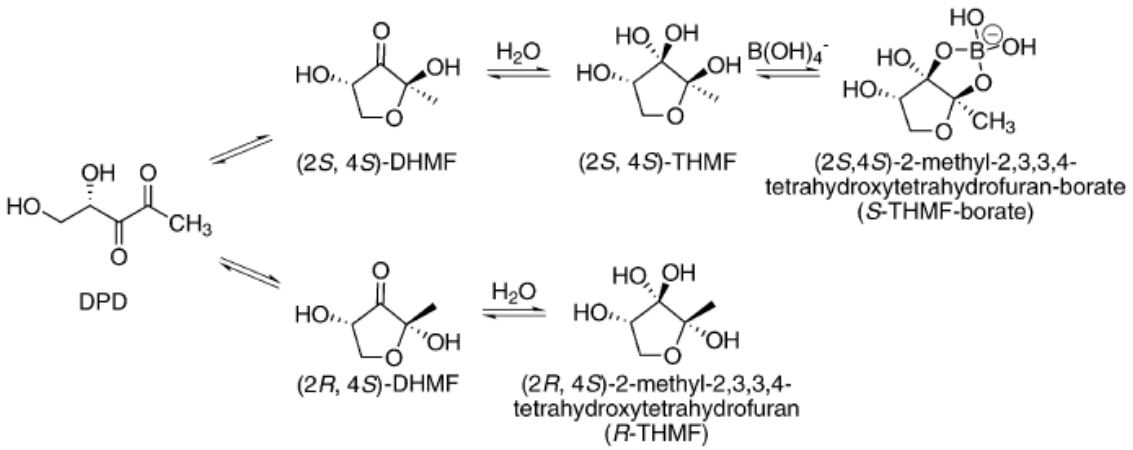

Figure 1-4. AI-2 family of molecules. DPD, a product of the activated methyl cycle can spontaneously cyclize intra-molecularly to form different cyclic forms of AI-2. Adapted from Lowery *et al.* [44].

The mechanism of AI-2 synthesis, secretion, uptake and signal transduction in *E. coli* is described in Figure 1-5 (The mechanism is similar to *S. typhimurium*) [66]. SAH, as described earlier is formed as an intermediate of the activated methyl cycle. The enzymes Pfs and LuxS convert SAH to DPD (releasing adenine and homocysteine respectively as intermediates in the process). DPD cyclizes to form AI-2, which is exported into the extra-cellular medium. AI-2 accumulates in the medium in response to increased cell population density. Once the AI-2 concentration in the medium exceeds a given threshold, which is indicative of a quorum of bacteria, the uptake and processing of AI-2 is triggered.

AI-2 is imported into the cells via the Lsr transporter. Once inside the cell, AI-2 is phosphorylated by the enzyme kinase, LsrK, to form phosphor-AI-2. Phospho-AI-2 binds to the repressor LsrR, which is attached to the promoter region of the *lsr* operon, causing it to detach from the promoter region thus de-repressing the *lsr* operon. The

expression of a number of genes (*lsrA, C, D, B, F, G* and *lsrR* and *K*) of varying functions is controlled by the *lsr* promoter region. The key points to note here are that AI-2 is converted from SAH by enzymes Pfs and LuxS and that once its concentration exceeds a threshold outside the cell; it triggers an uptake and signaling cascade that alters cellular response (expression of a variety of genes, proteins etc).

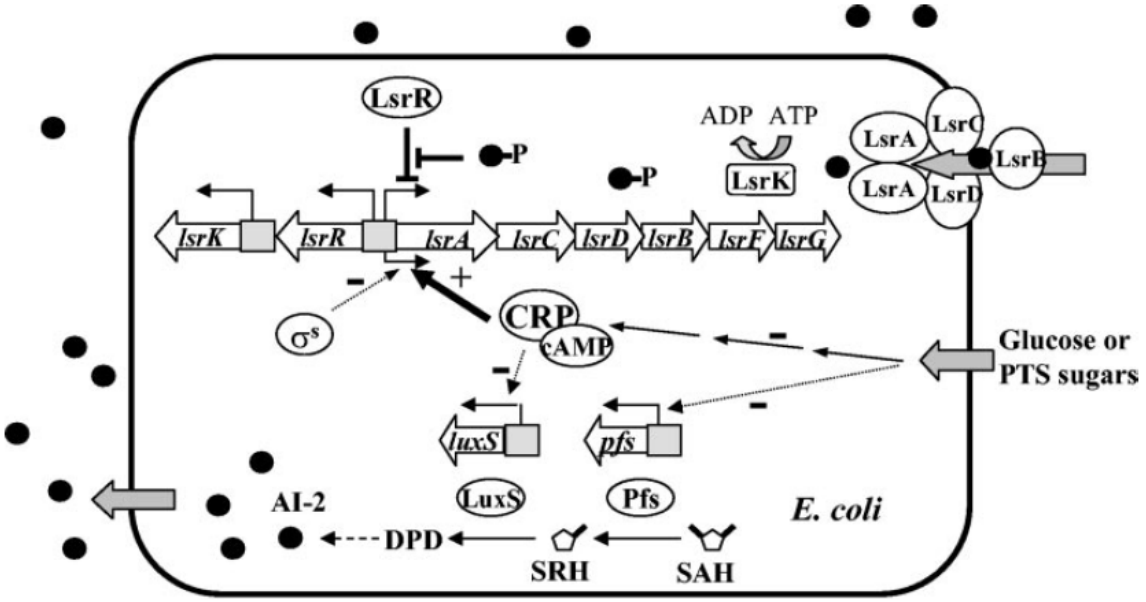

Figure 1-5. Synthesis, secretion, uptake and transduction of AI-2 in *E. coli*. Enzymes Pfs and LuxS convert SAH to DPD which cyclizes to form AI-2. AI-2 is secreted and is taken up via the Lsr transporter, is phosphorylated by LsrK, binds to repressor LsrR and de-represses the lsr operon (expressing genes lsrA, C, D, B, F, G and lsrR and K, which have varying functions). Adapted from Wang *et al.* [66].

1.4 Research Motivation

In the previous sections, a new approach to targeted delivery as well as background on AI-2 and AI-2 based QS was presented. While AI-2 has been observed to affect biofilm formation in both *E. coli* and *S. typhimurium*, the exact role of AI-2 and AI-2 based

signaling in both these organisms as well as other bacteria that are capable of producing and recognizing the AI-2 signal is not fully understood. Current methods to understand involve creation of *luxS* null mutants, i.e. creating bacterial strains that lack the enzyme LuxS and hence cannot produce AI-2. A criticism of using this approach is that LuxS plays a role in the activated methyl cycle which would be disturbed in the mutant cells. One way around this limitation is to create a method to externally (and controllably) deliver AI-2 to the cells. By doing so, one may deliver AI-2 to the cells without disrupting the native machinery and observe the effect of AI-2 on signal transduction and cellular response (cell phenotype).

Of the three methods of targeted delivery presented in section 1.1, pre-synthesizing AI-2, packaging it within a delivery mechanism and delivering it to targeted bacterial cells is not suitable as AI-2 is a transient molecule (exists in native systems on the order of hours) and may not be stable over the time scales of this method. The prodrug approach is also not convenient as it requires chemical synthesis of an inactive precursor of AI-2 that is activated in the presence of another activating molecule. The synthesis of a prodrug and activating molecule is not straight forward and requires careful design considerations. Therefore in this dissertation, the third method of delivery proposed earlier is used as it results in external delivery of AI-2 and overcomes the drawbacks of the first technique by synthesizing and delivering AI-2 at the target cells and does not involve design of a prodrug and activating molecule. Specifically the enzymes Pfs and LuxS are purified and the AI-2 biosynthesis pathway is reconstructed *in vitro* in a biological nanofactory as described later.

1.5 Global Objective, Global Hypothesis and Specific Aims

The global objective of this dissertation is to create a method to locally synthesize and deliver AI-2 to cells using biological nanofactories. The overall hypothesis of this work is "localized synthesis and delivery of AI-2 via biological nanofactories alters cellular response".

The specific aims of this research are: -

1. To create biological nanofactories for localized synthesize and delivery of AI-2.

Two types of nanofactories to achieve the same, magnetic and antibody nanofactories are described here.

2. To deploy the biological nanofactories to the targeted cells.

Here the nanofactories bind to the targeted cell surface and locally synthesize and deliver AI-2 there.

3. To observe the effect of localized synthesis and delivery AI-2 via biological nanofactories on targeted cell response.

The targeted cells sense the locally synthesized AI-2, uptake the signal molecule and produce and AI-2 specific cellular response which is measured.

1.6 Biological Nanofactories

A biological nanofactory is, as the name suggests, a nanometer sized biological factory. In its ideal form, a biological nanofactory comprises multiple functional modules attached together, each module performing a different function. When deployed, the nanofactories attach to the targeted cells, use raw materials in the vicinity of the cells and produce molecules-of-interest there via their biosynthetic machinery and thus alter

cellular response [73, 74]. Figure 1-6 shows a schematic of an ideal biological nanofactory which comprises of, but is not limited to, six functional modules: a structural scaffold or shell, transport to convey biomolecules to and from the environment, a sensing functionality, biochemical machinery to synthesize the molecules-of-interest, a mechanism for targeting the cell and externally triggered degradation to terminate treatment.

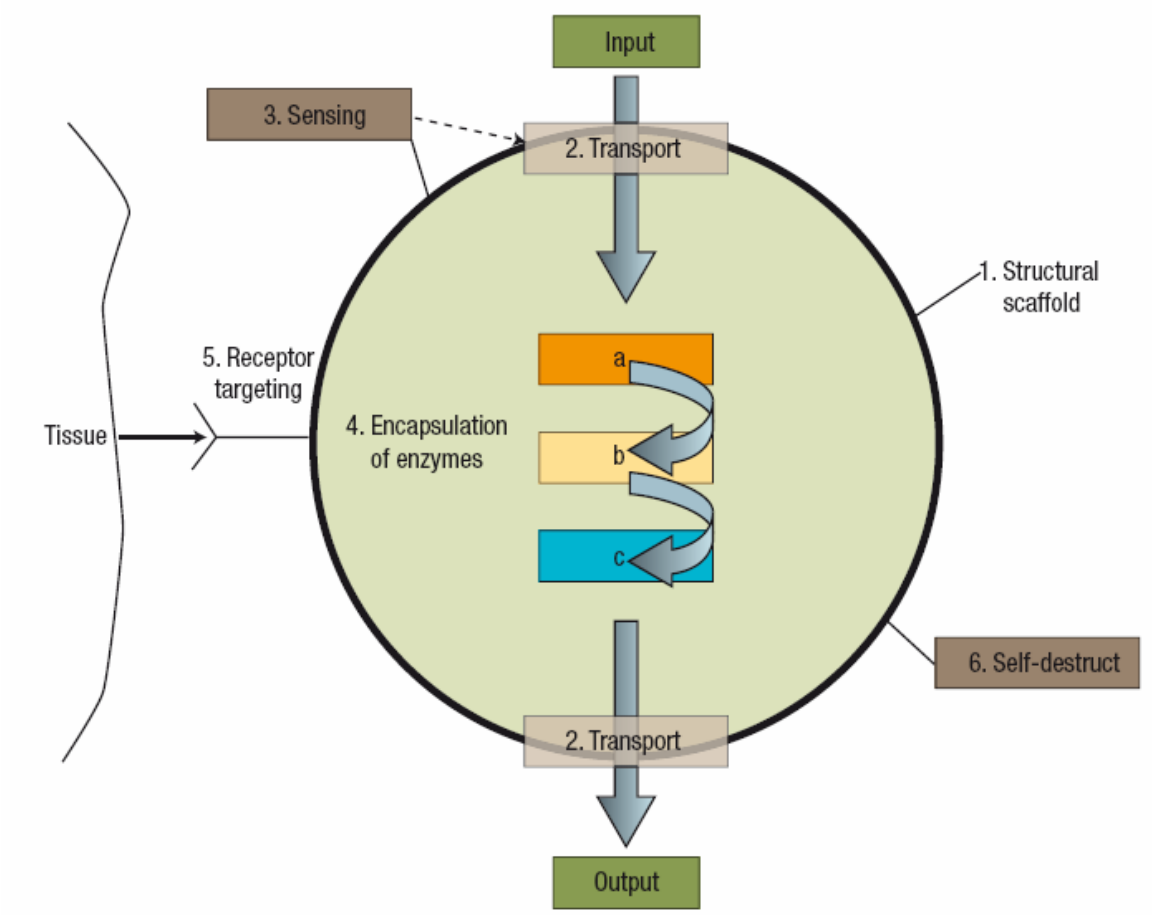

Figure 1-6. Schematic of an idealized biological nanofactory. An ideal nanofactory comprises six modules: a structural scaffold, transport to and from the scaffold, sensing, enzymes that synthesize the molecule-of-interest, a targeting element and a self destruct mechanism. Adapted from LeDuc *et al.* [74].

In this dissertation, two types of nanofactories which are working versions of the idealized biological nanofactory concept described above are presented: magnetic nanofactories and antibody nanofactories. Both nanofactories consist of AI-2 synthesis modules and cell targeting modules (Figure 1-7). Specifically the enzymes Pfs and LuxS are genetically cloned *in vitro*. These synthesis enzymes (synthesis module) are attached to the cell targeting module. For the magnetic nanofactories, targeting is achieved via chitosan functionalized magnetic nanoparticles. In the antibody nanofactories, targeting is achieved via antibodies. The nanofactories attach to QS bacteria (e.g. *E. coli, S. typhimurium*) via the targeting module; locally synthesize and deliver AI-2 in the vicinity of the bacteria. The bacteria sense and uptake the locally synthesized AI-2 and produce an altered response. The effect of the locally synthesized AI-2 on cellular response, specifically AI-2 based quorum sensing response is measured.

Figure 1-7. Scheme for altering QS response via localized synthesis and delivery of AI-2 via biological nanofactories. a. *In vitro* reconstruction of AI-2 synthesis pathway. b. Nanofactory assembly, targeting and localized synthesis and delivery of AI-2 alters bacterial QS response.

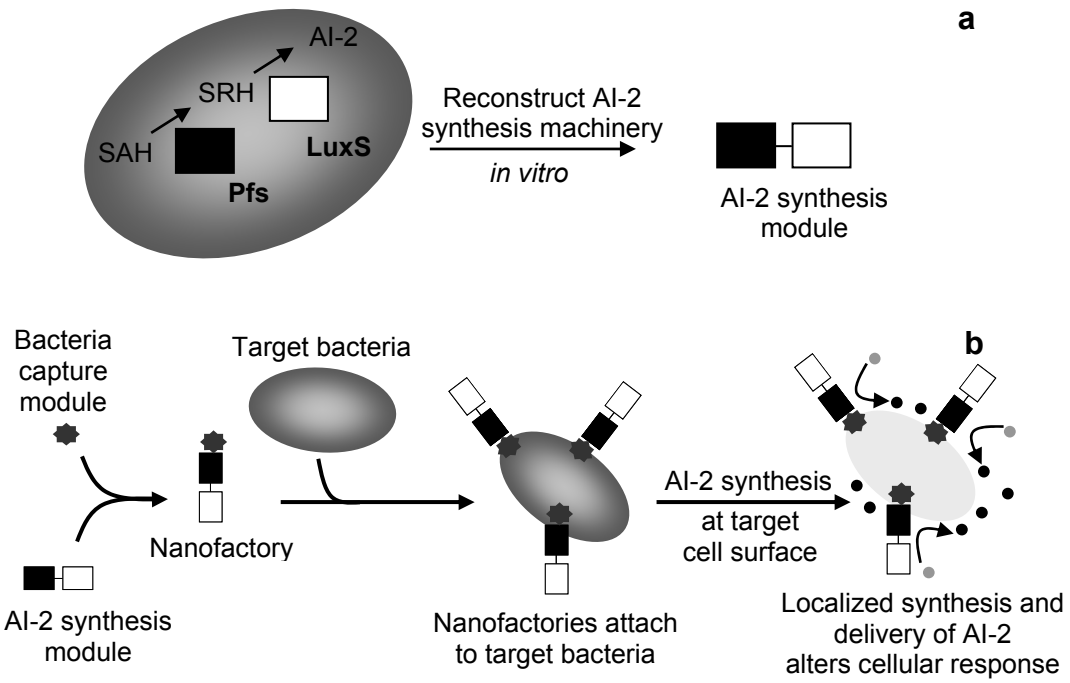

1.7 Dissertation Outline

Chapter 2 describes the *in vitro* expression and purification of the enzymes Pfs and LuxS and the synthesis of chitosan-mag magnetic nanoparticles. The assembly, deployment and cell capture of the magnetic nanofactories as well as the effect of synthesis and delivery of AI-2 by the magnetic nanofactories on native QS response of *E. coli* cultures are investigated in this chapter.

Chapter 3 describes the construction of a fusion protein HLPT that co-expresses both enzymes Pfs and LuxS. Comparison of the fusion protein performance versus that of the constituent enzymes over a wide range of conditions is investigated. The assembly of HLPT onto chitosan-mag nanoparticles and the effect of this nanofactory on AI-2 based cellular response in *E. coli* is investigated.

Chapter 4 describes the construction of a fusion protein HGLPT and its use in the creation of a self assembled antibody nanofactory. The effect of the antibody nanofactory on AI-2 based cellular response in *E. coli* and *S. typhimurium* is investigated.

Chapter 5 describes the construction of another fusion protein HG_3LPT and its use in the spatial assembly of *E. coli* cells in a microfluidics device. The effect of this construct on cellular response is investigated in the controlled conditions of a microfluidics device.

Chapter 6 summarizes the work in the previous chapters, describes the broader impact of the work and describes ongoing work that applies and/or builds on techniques devised in this work.

Chapter 2: Magnetic Nanofactories: Localized Synthesis and Delivery of Quorum Sensing Signaling Molecule Autoinducer-2 to Bacterial Cell Surfaces

2.1 Abstract

Magnetic 'nanofactories', for localized manufacture and signal-guided delivery of small molecules to targeted cell surfaces, are demonstrated. They recruit nearby raw materials for synthesis, employ magnetic mobility for capture and localization of target cells, and deliver molecules to cells triggering their native phenotypic response, but with user-specified control. Our nanofactories, which synthesize and deliver the "universal" bacterial quorum sensing signal molecule, autoinducer AI-2, to the surface of *E. coli*, are assembled by first co-precipitating nanoparticles of iron salts and the biopolymer chitosan. *E. coli* AI-2 synthases, Pfs and LuxS, constructed with enzymatically activatable "pro-tags", are then covalently tethered onto the chitosan. These enzymes synthesize AI-2 from metabolite S-adenosylhomocysteine. Chitosan serves as a molecular scaffold and provides cell capture ability; magnetite provides stimuli responsiveness. These magnetic nanofactories are shown to modulate the natural progression of quorum sensing activity. New prospects for small molecule delivery, based on localized synthesis, are envisioned.

2.2 Introduction

Localized delivery of a molecule-of-interest to a target cell surface is important in cell signaling [75-78]. When delivered locally, a signaling molecule can produce a higher signal

intensity that elicits an enhanced cellular response. For example, the localized delivery of growth factors has been shown to stimulate growth in targeted cells or tissue [79-81]. Various strategies have been employed to locally deliver signal molecules to target cells viz. using viral vectors [82], degradable polymeric scaffolds [83], liposomes [84] and nanoparticles [85]. All the above methods deliver signal molecules in their final form to their respective target cells. In this proof-of-concept paper, we are working with a novel and potentially programmable approach for the localized synthesis and delivery of a signaling molecule to a target cell surface using a magnetic 'nanofactory', which consists of enzymes with activatable 'pro-tags' conjugated to functionalized magnetic nanoparticles. Our technique differs from the above techniques in that it synthesizes the signal molecule from a precursor molecule at the surface of the target cell and locally delivers it (via the nanofactory). The rationale behind employing such a mode of localized synthesis and delivery is that we can control the amounts of signal molecule delivered to the target cell thus potentially enabling an *ex vivo* fine-tuning of cellular response.

A nanofactory is a nano-sized factory that combines three attributes: an ability to 'manufacture' the signaling molecule (synthesis ability), an ability to bind to the cell surface (cell capture ability) thus localizing the synthesized signaling molecule to the cell surface and an ability to be directed and recovered in response to an external stimulus (stimuli responsiveness). We introduce 'nanofactories' by demonstrating their assembly via biologically benign techniques and their use by locally synthesizing and delivering the quorum sensing signaling molecule autoinducer-2 (AI-2) at the surface of *Escherichia*

coli cells. The appropriate AI-2 specific cell response confirms altered phenotypic behavior and a functioning 'programmable' nanofactory.

AI-2 is an inter- and intra-species signaling molecule that plays a role in quorum sensing (QS) [43], a process that mediates inter- and intra-species bacterial communication resulting in coordinated multicellular behavior. Diverse cell processes such as bioluminescence, biofilm formation, virulence, antibiotic production and competence [45, 51, 71, 86-88] are in part, QS regulated. In *E. coli*, AI-2 is synthesized from S-adenosylhomocysteine (SAH) via a two-step enzymatic reaction involving the enzymes S-adenosylhomocysteine nucleosidase (Pfs) and S-ribosylhomocysteinase (LuxS) [66]. To confer AI-2 synthesis ability to the nanofactories, the enzymes Pfs and LuxS are attached to functionalized magnetic nanoparticles using activatable "pro-tags" at their C-termini (Figure 2-1).

In the first step, the magnetic carrier is synthesized by the dropwise addition of a mixture of ferric and ferrous salts ($[Fe^{3+}]/[Fe^{2+}] = 2$) and the biopolymer chitosan to a vigorously stirred base (NH_4OH) under an inert atmosphere. The resultant nano-sized co-precipitates contain both chitosan and magnetite (Fe_3O_4) called 'chitosan-mag' [89, 90]. Magnetite confers magnetic-responsiveness (stimuli responsiveness) to the nanofactory while chitosan serves a dual-role: it enables the nanofactory to attach to the target cell surface (cell capture ability) and it also provides amine-groups for attaching the enzymes Pfs and LuxS to the nanofactory.

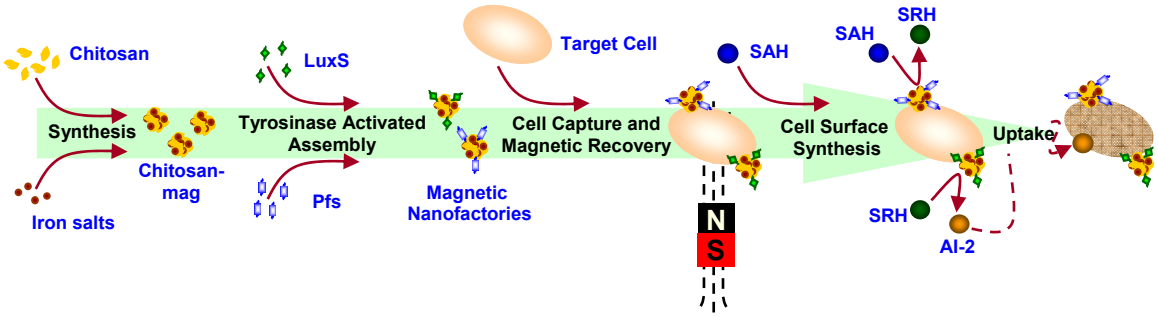

Figure 2-1. Overview of assembly and use of nanofactories to locally synthesize and deliver QS signaling molecule, AI-2, to a target cell. Synthesis of the magnetic carrier, chitosan-mag, by co-precipitation of iron salts and chitosan; attachment of pro-tagged Pfs and LuxS to chitosan-mag by 'activation' using tyrosinase to assemble magnetic nanofactories; capture of target cells by the magnetic nanofactories; recovery of captured cells using an external magnet; cell surface synthesis and delivery of AI-2 by enzymes Pfs and LuxS; uptake of AI-2 and production of cellular response (AI-2-dependent reporter).

This dual-role of chitosan is related to its unique pH-dependent solubility. The amine-groups of chitosan have a pK_a of about 6.3 [91, 92]. At a pH below the pK_a, most amine-groups are protonated and chitosan is positively charged and water soluble; at pH above the pK_a, most amine-groups are deprotonated and chitosan is neutral and insoluble in water.

Pfs with a pentatyrosine pro-tag at its C-terminus [$(His)_6$-Pfs-$(Tyr)_5$] is covalently assembled onto the available surface chitosan in chitosan-mag by activation using the enzyme tyrosinase. Upon the addition of tyrosinase, the tyrosine residues in the pro-tag are activated and form o-quinones that can then react with the amine-groups of chitosan [93-95]. Similarly, LuxS with the C-terminus pro-tag [$(His)_6$-LuxS-$(Tyr)_5$] is assembled onto chitosan-mag. The motivation for using pro-tags is that they are located at the C-termini of both Pfs and LuxS and extend away from their respective active sites. The addition of tyrosinase selectively activates the tyrosine residues of the tag and facilitates attachment of the enzymes via the tag to chitosan with intact enzymatic activity.

The nanofactories containing Pfs and those containing LuxS are then combined to obtain a suspension of magnetic nanofactories with AI-2 synthesis ability. These are added to a suspension containing the target cells (*E. coli*) where they bind to the cell surface via the available surface chitosan [89, 90] (chitosan molecules without attached enzymes). The nanofactories with the attached cells are recovered using an external magnetic field, resuspended in fresh medium or buffer and *in vitro* AI-2 is synthesized by the nanofactories, by addition of SAH, at the surface of the target cells. The *in vitro* synthesized AI-2 is delivered at the cell surface and taken up by the Lsr transporter producing an AI-2 specific transcriptional response which is measured by β-galactosidase

reporter activity. The interception of cell-cell communication and subsequent interruption of quorum-sensing behavior is a topic of intense interest because downregulating specific cell functions (e.g., cell attachment, virulence) that lead to pathology, but are not essential for a pathogen's viability, may lower the rate of emergence of resistant strains. We believe nanofactories offer many advantages relative to the localized delivery of small molecules, in that the molecule could eventually be synthesized and delivered at a site, at a prescribed concentration and time.

2.3 Materials and Methods

Chemicals

Chitosan (average molecular weight 50,000 g/mol), iron (II) chloride tetrahydrate ($FeCl_2.4H_2O$), iron (III) chloride hexahydrate ($FeCl_3.6H_2O$), isopropyl β-D-thiogalactopyranoside (IPTG), phosphate buffered saline (PBS, 9.6 g/L), tyrosinase (from mushroom), S-(5'-deoxyadenosin-5')-L-homocysteine (SAH), chloroform, sodium dodecyl sulfate salt (SDS, >98.5 %), o-nitrophenyl-β-D-galactopyranoside (ONPG), 2-mercaptoethanol, imidazole, zinc acetate dehydrate, and glycerol were all purchased from Sigma Aldrich. Glacial acetic acid (CH_3COOH), ampicillin sodium salt, kanamycin, Tris, sodium carbonate (Na_2CO_3), dibasic sodium phosphate ($Na_2HPO_4.7H_2O$), monobasic sodium phosphate ($NaH_2PO_4.H_2O$), potassium chloride (KCl), magnesium sulfate ($MgSO_4.7H_2O$), sodium chloride were all purchased from Fisher Scientific. Ammonium hydroxide (NH_4OH) was purchased from J. T. Baker. 5- (and 6)-carboxyfluorescein succinimidyl ester (NHS-fluorescein) and ((4'-aminoacetamido) methyl) fluorescein (amino-fluorescein) were purchased from Molecular Probes.

Synthesis of chitosan-mag and mag particles

A solution of chitosan (2.02 % w/w, pH 5.5) was prepared as described elsewhere [92]. 9.9 mL (0.2 g) chitosan solution, 0.795 g of $FeCl_2.4H_2O$ and 2.162 g of $FeCl_2.4H_2O$ were dissolved in 40 mL double distilled water. This reaction mixture, which contains 0.5 % chitosan, 0.2 M [Fe^{3+}], 0.1 M [Fe^{2+}] (i.e. [Fe^{3+}]/ [Fe^{2+}] = 2), was purged with N_2 gas and added dropwise to vigorously stirred 2M NH_4OH (pH 11.8), also previously purged with N_2). A positive N_2 pressure was maintained in the reaction chamber and care was taken to ensure that no bubbles were formed during the vigorous stirring (1500 – 2000 rpm). The resultant black precipitate that contains chitosan-mag particles was washed with copious amounts of double distilled water to remove the excess base and the pH of the suspension was brought to 7. For long term storage, a 10 mg/mL suspension of chitosan-mag was prepared in 0.5 % dilute acetic acid and stored at 4 ^{o}C for future use. For synthesis of mag, conditions identical to those used for the synthesis of chitosan-mag were used. However, no chitosan solution was used in the synthesis of mag.

Bacterial strains and growth media

The bacterial strains used in this study are listed in table 2-1. The Luria-Bertani broth contained 5 g/L of yeast extract (Sigma), 10 g/L of Bacto tryptone (Difco) and 10 g/L NaCl (J. T. Baker). The components of the Autoinducer Bioassay medium (AB) are described elsewhere [96].

Table 2-1. Bacterial strains, plasmids and oligonucleotide primers used in this study.

Strain or plasmid or primer	Relevant genotype and property	Reference
Escherichia coli strains		
W3110	Wild type	Laboratory stock
BL21	*F'* ompT hsdS$_B$ *($r_B^- m_B^-$) gal dcm*	[97]
ZK126	Wild type strain derivative, W3110 Δ*lacU160-tna2*	[98]
LW7	ZK126 Δ*luxS* :: Kan	[66]
DH5α	*recA1 supE44 endA1 hsdR17 gyrA96 relA1 thiΔ (lac-proAB)* F' [*traD36 proAB+ lacI^q lacZΔM15*]	Invitrogen
NC13	RK4353 *Δpfs (8-226)*::Kan	[99]
Vibrio harveyi strains		
BB170	BB120 *luxN* :: Tn*5* (sensor 1$^-$, sensor 2$^+$)	[100]
Plasmids		
pGFP	pTrcHisB derivative, *gfp*$^+$, Amp^r	[97]
pTrcHis-LuxS-Tyr	pTrcHisC derivative, W3110 *luxS*$^+$, Amp^r	This study
pTrcHis-Pfs-Tyr	pTrcHisC derivative, W3110 *pfs*$^+$, Amp^r	This study
pFZY1	*galK'-lacZYA* transcriptional fusion vector, Amp^r	[101]
pLW11	pFZY1 derivative, containing *lsrACDBFG* promoter region, Amp^r	[66]

Oligonucleotide primers

Name	Sequence	Relevant property
PfsF	CCGCTCGAGATATGAAAATCG GCATCATTG	Upstream primer for cloning *pfs* from W3110 contains *HindIII*
5TyrPfsR	CCCAAGCTTTTAATAATAATAA TAATAGCCATGTGCAAGTTTCT GCA	Downstream primer for cloning *pfs* from W3110 encodes 5-Tyr-tag and *XhoI*
LuxSF	CCGCTCGAGATATGCCGTTGTT AGATAGCT	Upstream primer for cloning *luxS* from W3110 contains *HindIII*
5TyrLuxSR	CCCAAGCTTCTAATAATAATAA TAATAGATGTGCAGTTCCTGCA ACT	Downstream primer for cloning *luxS* from W3110 encodes 5-Tyr-tag and *XhoI*

Plasmid construction

To express and purify Pfs with tyrosine tag (His-Pfs-Tyr) and LuxS with tyrosine tag (His-LuxS-Tyr), the plasmids pTrcHis-Pfs-Tyr and pTrcHis-LuxS-Tyr were constructed by PCR amplification of *pfs* (699 bp) and *luxS* (516 bp) from genomic DNA of *E. coli* strain W3110 (http://ecoli.aist-nara.ac.jp/) using the oligonucleotide primers listed in table 2-1. PCR reactions were carried out by using PCR Master Mix (Promega) and followed by gel purification with QIAquick gel extraction kit (Qiagen). PCR products were digested with *Hin*dIII and *Xho*I, and the products were extracted by gel purification and then inserted into pTrcHisC (Invitrogen). To verify the integrity of all constructs, DNA sequencing was performed at the DNA core facility of the Center for Biosystems Research (University of Maryland Biotechnology Institute). To obtain purified His-pfs-Tyr and His-luxS-Tyr, pTrcHis-pfs-Tyr and pTrcHis-luxS-Tyr plasmids were transformed into DH5α (defective *luxS*) and NC13 (*pfs* knockout), respectively. In this way, there is no contaminating Pfs in LuxS preparations and vice versa.

Purification of $(His)_6$-Pfs-$(Tyr)_5$ and $(His)_6$-LuxS-$(Tyr)_5$

E. coli DH5α pTrcHis-Pfs-Tyr [for Pfs: $(His)_6$-Pfs-$(Tyr)_5$] and *E. coli* NC13 pTrcHis-LuxS-Tyr [for LuxS: $(His)_6$-LuxS-$(Tyr)_5$] were separately cultured at 37 ^oC and 250 rpm in LB medium supplemented with ampicillin at 50 μg/mL. When the optical densities (OD_{600}) of the cell cultures were between 0.4 - 0.6, IPTG was added to induce enzyme production (for Pfs culture: final concentration used was 1 mM IPTG, for LuxS culture: final concentration used was 1mM IPTG and 0.1 mM zinc acetate). After 6 hr, cells were collected by centrifugation at 6,000 xg for 20 minutes at 4 ^oC. The cells were stored at -

20 ^{o}C or directly resuspended in PBS + 10 mM imidazole. The resuspended cells were lysed by sonication using Sonic Dismembrator 550 (Fisher Scientific). After sonication, the soluble cell extract was collected by centrifugation at 14,000 xg for 15 minutes at 4 ^{o}C. The soluble extract was filtered using a 0.22 μm polyether sulfone, low protein binding filter (Millipore). The filtered extract was then loaded on a pre-equilibrated immobilized metal-ion affinity chromatography (IMAC) column (HiTrap Chelating HP, Amersham Biosciences). The sample was washed with varying amounts of phosphate buffer, sodium chloride and imidazole (Wash 1: 20 mM PO_4^{3-}, 250 mM NaCl and 10 mM imidazole; Wash 2: 20 mM PO_4^{3-}, 250 mM NaCl and 50 mM imidazole). The sample was then eluted with 20 mM PO_4^{3-}, 250 mM NaCl and 350 mM imidazole and dialyzed overnight into PBS at 4 ^{o}C. For long term storage, glycerol was added to the enzyme solution (final glycerol concentration 30 %) and the samples were stored at -80 ^{o}C until use.

Reaction with NHS-fluorescein and amino-fluorescein

Chitosan-mag and mag in dilute CH_3COOH (0.5 mg/mL, pH 6) were separately reacted with either NHS-fluorescein or amino-fluorescein in double distilled water (5 μg/mL). The reaction mixture was maintained at pH 6 by PBS. The reaction was allowed to proceed at room temperature for 30 minutes. After reaction, the particles were recovered using a magnetic stand (Promega MagneSphere® stand Z5342). The particles were collected within 3 minutes. After collection, the particles were washed with copious amounts of double distilled water and resuspended in dilute CH_3COOH, using the magnetic stand for collection after each wash. The fluorescence of the particles was

measured using a fluorescence plate reader (Perkin Elmer LS 5S, excitation wavelength 480 nm, slit width 10 nm, emission wavelength 510 nm, slit width 20 nm, emission cut-off 515 nm).

Cell capture using chitosan-mag

E. coli BL21 pGFP was cultured at 37 ^{o}C and 250 rpm in LB medium supplemented with ampicillin at 50 μg/mL. When the optical density OD_{600} of the cell culture was between 0.4 - 0.6, IPTG was added to induce GFP production (final concentration used was 1 mM IPTG). After 6 hour induction, cells were collected by centrifugation at 6,000 xg for 10 minutes at room temperature. The cells were resuspended in water with the pH adjusted using dilute CH_3COOH where needed. The pH was varied from 4 to 7. For cell capture chitosan-mag in dilute CH_3COOH (0.5 mg/mL, pH varied from 4 to 7) was used. Capture was carried out at room temperature by using the cell suspension with the appropriate chitosan-mag suspension at the identical pH for 30 minutes. After capture, the particles were collected using the magnetic stand (specifications above) and washed thrice with double distilled water each time collecting the particles with the magnetic stand. After washing the particles were suspended in double distilled water at appropriate pH. The optical densities OD_{600} of the cell suspension before capture, of the supernatant after capture and of the three washes were measured. The optical density measurements were made simultaneously after the final wash and the amount of growth taking place during the capture and wash process was assumed to be minimal. To determine the amount of cells on the particles, the fluorescence of the resuspended particles with the attached cells was measured using a fluorescence plate reader mentioned above (excitation wavelength

395 nm, slit width 10 nm, emission wavelength 510 nm, slit width 10 nm, emission cut-off 430 nm). To determine the amount of cells captured in terms of difference in optical density, the following formula was used: $\Delta OD_{600} = OD_{cellsuspension} - OD_{supernatant} - OD_{washes}$ accounting appropriately for dilution.

Nanofactory assembly: attaching $(His)_6$-Pfs-$(Tyr)_5$ and $(His)_6$-LuxS-$(Tyr)_5$ to chitosan-mag

Chitosan-mag in dilute CH_3COOH (0.5 mg/mL, pH 6) was reacted with $(His)_6$-Pfs-$(Tyr)_5$ of varying concentrations (10-150 µg/mL) using activating enzyme, tyrosinase (100 U/mL). The reaction was carried out for 1 hour at 37 ^oC. After reaction, the particles with the attached Pfs (now referred to as nanofactories) were collected using a magnetic stand (details above). The nanofactories were washed thrice with double distilled water to remove unbound Pfs and resuspended and stored until further use. Similarly, chitosan-mag in dilute CH_3COOH (0.5 mg/mL, pH 6) was reacted with $(His)_6$-LuxS-$(Tyr)_5$ of varying concentrations (10-150 µg/mL) using activating enzyme tyrosinase (100 U/mL) and treated as above to obtain nanofactories with bound LuxS.

***In vitro* synthesis of AI-2**

The nanofactories containing Pfs and those containing LuxS were combined to obtain nanofactories with AI-2 synthesis ability. The *in vitro* synthesis of AI-2 was carried out by the addition of SAH (0.5 mM in 100 mM Tris-HCl buffer pH 7.8) to the nanofactories (1 mg/mL, 0.5 mg chitosan-mag with bound Pfs and 0.5 mg chitosan-mag with bound LuxS, pH 6). The reaction was carried out for 2 hours at 37 ^oC. After the specified time

the reaction was arrested using chloroform. The nanofactories were centrifuged at 12000 xg for 5 minutes. The 'enzyme-free' supernatants (now containing in vitro AI-2) were collected and stored at -20 ^{o}C until further use.

AI-2 activity assay

The AI-2 activity assay was carried out as described elsewhere . Briefly, 20 µl of AI-2 assay sample (collected during the above synthesis reaction) was mixed with 180 µl of BB170 suspension prepared by 5000-fold dilution of an overnight culture with AB medium. AB medium was used as negative control and a 4 hr conditioned LB medium from *E. coli* W3110 grown at 250 rpm was used as a positive control. Bioluminescence obtained from experimental samples was normalized to the bioluminescence obtained for the negative control. All assays were repeated at least thrice with separately prepared samples to confirm the reproducibility of AI-2 activity.

Localized synthesis and delivery of AI-2 at cell surface using magnetic nanofactories

E. coli ZK126 pLW11 and *E. coli* LW7 pLW11 were pre-cultured overnight at 37 ^{o}C and 250 rpm in LB medium supplemented with ampicillin at 100 µg/mL. 0.5 mL of these overnight pre-cultures was diluted in 49.5 mL LB medium supplemented with 60 µg/mL ampicillin. These cultures were grown at 30 ^{o}C at 250 rpm. The nanofactories were assembled as mentioned above. At 2-hour intervals (from 0 – 8 hours), samples from these cell cultures were withdrawn. For each 2-hour sample, the cells were collected by centrifugation at 6,000 xg for 10 minutes at room temperature. Cell suspensions were prepared in 10 mM Phosphate Buffer (PB, pH 6). Cell capture was carried out at room

temperature using the magnetic nanofactories (1 mg/mL chitosan-mag, 0.5 mg chitosan-mag with bound Pfs, 0.5 mg of chitosan-mag with bound LuxS, pH 6) or just chitosan-mag (negative control, 1 mg/mL, pH 6). The nanofactories or chitosan-mag with captured cells were recovered by using a magnetic stand (specifications above). The nanofactories or chitosan-mag were washed thrice and resuspended in PB (pH 6). OD_{600} of the cell suspensions, supernatants and washes were measured as mentioned above to determine the amount of captured cells as mentioned above. *In vitro* AI-2 was synthesized at the surface of the cells captured by the nanofactories or chitosan-mag by adding 0.5 mM SAH (37 ^{o}C, 2 hour synthesis). After synthesis, the nanofactories and chitosan-mag with attached cells were recovered using the magnetic stand. A Miller assay [102] was performed to determine the AI-2 dependent β-galactosidase expression for the cells captured by the nanofactories and chitosan-mag.

To study the effect of localized synthesis and delivery, *in vitro* AI-2 was synthesized at the surface of the cells (*E. coli* LW7 pLW11; 8 hour time-point) captured by the magnetic nanofactories (1 mg/mL, 0.5 mg chitosan-mag with bound Pfs, 0.5 mg of chitosan-mag with bound LuxS, pH 6) by adding 0.5 mM SAH (37 ^{o}C, 2 hour synthesis) to the reaction mixture. After synthesis, the nanofactories were recovered using the magnetic stand and the AI-2 dependent Miller units of β-galactosidase expression of captured cells was determined. The β-galactosidase expression was compared with that obtained for cells captured by chitosan-mag (1mg/mL) with 50 μg/mL each of unbound Pfs and LuxS and 0.5 mM SAH (37 ^{o}C, 2 hour synthesis) added to the reaction mixture, cells captured by chitosan-mag (1mg/mL) with 0.5 mM SAH (37 ^{o}C, 2 hour synthesis) added to the reaction mixture, unattached (free) cells with 50 μg/mL each of unbound Pfs

and LuxS and 0.5 mM SAH (37 ^{o}C, 2 hour synthesis) added to the reaction mixture or unattached cells with 0.5 mM SAH (37 ^{o}C, 2 hour synthesis) added to the reaction mixture.

Electron microscopy

Transmission electron microscopy (TEM) images of the chitosan-mag particles were taken using a Zeiss EM10 CA microscope at the University of Maryland Biological Ultrastructure Facility. For the scanning electron microscopy (SEM) images of the nanofactories attached to the target cells, the nanofactories were assembled as described above and the cell capture was carried out as mentioned above at the 8 hour time-point. After cell capture, the nanofactories were recovered and the washed thrice to remove any uncaptured cells or traces of cell broth with double distilled water. The cells captured on the nanofactories were first fixed with 2 % glutaraldehyde and then with 1 % osmium tetroxide. The samples were then dehydrated with 100 % ethanol and dried using critical point drying technique. The samples were then mounted and coated with gold (Au): palladium (Pd) alloy and viewed using a Hitachi S-4700 microscope. For TEM images of the nanofactories attached to the cells, after capture the particles with attached cells were fixed first in 2 % glutaraldehyde, then in 1% osmium tetroxide and finally in 2 % uranyl acetate. The fixed samples were dehydrated in 100 % ethanol. The samples were progressively infiltrated with increasing amounts of Spurr's resin mixture in propylene oxide. Following this, the samples were embedded in fresh Spurr's resin and incubated at 70 ^{o}C. After curing at the 70 ^{o}C, the samples were sectioned using a diamond tip microtome and the sections were viewed using a Zeiss EM10 CA microscope.

Statistical Analysis

To determine significant differences between different groups of data for a single experiment, a single-factor ANOVA test was performed. The data were tested to see if they fulfilled the homogeneity of variance assumption. For experiments that had more than two groups of data, multiple comparison tests were performed to determine which group/groups were significantly different (higher or lower) than other groups. * indicates that the group is significantly different from other groups (higher or lower, $p < 0.01$)

2.4 Results

Synthesis of the magnetic carrier with accessible surface amine-groups of chitosan

The first step in the assembly of a magnetic nanofactory is the synthesis of the magnetic carrier 'chitosan-mag' (Figure 2-1) by the dropwise addition of a mixture of ferrous and ferric chloride and chitosan into a vigorously stirred base (NH_4OH) under anoxic conditions (co-precipitation). Figure 2-2a shows a transmission electron micrograph of the resultant chitosan-mag nanoparticles (average particle size ~ 10 nm). Surface accessibility of the amine-groups of chitosan (0.5 mg/mL, pH 6) is tested by labeling the nanoparticles with an amine-reactive fluorescent dye (5- (and 6)-carboxyfluorescein succinimidyl ester (NHS-fluorescein), 5 μg/mL, 30 minutes reaction at room temperature) [103]. After reaction with NHS-fluorescein, the particles are collected using an external magnet and unreacted dye is removed by washing with double distilled water. Figure 2-2b shows the Normalized relative fluorescence units (RFU) of NHS-fluorescein-labeled chitosan-mag particles compared to identically prepared controls (chitosan-mag

particles reacted with ((4'-aminoacetamido) methyl) fluorescein (amino-fluorescein) which is not directly amine-reactive, NHS-fluorescein-labeled magnetite (mag) nanoparticles without chitosan and mag particles reacted with amino-fluorescein). The fluorescence of chitosan-mag labeled with NHS-fluorescein is ~ 13.5 fold higher than that of chitosan-mag without NHS-fluorescein, ~ 4.5 fold higher than chitosan-mag reacted with amino-fluorescein, ~ 9.5 fold higher than mag with NHS-fluorescein and ~ 15.5 fold higher than mag with amino-fluorescein. These results confirm that amine-reactive NHS-fluorescein preferentially binds to chitosan and that chitosan-mag particles have abundant amine-reactive sites.

Cell capture using chitosan-mag (cell capture ability)

Chitosan-mag particles (0.5 mg/mL) are tested for their ability to capture cells via accessible surface chitosan (cell capture ability) by adding the particles to a suspension containing fluorescing cells [*E. coli* BL21 pGFP induced with 1 mM IPTG to produce green fluorescent protein (GFP) [97]]. The particles are contacted with the fluorescing cells for 30 minutes at room temperature. Because chitosan's amines confer pH-sensitive net charge, we investigated the effect of pH on cell capture over a range of pH (from pH 4 to 7). After capture, the particles with the attached cells are recovered with an external magnet and rinsed 3 times with double distilled water to remove the unbound cells.

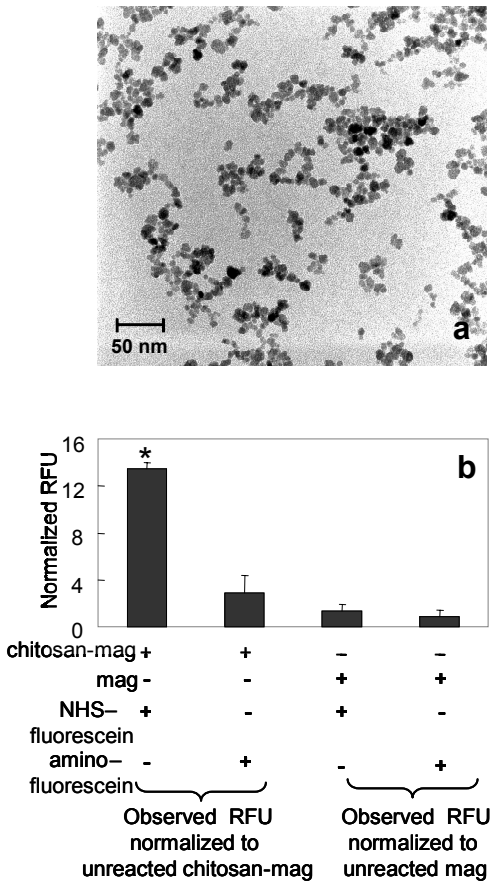

Figure 2-2. Synthesis of the magnetic carrier chitosan-mag with accessible surface amine-groups of chitosan. (a) TEM of the synthesized chitosan-mag particles. (b) Normalized Relative Fluorescence Units (Normalized RFU) produced by reacting chitosan-mag and mag with either NHS-fluorescein (amine-group reactive dye) or amino-fluorescein (control dye). * indicates significant difference ($p < 0.01$).

The optical density at 600 nm (OD_{600}) of the cell suspension before capture, the supernatant after capture and the washes are measured to estimate the amount of captured cells. The difference in optical density, ΔOD_{600}, ($\Delta OD_{600} = OD_{cellsuspension} - OD_{supernatant} - OD_{washes}$ accounting appropriately for the dilutions) corresponds to the optical density of the captured cells. The fluorescence of the resuspended particles with the attached cells is also measured using a fluorescence plate reader as a second way of estimating the amount captured cells. Figure 2-3 shows ΔOD_{600} (the optical density of the captured cells) and the measured normalized RFU of the particles plus attached cells (fluorescence of chitosan-mag with captured cells divided by that of chitosan-mag without cells) as a function of pH. The cell capture by chitosan-mag is observed to be higher at lower pH ($\leq$ 6) and decreases as the pH is increased to 7. The capture was found to remain low when the pH was increased above 7 (data not shown) [89]. This indicates that chitosan-mag can be used for cell capture (pH $\leq$ 6). We use pH 6 for subsequent experiments involving cell capture.

Assembly of magnetic nanofactories: attaching Pfs and LuxS to chitosan-mag via tyrosinase activatable pro-tags (synthesis ability)

The QS enzymes, Pfs and LuxS, are both engineered to have hexahistidine-tags at their N-termini and pro-tags (pentatyrosine-tags) at their C-termini [viz. $(His)_6$-Pfs-$(Tyr)_5$ and $(His)_6$-LuxS-$(Tyr)_5$]. The hexahistidine tags at the N-termini are used to obtain the purified enzymes via immobilized metal ion affinity chromatography (IMAC). The pro-tags at the C-termini are used to increase the amount of accessible tyrosine residues for the reaction conjugating the enzymes to chitosan.

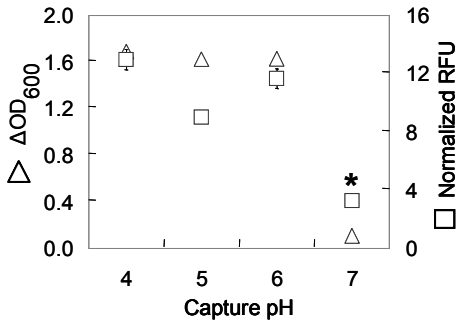

Figure 2-3. Cell capture using chitosan-mag (cell capture ability). Optical density corresponding to the amount of cells captured by chitosan-mag as a function of pH (ΔOD600, triangles) and measured normalized RFU of chitosan-mag with attached fluorescing cells (captured cells) as a function of pH (squares). * indicates significant difference ($p < 0.01$).

They facilitate formation of the enzyme-chitosan conjugate with intact enzymatic activity. Tyrosinase is used to activate the pro-tag; it converts accessible tyrosine residues to reactive o-quinones [93-95]. These electrophilic o-quinones can then react non-enzymatically with the nucleophilic amine-groups of accessible surface chitosan to form Schiff bases or Michael-type adducts that couple the enzymes on to chitosan [104] (Figure 2-4a and Figure 2-5).

In our experiments, we first attach Pfs to chitosan-mag (0.5 mg/mL, pH 6) by activation of its pro-tag using tyrosinase (100 U/mL). The concentration of added Pfs is varied [10 μg/mL (0.34 μM), 50 μg/mL (1.70 μM) or 150 μg/mL (5.10 μM)]. After reaction, the nanofactories with Pfs are recovered by an external magnet and rinsed thrice with distilled water to remove any unbound enzyme. Similarly, we assemble magnetic nanofactories with LuxS by attaching LuxS to chitosan-mag (0.5 mg/mL, pH 6) using tyrosinase (100 U/mL) and varying concentrations of added LuxS [concentrations 10 μg/mL (0.40 μM), 50 μg/mL (2.00 μM) or 150 μg/mL (6.00 μM)]. Studies calculating the amount of pro-tagged proteins bound to chitosan (i.e. mg of bound protein/mg of chitosan) upon tyrosinase activation can be found elsewhere [104]. The nanofactories with Pfs and those with LuxS are then combined to form a single solution with AI-2 synthesis ability (containing both types of magnetic nanofactories). The nanofactories synthesize *in vitro* AI-2 upon addition of the substrate SAH (Figure 2-4a; 0.5 mM, 37 ^{o}C, 2 hr reaction). The reaction is arrested and the reaction mixture is analyzed to determine the amount of *in vitro* AI-2.

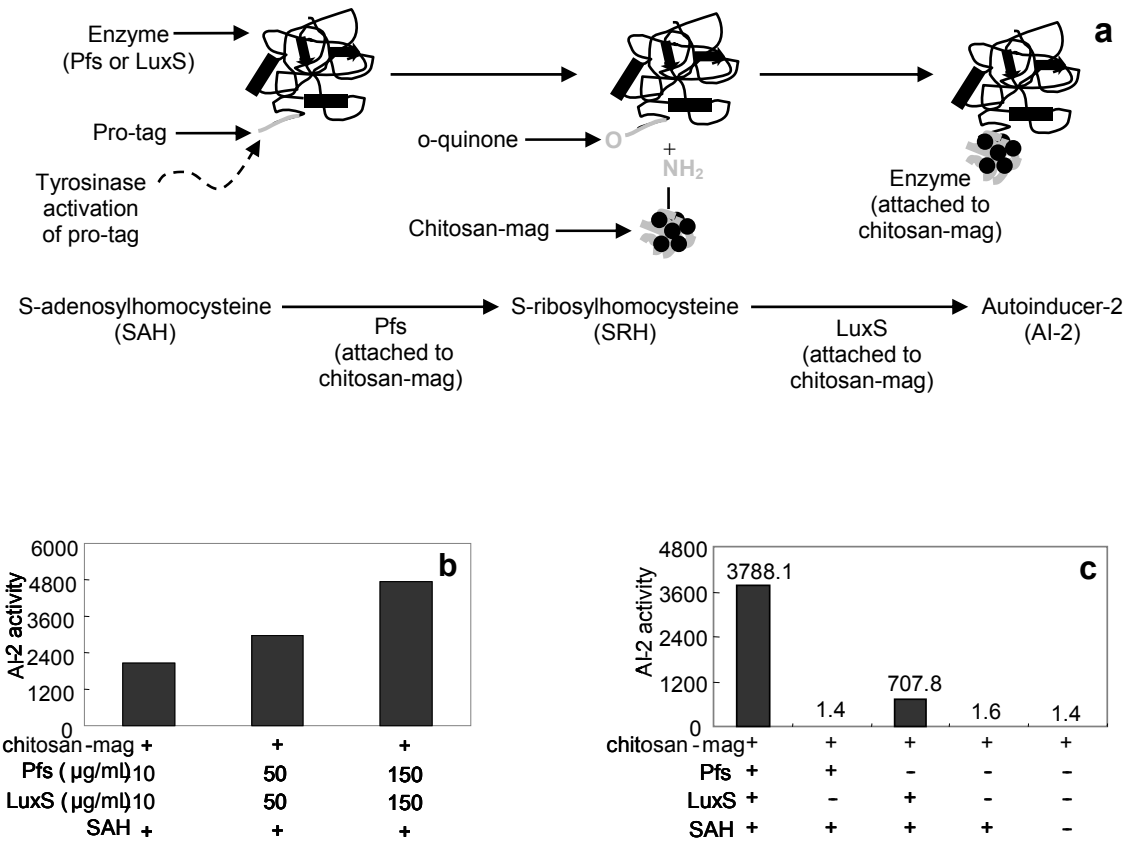

Figure 2-4. Assembly of the magnetic nanofactories: attaching Pfs and LuxS to chitosan-mag via tyrosinase activatable pro-tags (synthesis ability). (a) Attachment of the enzymes to chitosan-mag by activation of the pro-tags using tyrosinase; synthesis of AI-2 from substrate (SAH), the two-step synthesis is catalyzed by the enzymes Pfs and LuxS. (b) AI-2 activity observed in reporter strain in response to in vitro AI-2 synthesized by adding SAH to nanofactories containing varying (increasing) amounts of added Pfs and LuxS. (c) AI-2 activity observed in reporter strain in response to in vitro AI-2 synthesized by adding SAH to either the nanofactories or one or more element of the nanofactory.

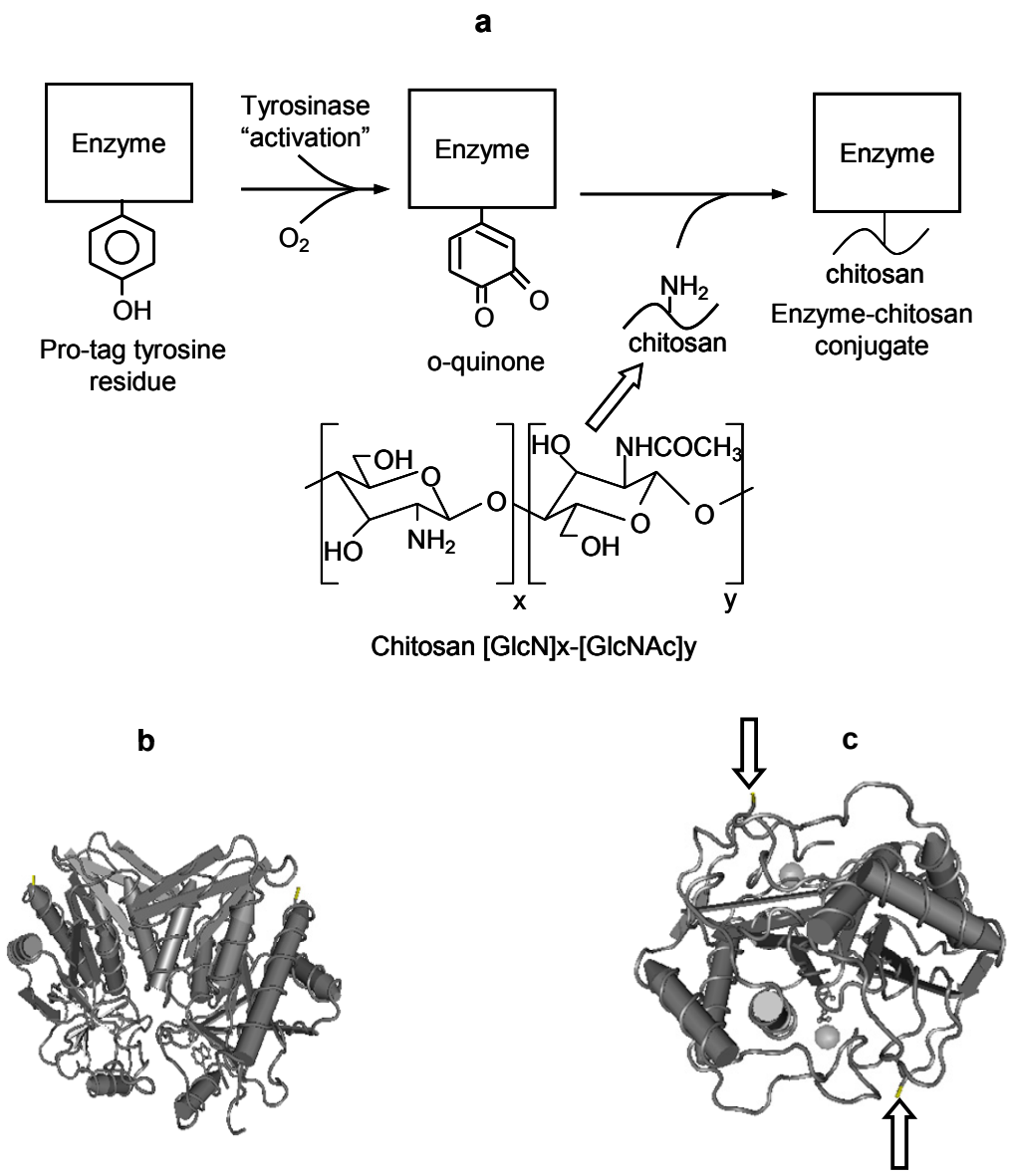

Figure 2-5. Attaching Pfs and LuxS with C-termini pro-tags to chitosan via tyrosinase. (a) Tyrosinase activates the tyrosine residues of the C-terminus pro-tag to generate reactive o-quinones that can react with the amine-groups of chitosan attaching the enzymes to chitosan. (b) Crystal structure of Pfs dimer [105], arrows show position of the C-termini pro-tag. (c) Crystal structure of LuxS dimer [106], arrows show position of the C-termini pro-tag.

Here, 'enzyme-free' solutions containing AI-2 are added to a suspension containing a reporter bacterial strain *Vibrio harveyi* BB170 [100] which produces light in response to added AI-2 [107]. The luminescence produced indicates the AI-2 activity in the added sample. Figure 2-4b shows the AI-2 activity (luminescence produced by *V. harveyi* with AI-2 in added sample divided by that produced without AI-2 in added sample) for varying amounts of added enzymes (Pfs and LuxS, 10-150 μg/mL). The AI-2 activity increases with increasing amounts of added enzymes.

For *in vitro* AI-2 synthesis ability, we expect that both types of nanofactory (i.e. with attached Pfs and LuxS) and substrate SAH need to be present. To test this, *in vitro* AI-2 synthesis was carried out using combinations of the above elements (when used: 1 mg/mL chitosan-mag, 0.5 mM SAH, 50 μg/mL Pfs and 50 μg/mL LuxS). Figure 2-4c shows that the observed AI-2 activity is much higher when all elements for AI-2 synthesis are simultaneously present, ~ 4 fold lower in the case of nanofactories with only attached LuxS and added SAH, and negligible for all other cases.

Localized synthesis and delivery of *in vitro* AI-2 at the cell surface using magnetic nanofactories

To demonstrate user-specified localized synthesis and delivery of AI-2, cultures of *E. coli* are grown in shake flask cultures, exposed to magnetic nanofactories, and evaluated for phenotypic response in a set of controlled experiments. The magnetic nanofactories are assembled (1 mg/mL chitosan-mag; 0.5 mg chitosan-mag with 50 μg/mL Pfs and 0.5 mg chitosan-mag with 50 μg/mL LuxS) and added to a growing suspension of either *E. coli* ZK126 pLW11 [98] or *E. coli* LW7 pLW11 (pH 6) for cell capture [66]. *E. coli* ZK126 is a *lac*

null mutant while *E. coli* LW7 is a *lac* and *luxS* double mutant. The plasmid, pLW11, employs the *lsr* promoter (AI-2 responsive) to drive β-galactosidase expression [66].

Cell capture is performed at 2-hour intervals throughout the experiments (from inoculation to stationary phase). There is no apparent difference in capture efficiency due to the added enzymes in the case of the nanofactories (Figure 2-6a and b). After capture, the nanofactories with the attached cells are recovered using an external magnet and unbound cells are rinsed off (phosphate buffer, PB).

After capture, *in vitro* AI-2 is synthesized by the nanofactories at the cell surface by the addition of SAH (0.5 mM, 37 ^{o}C, 2 hr reaction). Functioning nanofactories are demonstrated by AI-2 synthesis and delivery at the surface of these cells, followed by AI-2 transport and altered gene expression (as determined by AI-2 dependent β-galactosidase expression). In Figure 2-6c and 6d, AI-2 dependent β-galactosidase expression is compared to the negative controls (Figure 2-6c for *E. coli* ZK126 pLW11 and Figure 2-6d for *E. coli* LW7 pLW11). In the case of LuxS^{+} cells (ZK126), which synthesize their own AI-2, the increase in β-galactosidase expression is enhanced ~ 4-fold due to the AI-2 synthesized at the cell surface. In the case of *luxS*$^{-}$ cells (LW7), the increase is >10-fold. These results clearly indicate altered phenotypic behavior and a functioning 'programmable' nanofactory. Figure 2-6e and 6f show SEM and TEM images of the nanofactories attached to *E. coli* LW7 pLW11.

To study the benefit of localized synthesis and delivery of AI-2, the nanofactories are compared to various other configurations using either free cells or cells attached to chitosan-mag (1 mg/mL) either with or without the addition of free enzymes (Pfs and LuxS 50 μg/mL). The control experiments are designed to synthesize equivalent levels

of AI-2. In Figure 2-6g, the cell response to AI-2 delivered locally via nanofactories is 2-fold higher than that observed for delivery by diffusion from the bulk. Our cell surface approach using the magnetic nanofactories produces the highest AI-2 dependent β-galactosidase expression indicating that localized synthesis and delivery of AI-2 results in an increased AI-2 specific transcriptional response.

Figure 2-6. Localized synthesis and delivery of *in vitro* AI-2 at the target cell surface using magnetic nanofactories. (a) $LuxS^{+}$: Cell capture using magnetic nanofactories: Δ optical density of cells captured by the nanofactories at various time-points for *E. coli* ZK126 pLW11 ($\Delta OD_{600;}$ columns) and corresponding growth curve. (b) $LuxS^{-}$: Cell capture using magnetic nanofactories: Δ optical density of cells captured by the nanofactories at various time-points for *E. coli* LW7 pLW11 ($\Delta OD_{600;}$ columns) and corresponding growth curve. (c) $LuxS^{+}$: AI-2 dependent β-galactosidase activity produced in response to synthesis and delivery of AI-2 by nanofactories to the surface of the target cells (*E. coli* ZK126 pLW11, Miller units). * indicates significant difference ($p < 0.01$) (d) $LuxS^{-}$: AI-2 dependent β-galactosidase activity produced in response to synthesis and delivery of AI-2 by nanofactories to the surface of the target cells (*E. coli* LW7 pLW11, Miller units). * indicates significant difference ($p < 0.01$). (e) SEM of the nanofactories attached to the target cells, *E. coli* LW7 pLW11. (f) TEM of nanofactories attached to the target cells, *E. coli* LW7 pLW11. (g) AI-2 dependent β-galactosidase activity produced in response to localized synthesis and delivery of AI-2 by nanofactories to the surface of the target cells (*E. coli* LW7 pLW11) compared to that produced using other techniques of AI-2 synthesis and delivery. * indicates significant difference ($p < 0.01$).

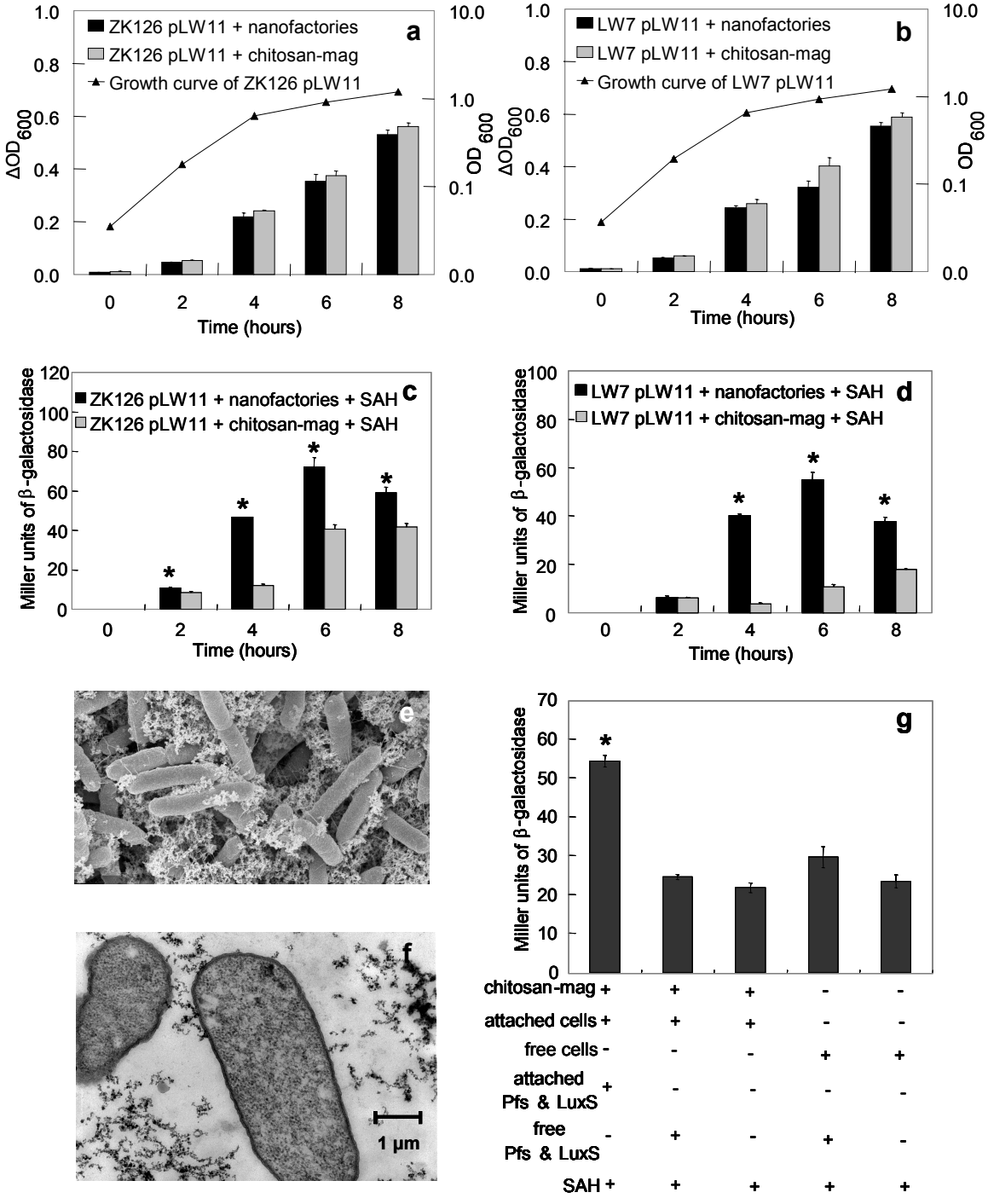

2.5 Discussion

We have demonstrated magnetic nanofactories for the localized synthesis and delivery of the QS signaling molecule AI-2 to the surface of *E. coli*. Our magnetic nanofactories consist of *E. coli* AI-2 synthases, Pfs and LuxS, attached to nano-sized co-precipitates of chitosan-mag (Figure 2-2a). They possess the ability to manufacture AI-2 (via attached Pfs and LuxS; synthesis ability), to attach to the cell surface (via chitosan; cell capture ability) and to be directed and recovered in response to an external magnetic field (via magnetite; stimuli responsiveness).

The biopolymer chitosan serves a dual role in the nanofactory viz. enabling cell capture and providing amine groups to attach Pfs and LuxS. This dual role is attributed to chitosan's unique pH-dependent behavior, particularly the reversible protonation-deprotonation of the amine-groups of chitosan. The decrease in the cell capture ability of chitosan-mag as the pH is increased above 6 (Figure 2-3) is due to the increased extent of amine deprotonation at pH values above their pK_a (no net charge). For attaching QS enzymes, chitosan's amine-groups should be in nucleophilic (neutral) form.

We selected a pH of 6 for our work because at this pH there are sufficient deprotonated amines for enzyme assembly while retaining protonated amines needed for capture (Fig. 2-6a and 6b). Incidentally, as noted by capture efficiency experiments (Figure 2-6a and 6b) and enzyme loading experiments (Figure 2-4b) we have not exhausted the available amines from chitosan for either capture or enzyme loading. This may be advantageous should one need to assemble a cell-specific targeting moiety to the nanofactories.

The enzymes Pfs and LuxS contain activatable pro-tags at their C-termini. The pro-tag extends away from the active site of both enzymes and also provides tyrosine residues for the activation by tyrosinase hence facilitating the attachment of the enzymes to chitosan-mag with intact activity (due to the mild reaction conditions; Figure 2-4b). This report is the first demonstration of small molecule synthesis using enzymes with engineered pro-tags.

The nanofactories with synthesis ability, cell capture ability and stimuli responsiveness are used to capture the strains *E. coli* ZK126 pLW11 (Figure 2-6a) and *E. coli* LW7 pLW11 (Figure 2-6b, 6e and 6f). The synthesis and delivery of AI-2 at the surface of the captured cells using the nanofactories results in increased AI-2 dependent β-galactosidase expression for both strains (Figure 2-6c and 6d). The use of nanofactories for the localized synthesis and delivery of AI-2 also produces an increase in AI-2 dependent β-galactosidase expression when compared to other techniques of synthesis and delivery of AI-2 (Figure 2-6g) indicating the benefit of localized synthesis and delivery in producing increased AI-2 specific transcriptional response (β-galactosidase reporter expression).

We believe our work is significant for the following reasons. Our technique of using magnetic nanofactories to locally synthesize and deliver signaling molecules to target cell surfaces is novel. The magnetic nanofactories have diverse, yet co-existent attributes of small molecule synthesis ability, cell capture ability and responsiveness to external magnetic fields which make them suitable for use in localized cell surface synthesis and delivery applications. The cell capture ability of the nanofactories is based on the simple, reversible pH-dependent properties of chitosan. While this charge based

capture of cells by chitosan is non-specific, specificity can be bestowed to the nanofactory by using an appropriate antibody to a particular region of the target cell. Standard amine-group chemistry of chitosan can be used to attach the antibody to the nanofactory. Further investigations on this aspect are currently in progress. An external (non-invasive) magnetic field is used to recover the nanofactories with attached cells and confine them to a specific location for further analysis. The increase in AI-2 specific transcriptional response (β-galactosidase reporter expression) particularly at earlier times (4- and 6- hour time-points) for both strains indicates functioning and programmable nanofactories that are successful in intercepting and modulating cell-cell communication. Thus we have a facile tool to modulate QS with a view to understanding and controlling QS-based phenomena such as biofilm formation, pathogenicity, and antibiotic resistance. Finally, we believe nanofactories offer many advantages relative to the localized delivery of small molecules, in that the molecule could eventually be synthesized and delivered at a site, at a prescribed concentration and time.

2.6 Acknowledgements

Partial support of this work was provided by the National Science Foundation (Grant No. BES-0124401) and the Bioengineering Graduate Program of the University of Maryland (fellowship to RF).

Chapter 3: AI-2 Biosynthesis Module in a Magnetic Nanofactory Alters Bacterial Response via Localized Synthesis and Delivery

3.1 Abstract

Nanofactories are nano-dimensioned and comprised of modules serving various functions that alter the response of targeted cells when deployed by locally synthesizing and delivering cargo to the surfaces of the targeted cells. In its basic form, a nanofactory consists of a minimum of two functional modules: a cell capture module and a synthesis module. In this work, magnetic nanofactories that alter the response of targeted bacteria by the localized synthesis and delivery of the 'universal' bacterial quorum sensing signal molecule autoinducer AI-2 are demonstrated. The magnetic nanofactories consist of a cell capture module (chitosan-mag nanoparticles) and an AI-2 biosynthesis module that contains both AI-2 biosynthetic enzymes Pfs and LuxS on a fusion protein (His-LuxS-Pfs-Tyr, HLPT) assembled together. HLPT is hypothesized to be more efficient than its constituent enzymes (used separately) at conversion of the substrate SAH to product AI-2 on account of the proximity of the two enzymes within the fusion protein. HLPT is demonstrated to be more active than the constituent enzymes, Pfs and LuxS, over a wide range of experimental conditions. The magnetic nanofactories (containing bound HLPT) are also demonstrated to be more active than free, unbound HLPT. They are also shown to elicit an increased response in targeted *Escherichia coli* cells, due to the localized synthesis and delivery of AI-2, when compared to the response produced by the addition of AI-2 directly to the cells. Studies investigating the universality of AI-2 and unraveling AI-2 based quorum sensing in bacteria using magnetic nanofactories are envisioned. The prospects of using such multi-modular nanofactories in developing the next generation of

antimicrobials based on intercepting and interrupting quorum sensing based signaling are discussed.

3.2 Introduction

A key requisite in targeted delivery for biological applications is localizing the delivered cargo within a targeted region (usually cells or tissue). This facilitates the specific effects of the delivered cargo within the target area and minimizes its non-specific effects elsewhere. The most widely used techniques involve packaging the cargo in its final and active form within a delivery vehicle that transports the cargo to the target site. A variety of delivery vehicles such as polymeric scaffolds, liposomes, nanoparticles or viral vectors have been investigated in the literature [108-110]. Other techniques of targeted delivery employ delivery of an inactive prodrug which is converted to its active form at the target site [111, 112]. We are investigating a fundamentally different approach that uses a nanofactory to locally synthesize and deliver active cargo from an added precursor at a target site.

As defined previously, a nanofactory is a nano-dimensioned factory that is comprised of a synthesis module and a cell capture module assembled together (Figure 3-1) [73, 74]. When deployed, the nanofactories bind to the target cell surface via the cell capture module. Upon addition of a precursor, the synthesis module locally synthesizes the active cargo at the surface of the target cell thereby localizing its effect within the targeted region.

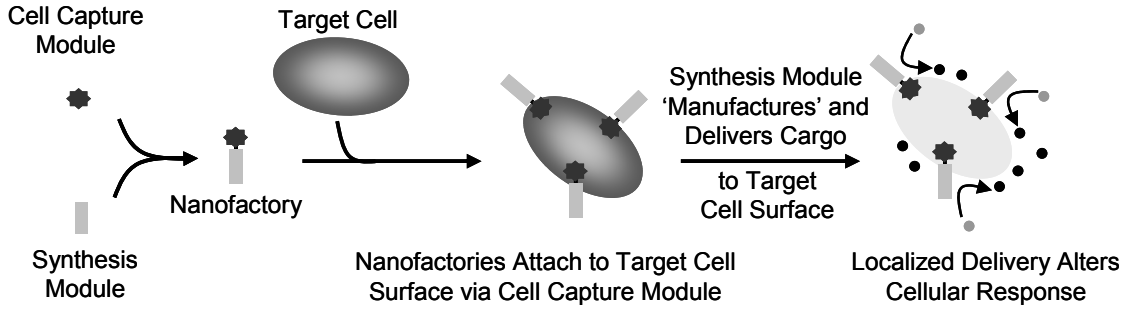

Figure 3-1. Using a nanofactory to alter cellular response via localized synthesis and delivery. A nanofactory, which consists of a cell capture module and synthesis module assembled together, binds to targeted cells via the cell capture module and synthesizes the cargo to be delivered locally at the cell surface using the synthesis module, thereby altering its response.

The reasoning behind using a synthesis and delivery approach is that one can control the amount of cargo delivered to the target site by controlling the amount of added precursor and by doing so modulate the response of the targeted cells. In theory, this concept of a two-module nanofactory can be extended to a multi-modular nanofactory where the added modules confer additional functions or features to the nanofactory which are end-use specific.

In our work we use magnetic nanofactories to locally synthesize and deliver the quorum sensing (QS) signal molecule autoinducer-2 (AI-2) to bacterial cell surfaces and investigate its effect on cellular response. QS is a commonly observed phenomenon whereby bacteria coordinate their intra- or inter-species behavior via the production, secretion, sensing and uptake of small signal molecules called autoinducers [45, 113-115]. QS has been shown to play a role in coordinated bacterial response such as antibiotic production, biofilm formation, bioluminescence, competence and virulence [57, 116-118]. In *E. coli*, AI-2 is synthesized from the toxic metabolite S-adenosylhomocysteine (SAH) via a two-step enzymatic reaction involving the enzymes S-adenosylhomocysteine nucleosidase (Pfs) and S-ribosylhomocysteinase (LuxS) (Figure 3-2a) [66]. AI-2 based signaling has been observed in many Gram negative [119-121] and Gram positive bacteria [122, 123] and is therefore referred to as the 'universal' signaling molecule.

In this work, we extend the concepts demonstrated in our previous study using magnetic nanofactories [73] where the nanofactories comprised of purified Pfs and LuxS attached to separate chitosan-mag nanoparticles. The Pfs nanofactories were then combined with LuxS nanofactories to create a suspension with AI-2 biosynthesis capability. Here, we construct a plasmid that expresses the AI-2 biosynthesis module

which contains both Pfs and LuxS on a single fusion protein (His-LuxS-Pfs-Tyr: HLPT, Figure 3-2b). By having the two enzymes adjacent to each other on a single fusion protein, we believe that we can minimize the time required for the products of the Pfs reaction to diffuse to the LuxS reaction sites. At the same time, we believe that the creation of a fusion protein results in minimal loss of the intrinsic activities of the constituent enzymes (Pfs and LuxS) within the fusion protein.

HLPT is then assembled onto the cell capture module, chitosan-mag, to create the magnetic nanofactories (Figure 3-2c). Chitosan-mag contains the biopolymer chitosan co-precipitated with iron oxide (mag) nanoparticles [89, 90]. Chitosan is a positively charged amine-group containing polysaccharide and has been shown to attach to many Gram positive and Gram negative bacteria and confers the cell capture attribute to the nanofactory. The positively charged amine groups of chitosan can bind to negatively charged bacterial cell surfaces (measured by their zeta potential). The strength and reversibility of this interaction is described in detail in the literature [89, 90]. Mag confers the attribute of magnetic responsiveness to the nanofactory that allows them to be recovered in the presence of a magnetic field which is an added feature of the nanofactory.

The magnetic nanofactories are deployed and attach to the surface of targeted *E. coli* cells via chitosan (Figure 3-2d). Once attached, the nanofactories synthesize AI-2 upon addition of the substrate SAH.

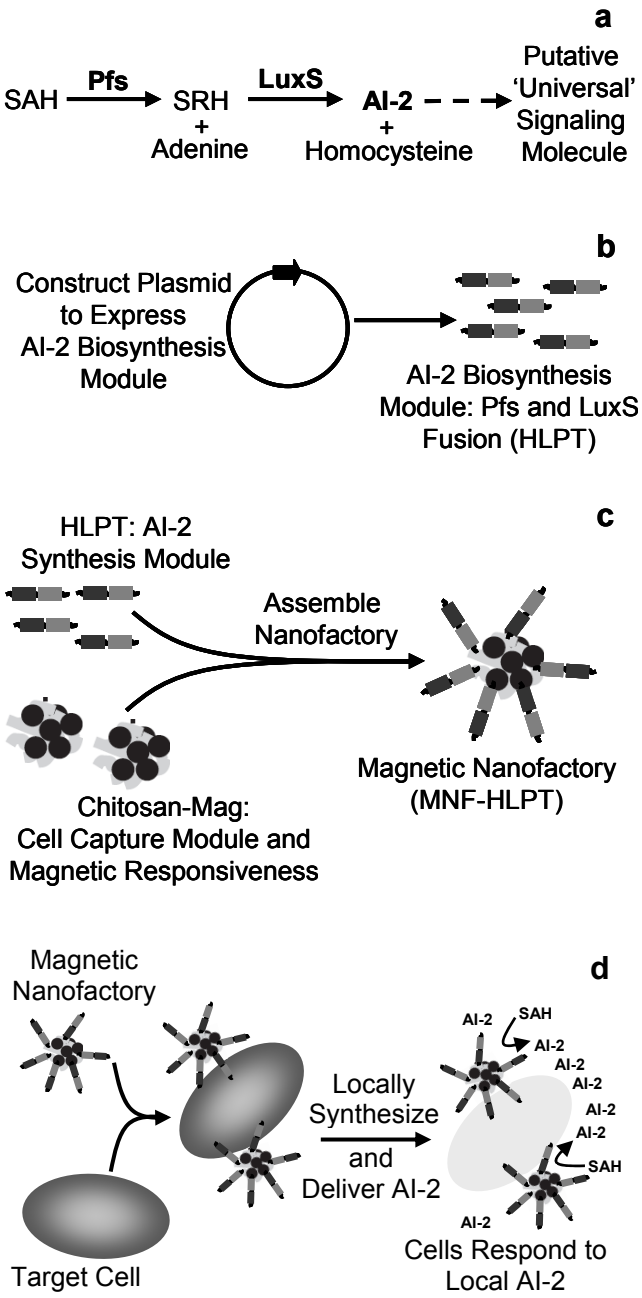

Figure 3-2. Altering bacterial response using magnetic nanofactories. a. Schematic depicting the biosynthesis of signal molecule AI-2 from substrate SAH in *E. coli* catalyzed by enzymes Pfs and LuxS. b. Construction of plasmid pHLPT that expresses the AI-2 biosynthesis module on a single fusion protein, HLPT. c. Assembly of the magnetic nanofactory (MNF-HLPT) by contacting the AI-2 biosynthesis module, HLPT, with the cell capture module, chitosan-mag. d. Using the magnetic nanofactory to locally synthesize and deliver AI-2 at the target cell surface thereby altering cellular response.

The effect of the localized synthesis and delivery on AI-2 specific cellular response is investigated by relating the amount of AI-2 that is delivered to the target cell (outside the target cell) to the production of AI-2 specific β-galactosidase reporter (within the target cell).

The specific aims of this work are to demonstrate construction of the AI-2 biosynthesis module (HLPT); to test the activity of HLPT and compare it to that of the constituent enzymes, Pfs and LuxS, over a wide range of reaction conditions; to compare the activity of the magnetic nanofactory (containing bound HLPT) to that of free, unbound HLPT and finally to investigate the effect of localized synthesis and delivery of AI-2 via the magnetic nanofactories on cellular response and to compare it with that produced by the direct addition of AI-2 to the target cells.

The emergence of antibiotic resistant microbial strains [71, 124] poses a constant threat to human health and places an emphasis on developing new approaches to tackle bacterial pathogenicity. The interception and subsequent interruption of QS based signaling is believed to be important in the development of the next generation of antimicrobials. Specifically, the downregulation of QS related cell functions associated with pathogenicity (e.g. pili formation) but not essential for a pathogen's viability is believed to reduce selective pressure on the pathogen to produce antibiotic resistant strains [71]. A first step toward developing QS based antimicrobials involves understanding quantitatively the effect of a QS signals on bacterial response. The magnetic nanofactories provide a means to do the same by controllably delivering AI-2 to the targeted bacteria.

3.3 Materials and Methods

Chemicals

Chitosan (medium molecular weight 200,000 g/mol), iron (II) chloride tetrahydrate ($FeCl_2.4H_2O$), iron (III) chloride hexahydrate ($FeCl_3.6H_2O$), isopropyl β-D-thiogalactopyranoside (IPTG), phosphate buffered saline tablets (10 mM phosphate buffer, 2.7 mM KCl and 137 mM NaCl, pH 7.4), S-(5'-deoxyadenosin-5')-L-homocysteine (SAH), chloroform, sodium dodecyl sulfate salt (SDS, >98.5 %), o-nitrophenyl-β-D-galactopyranoside (ONPG), 2-mercaptoethanol, imidazole and 5,5'-Dithiobis (2-nitrobenzoic acid) (DTNB) were all purchased from Sigma Aldrich. Glacial acetic acid (CH_3COOH), ampicillin sodium salt, kanamycin, Tris, sodium carbonate (Na_2CO_3), dibasic sodium phosphate ($Na_2HPO_4.7H_2O$), monobasic sodium phosphate ($NaH_2PO_4.H_2O$), potassium chloride (KCl), magnesium sulfate ($MgSO_4.7H_2O$), hydrochloric acid (HCl), sodium hydroxide (NaOH) and sodium acetate trihydrate ($CH_3COONa.3H_2O$) were all purchased from Fisher Scientific. Ammonium hydroxide (NH_4OH) was purchased from J. T. Baker. Bugbuster HT was purchased from Novagen and protein assay dye reagent concentrate was purchased from BioRad laboratories.

Plasmid construction

To construct the plasmid pTrcHis-LuxS-Pfs-Tyr (pHLPT) that expresses the AI-2 biosynthesis module containing enzymes Pfs and LuxS as a fusion, the forward and reverse oligonucleotide primers listed in table 3-1 were used to amplify the *luxS* gene (609 bp) from plasmid pTrcHis-LuxS-Tyr [73]. The PCR reactions were carried out using Vent DNA polymerase (New England Biolabs; NEB).

Table 3-1. List of bacterial strains, plasmids and primers used in this study.

Strain, plasmid or primer	Relevant genotype and/or property	Reference
Escherichia coli strains		
W3110	Wild type	Laboratory stock
BL21 luxS$^-$	*F'* ompT hsdS$_B$ *($r_B^- m_B^-$) gal dcm* Δ*luxS* :: Kan	Laboratory Stock
NC13	RK4353 *Δpfs (8-226)*::Kan	[99]
DH5α	*recA1 supE44 endA1 hsdR17 gyrA96 relA1 thiΔ (lac-proAB)* F' [*traD36 proAB+ lacI^q lacZΔM15*]	Invitrogen
ZK126	Wild type strain derivative, W3110 Δ*lacU160-tna2*	[98]
LW7	ZK126 Δ*luxS* :: Kan	[66]
TOP10	*F- mcrA Δ(mrr-hsdRMS-mcrBC) φ80lacZΔM15 ΔlacX74 deoR nupG recA1 araD139 Δ(ara-leu)7697 galE15 galK16 rpsL(Str^R) endA1 λ$^-$*	Invitrogen
Vibrio harveyi strains		
BB170	BB120 *luxN* :: Tn*5* (sensor 1$^-$, sensor 2$^+$)	[100]
Plasmids		
pTrcHis-LuxS-Tyr	pTrcHisC derivative, W3110 *luxS*$^+$, Amp^r	[73]
pTrcHis-Pfs-Tyr	pTrcHisC derivative, W3110 *pfs*$^+$, Amp^r	[73]
pFZY1	*galK'-lacZYA* transcriptional fusion vector, Amp^r	[101]
pLW11	pFZY1 derivative, containing *lsrACDBFG* promoter region, Amp^r	[66]
pCR-LuxS	pCR-Blunt II-TOPO derivative, *luxS*$^+$, Kan^r	This study
pHLPT	pTrcHisC derivative, W3110 *pfs*$^+$, *luxS*$^+$, Amp^r	This study

Oligonucleotide primers

Name	Sequence	Relevant property
C1-5'	5'- GGC TAG CAT GAC TGG TGG -3'	Upstream primer for cloning *luxS* from pTrcHis-LuxS-Tyr, contains *Nhe*I
C1-3'	5'- TAG ATC TTT CGG CCG ATG TGC AGT TCC T -3'	Downstream primer for cloning *luxS* from pTrcHis-LuxS-Tyr, contains *Bgl*II

The 609 bp fragment containing *luxS* was isolated and purified using the QIAquick gel extraction kit (Qiagen). The blunt end fragment was then inserted into pCR-Blunt II-TOPO (Invitrogen). The intermediate plasmid (pCR-LuxS) was transformed into the strain *E. coli* TOP10 (Invitrogen). The integrity of the intermediate construct was verified by sequencing the plasmid at the DNA core facility at the Center for Biosystems Research, University of Maryland Biotechnology Institute. The fragment containing *luxS* was extracted by digesting pCR-LuxS using the restriction endonucleases *Nhe*I and *Bgl*II (NEB), isolated and purified using the QIAquick gel extraction kit. The purified fragment was then inserted into the destination vector pTrcHis-Pfs-Tyr , previously cut using the endonucleases *Nhe*I and *BamH*I, by ligation using the Quick ligation kit (NEB) to generate the final plasmid pHLPT. pHLPT was transformed into the expression strain *E. coli* BL21 luxS$^-$ (a *luxS* knockout, table 3-1) and its integrity was verified by sequencing at the DNA core facility.

Growth media

The Luria-Bertani (LB) medium used for bacterial growth contains 5 g/L of yeast extract (Sigma), 10 g/L of Bacto tryptone (Difco) and 10 g/L NaCl (J. T. Baker). The components of the Autoinducer Bioassay medium (AB) are described elsewhere [96].

Expression and purification of His-LuxS-Pfs-Tyr (HLPT), Pfs and LuxS

E. coli BL21 luxS$^-$ pHLPT was cultured at 37 ^oC and 250 rpm in LB medium supplemented with ampicillin at a concentration of 50 μg/mL. When the optical density (OD_{600}) of the cell culture was between 0.4 - 0.6, IPTG was added to induce fusion

protein, HLPT, production (final IPTG concentration used was 1 mM). After a 6 hr induction period at the same culture conditions, the cells were harvested by centrifugation at 6,000 xg for 30 minutes at 4 ^{o}C. The cells were stored at -20 ^{o}C or directly resuspended in the cell lysis reagent, Bugbuster HT. The lysis reaction was allowed to proceed for 30 minutes at room temperature and 100 rpm. After the said lysis time, the samples were centrifuged at 12000 xg at 4 ^{o}C for 20 minutes. The clarified supernatant containing the overexpressed HLPT was contacted with TALON® metal affinity resin (Clontech) suspended in binding buffer (10 mM PO_4^{3-} and 10 mM imidazole) for 30 minutes at room temperature and 100 rpm. The resin containing the bound HLPT was rinsed thrice with wash buffer (10 mM PO_4^{3-}) and treated with the elution buffer (10 mM PO_4^{3-} and 250 mM imidazole). For complete elution, the resin was subjected to a second elution under identical conditions. The eluted HLPT was desalted using Zeba desalt spin columns (Pierce Biotechnology) to remove excess salts in the buffer exchange mode (where the elution buffer was exchanged for 10 mM sodium phosphate buffer pH 6; PB6). Prior to determining the concentration of HLPT, the samples were filtered using a 0.22 μm polyether sulfone, low protein binding filter (Millipore). The concentration of HLPT in 10 mM PB6 was quantified by measuring the absorbance of the samples at 280 nm (OD_{280}) and confirmed using the BioRad protein assay as per the manufacturer's specifications (website: http://www.bio-rad.com). For Pfs expression and purification, the cell strain *E. coli* DH5α carrying plasmid pTrcHis-Pfs-Tyr was used while for LuxS expression and purification, the cell strain *E. coli* NC13 carrying plasmid pTrcHis-LuxS-Tyr was used under experimental conditions identical to those used for HLPT expression and purification described above.

Protein sizing and analysis assay using LabChip®

The sizing and analysis of HLPT, Pfs and LuxS was performed using a LabChip® Protein 200 plus kit (Agilent Technologies). Briefly 1 μg each of purified HLPT (molecular weight 50093 Daltons), Pfs (molecular weight 29716 Daltons) and LuxS (molecular weight 24778 Daltons) were loaded per well in the chip and the assay was conducted according to the manufacturer's specifications (website: http://www.chem.agilent.com).

Synthesis of *in vitro* AI-2

In vitro AI-2 was synthesized by adding 1 μM of the fusion protein, HLPT, to 100 μM of the substrate, SAH, in 10 mM PB6. The reaction was carried out at 37 ^{o}C for 2 hours. After the said reaction time, the samples were withdrawn, chloroform was added to the samples to arrest the reaction and the samples were centrifuged at 14000 rpm on a benchtop centrifuge (Eppendorf 5417 C). The aqueous supernatants containing *in vitro* AI-2 (in addition to enzymatic reaction byproducts and unreacted SAH) were collected and filtered through a 0.22 μm filter (Millipore). The samples were either immediately quantified using the techniques for AI-2 activity estimation mentioned subsequently or stored at – 20 ^{o}C for up to a week until assayed. As controls, 1 μM HLPT was replaced by equimolar amounts of Pfs and LuxS (1 μM Pfs and 1 μM LuxS), Pfs (1 μM) or LuxS (1 μM).

Estimation of AI-2 activity (using the *V. harveyi* bioluminescence assay)

The estimation of AI-2 activity was performed by measuring the AI-2 dependent bioluminescence produced in the bacterial reporter *V. harveyi* as described elsewhere [107]. Briefly, 20 µL of sample (collected during the above synthesis reactions) was added to 180 µL of *V. harveyi* BB170 suspension prepared by 5000-fold dilution of an overnight culture of the same strain into fresh AB medium. 10 mM PB6 was used as the negative control and the cell-free supernatants obtained by centrifuging a 4 hr culture of the wild type strain *E. coli* W3110 grown in LB medium at 37 ^{o}C and 250 rpm (conditioned medium) was used as the positive control. The bioluminescence produced in the reporter was measured for all samples. AI-2 activity in a given sample was calculated by dividing the bioluminescence produced by a given sample by that produced in the negative control under identical reaction conditions. To verify reproducibility of the results, each sample type was analyzed by using at least three separately prepared experimental replicates ($n \geq 3$).

Estimation of AI-2 concentration (by quantification of free thiols using DTNB)

The reaction catalyzed by LuxS results in the formation of equimolar amounts of AI-2 and homocysteine [56, 125]. Therefore, the concentration of AI-2 can be equated to the concentration of homocysteine generated in the AI-2 synthesis reaction which can be estimated by its free thiol group (-SH). To estimate homocysteine, 100 µL of sample collected above was added to DTNB reagent (100 µM DTNB, 2.5 mM sodium acetate in 0.1 M Tris buffer, pH 8). The reaction was carried out at room temperature for at least 15 minutes. After the reaction, the absorbance at 412 nm (OD_{412}) was measured and the concentration of homocysteine calculated using molar extinction coefficient (13600 M^{-1}

cm^{-1}) of the reaction product 5-thio-2-nitrobenzoic acid (TNB) [126]. Each sample type had at least three separately prepared experimental replicates ($n \geq 3$).

Effect of synthesis time and temperature on AI-2 concentration

To investigate the effect of synthesis time on the AI-2 generation, samples containing 1 µM HLPT and 100 µM SAH in 10 mM PB6 were incubated at 37 ^{o}C. At various synthesis times (t = ½ hr, 1 hr, 2 hr and 4 hr), aliquots of sample were withdrawn, processed and the concentration of AI-2 estimated using DTNB as described above. For controls, HLPT was replaced by equimolar amounts of Pfs and LuxS (1 µM Pfs and 1 µM LuxS), Pfs (1 µM) or LuxS (1 µM).

To investigate the effect of synthesis temperature, samples containing 1 µM HLPT and 100 µM SAH in 10 mM PB6 were incubated at various temperatures (4 ^{o}C, room temperature, 30 ^{o}C, 37 ^{o}C) for two hours. Controls identical to earlier experiments were also performed. After the said reaction time, the samples were withdrawn, processed and estimated as described above.

Preparation of chitosan-mag nanoparticles

Chitosan-mag was prepared as described in our previous study [73]. Briefly, 20 mL of a reaction mixture (previously purged with nitrogen to removed dissolved oxygen) consisting of 13.5 mM Fe^{2+}, 27 mM Fe^{3+} ($[Fe^{3+}]/[Fe^{2+}] = 2$) and 1 % chitosan (reaction mixture pH 0.5) was added dropwise to 2 M NH_4OH (also previously purged with nitrogen, pH 11) which was vigorously stirred. The resultant black precipitate was collected by decanting the supernatant and was washed with copious amounts of de-

ionized water to wash off the excess base. After washing, the pH of the solution was lowered to a neutral pH using 0.5 % acetic acid. The precipitate was collected by centrifuging at 12000 xg for 10 minutes and resuspended in 0.5 % acetic acid. To break up any aggregates formed during the synthesis reaction, the suspension was sonicated for 30 minutes using Sonic Dismembrator 550 (Fisher Scientific). The resulting suspension containing chitosan-mag nanoparticles was filtered through a 0.22 μm filter to sterilize the particles for use with bacterial cells and the concentration (mg/mL) of the suspension estimated. Chitosan-mag was also prepared by varying the proportions of chitosan and iron salts used in the synthesis reaction and it resulted in chitosan-mag nanoparticles of varying accessible surface amine concentrations.

Assembly of the magnetic nanofactories

The magnetic nanofactories consist of an AI-2 biosynthesis module (HLPT) and an *E. coli* binding module (chitosan-mag). HLPT and chitosan-mag were prepared as described earlier. To assemble the nanofactories, a solution containing 1 μM HLPT and 1 mg/mL chitosan-mag in 10 mM PB6 was incubated at 30 ^{o}C for 1 hour. HLPT adsorbs on to chitosan-mag thereby combining the AI-2 biosynthesis and cell capture modules forming the nanofactory, MNF-HLPT. MNF-HLPT was also made by varying the ratio of HLPT to chitosan-mag.

Comparing the activities of the magnetic nanofactories and free enzymes

To test MNF-HLPT, for its AI-2 synthesis capability, MNF-HLPT was incubated with the substrate SAH. MNF-HLPT used contained 0.25 mg/mL chitosan-mag and 0.25 μM

assembled HLPT and was incubated with 250 μM SAH in 10 mM PB6 at 30 ^{o}C for 2 hours. After the said reaction period, the particles were collected with a magnetic stand (Promega MagneSphere® stand Z5342). When needed, 1 M NaOH was added to the sample to assist in the particle precipitation. The supernatants were collected, treated with chloroform to arrest the reaction and the AI-2 concentration was estimated as described earlier. The performance of MNF-HLPT was compared with that of an equimolar amount of free (unbound) HLPT at reaction conditions identical to those used for MNF-HLPT.

Altering cellular response via localized synthesis and delivery of AI-2 using the magnetic nanofactories

E. coli LW7 pLW11 (*lac*$^{-}$ *luxS*$^{-}$, AI-2 responsive *lsr-lacZ* on pLW11) was pre-cultured overnight at 37 ^{o}C and 250 rpm in LB medium supplemented with ampicillin at a concentration of 100 μg/mL. 0.5 mL of the overnight culture was added to 49.5 mL fresh LB medium supplemented with 60 μg/mL ampicillin. The culture was grown at 30 ^{o}C and 250 rpm for 7 hours. After the said growth period, the cells were withdrawn and recovered by spinning at 12000 xg for 5 minutes. A suspension of the cell strain in 10 mM PB6 was prepared.

The magnetic nanofactories were assembled as described above. After assembly 0.5 mL of the magnetic nanofactories (MNF-HLPT: 4 μM HLPT attached to 1 mg/mL chitosan-mag in 10 mM PB6) was added to 0.5 mL of the *E. coli* LW7 pLW11 suspension. Cell capture was carried out for 30 minutes at room temperature. The nanofactories with the bound cells were recovered by using the magnetic stand and

resuspended in 0.5 mL 10 mM PB6. The amount of bound cells was estimated by measuring the optical density (OD_{600}) of the cell suspension before capture and of the supernatant after capture ($OD_{bound\ cells} = OD_{600,cell\ suspension} - OD_{600,supernatant}$).

The above solution was added to SAH (final concentration 0.5 mM SAH in 10 mM PB6) and the samples were incubated at 37 ^{o}C for 2 hours. After the reaction, the nanofactories with the bound cells were recovered with a magnetic stand. The supernatants (containing AI-2) were collected and the amount of AI-2 delivered to the cells by the nanofactories was estimated using the method described above (using DTNB). A Miller assay [102] was performed to determine the AI-2 dependent β-galactosidase expression of the cells captured by the nanofactories. The AI-2 dependent β-galactosidase expression produced by MNF-HLPT was compared with that produced by the direct addition of *in vitro* AI-2 (150 μM) to the cells, cells captured by chitosan-mag only (hence no AI-2) and that of free cells (no AI-2), all treated identically.

3.4 Results

Construction of the AI-2 biosynthesis module (HLPT)

We constructed plasmid pHLPT to expresses the AI-2 biosynthesis module on a single fusion protein (plasmid map, Figure 3-3a). When induced, pHLPT expresses fusion protein His-LuxS-Pfs-Tyr (HLPT), which contains both the AI-2 biosynthesis enzymes Pfs and LuxS. HLPT possesses the ability to synthesize the signal molecule AI-2 upon addition of the substrate SAH. The fusion protein was purified using immobilized metal ion affinity chromatography and analyzed for its size using LabChip®. Purified HLPT possesses the correct size (50093 Da) calculated from the primary amino acid sequence

of the protein. The size of HLPT is shown in relation to that of its constituent enzymes Pfs (29716 Da) and LuxS (24778 Da) in Figure 3-3b.

Testing the activity of HLPT

In vitro AI-2 was synthesized by adding HLPT to substrate SAH (synthesis time = 2 hours, temperature = 37 ^{o}C). Controls using Pfs and LuxS were performed as described earlier. The reaction products were analyzed either for their AI-2 activity using the *V. harveyi* bioluminescence assay or for their AI-2 concentration by quantification of free thiols using DTNB. Figure 3-4a shows that HLPT produces higher AI-2 activity in the reporter strain as compared to the controls. Figure 3-4b shows that the homocysteine concentration (hence AI-2 concentration) is the highest when using HLPT. Taken together, the results in Figure 3-4 indicate that the AI-2 biosynthesis module (HLPT) produces the highest conversion of substrate SAH to product AI-2 (+homocysteine) under the stated reaction conditions.

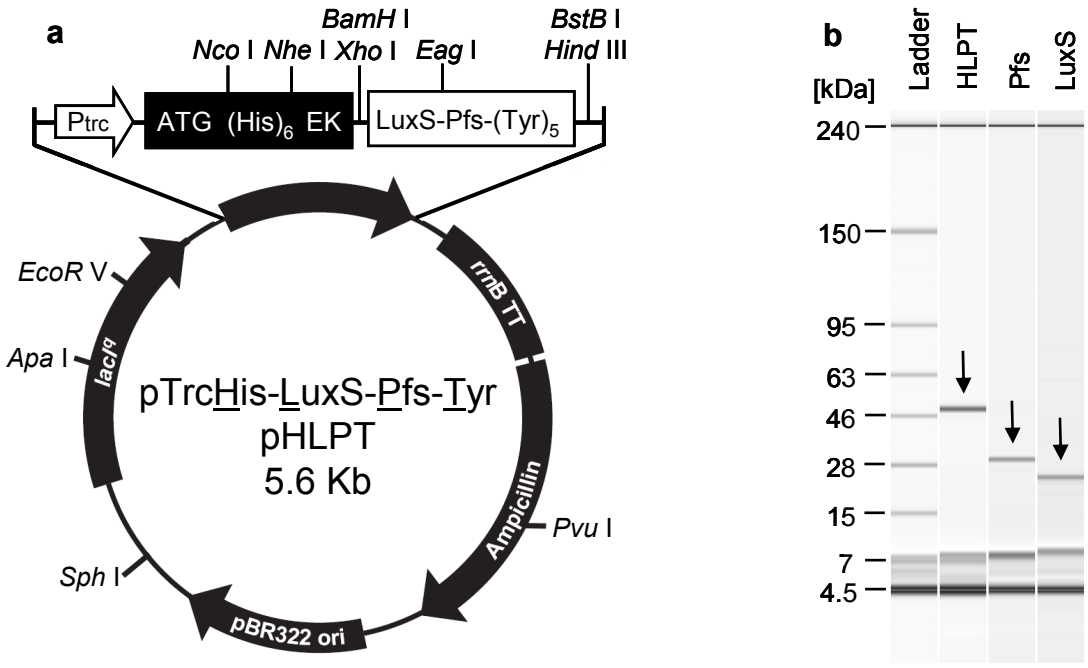

Figure 3-3. Construction and expression of HLPT. a. Plasmid map depicting the features of the plasmid pHLPT that expresses the fusion protein HLPT. b. Analysis of HLPT using LabChip®. HLPT predicted theoretical molecular weight is 50093 Da, Pfs molecular weight is 29716 Da and LuxS molecular weight is 24778 Da.

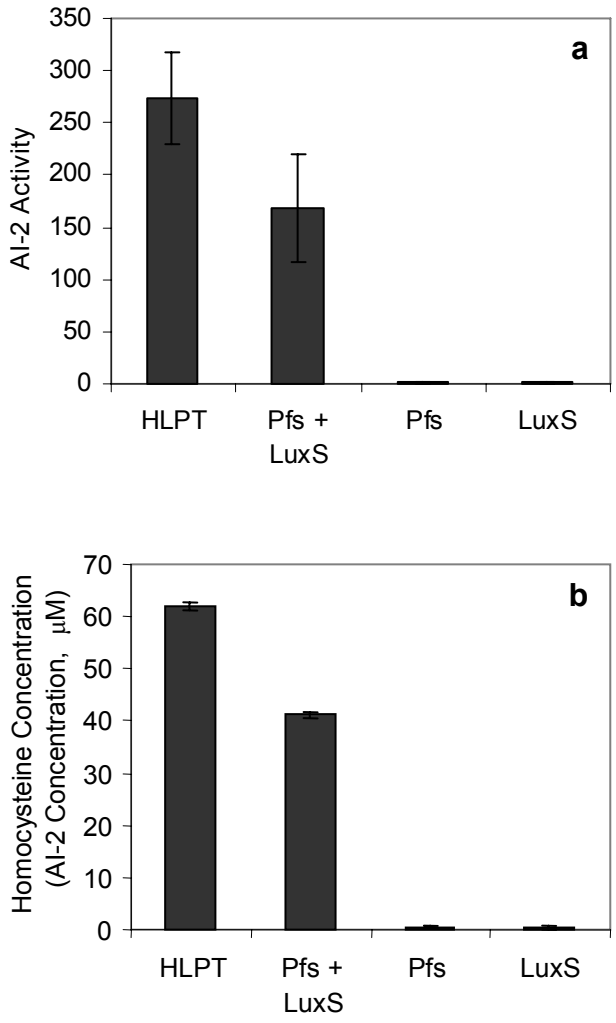

Figure 3-4. Testing the activity of HLPT and comparing it to equimolar amounts of Pfs and LuxS, Pfs only and LuxS only using the a. *V. harveyi* bioluminescence assay and b. free thiol quantification via DTNB.

Investigating the effect of synthesis time and temperature on the activity of HLPT

Figure 3-5 shows the effect of synthesis time and synthesis temperature on product formation. Figure 3-5a shows that HLPT produces higher concentrations of AI-2 than equimolar amounts of Pfs and LuxS over the entire time period investigated (4 hours at 37 ^{o}C). The ratio of average concentration of AI-2 produced using HLPT to that produced using Pfs and LuxS is higher initially (t = 30 minutes) and decreases as time proceeds (t = 30 minutes, ratio = 1.6; t = 1 hour, ratio = 1.5; t = 2 hours, ratio = 1.4 and t = 4 hours, ratio = 1.2). Figure 3-5b shows that HLPT produces higher concentrations of AI-2 than equimolar amounts of Pfs and LuxS over the synthesis temperatures investigated (T = 4 ^{o}C, Room temperature 23 ^{o}C, 30 ^{o}C and 37 ^{o}C, t = 2 hours). A similar trend was observed where the ratio of average concentration of AI-2 produced using HLPT to that produced using Pfs and LuxS is higher at a lower temperature (T = 4 ^{o}C) and decreases as with increasing temperature (T = 4 ^{o}C, ratio = 4.9; T = 23 ^{o}C, ratio = 2.7; T = 30 ^{o}C, ratio = 2.1 and T = 37 ^{o}C, ratio = 1.6). Taken together, Figure 3-5 indicates that HLPT produces the highest conversion of substrate (SAH) to product (AI-2 + homocysteine) over a wide range of reaction conditions. We therefore select HLPT for future experiments as it has higher activity (produces higher concentrations of AI-2) than Pfs and LuxS under the experimental conditions used.

Comparing the activity of the magnetic nanofactory, MNF-HLPT, to free HLPT

As noted earlier, HLPT adsorbs onto chitosan-mag forming MNF-HLPT. *In vitro* AI-2 was synthesized using either MNF-HLPT or equimolar amounts of free HLPT (2 hours, 30 ^{o}C).

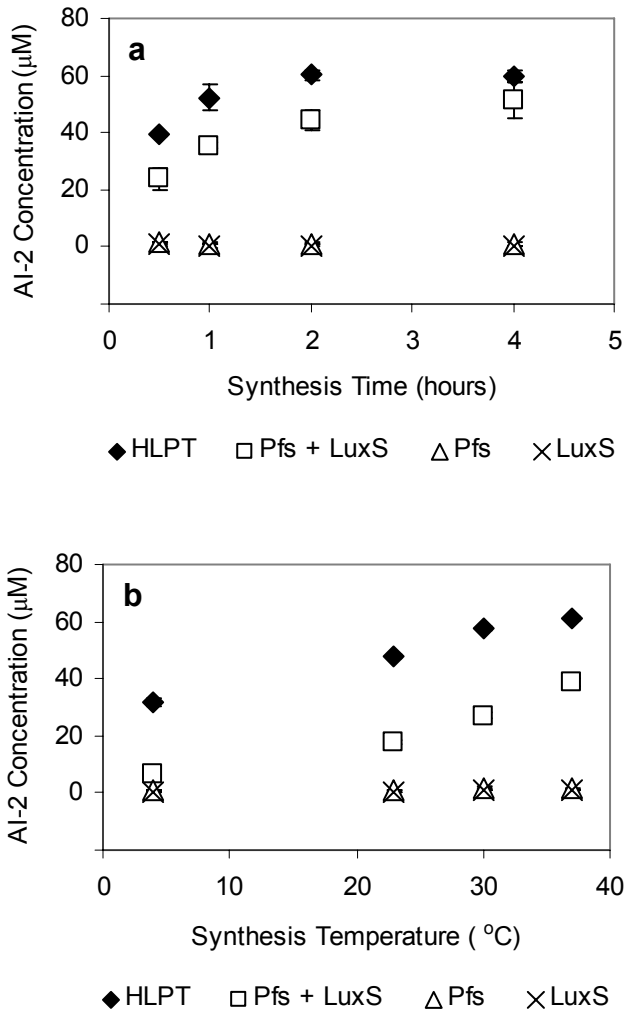

Figure 3-5. Comparing the activity of HLPT to equimolar amounts of Pfs and LuxS, Pfs only and LuxS only as a function of a. synthesis time (maintaining a constant reaction temperature of 37 ^{o}C) and b. synthesis temperature (maintaining a constant reaction time of 2 hours) .

Figure 3-6 shows that MNF-HLPT produces higher concentrations of AI-2 than free HLPT under the stated reaction conditions (ratio = 1.6). The result indicates that enzyme immobilization resulted in higher enzymatic activity under the reaction conditions used. We therefore use MNF-HLPT in future experiments to deliver AI-2 to targeted *E. coli* cells.

Altering cellular response via localized synthesis and delivery of AI-2 using MNF-HLPT

MNF-HLPT was added to a suspension of the reporter strain *E. coli* LW7 pLW11 (*lac*$^-$ *luxS*$^-$, AI-2 responsive *lsr-lacZ* on pLW11). MNF-HLPT locally synthesizes and delivers AI-2 at the surface of the reporter cell upon addition of substrate SAH. The local AI-2 is taken up by the reporter and induces plasmid pLW11 to produce AI-2-dependent β-galactosidase which is measured by a Miller assay.

The response produced by MNF-HLPT in the reporter was compared to that produced by direct addition of *in vitro* AI-2 (10 fold higher concentration, synthesized previously) and controls without any added or intrinsic AI-2 (chitosan-mag and free cells). Figure 3-7a shows the concentrations of AI-2 delivered to the cells and Figure 3-7b shows the resultant AI-2-dependent response (β-galactosidase production). The direct addition of AI-2 (150 μM) to the cells results in a response that is 1.4 times (36 Miller units) that of the native response of the cells (no AI-2, 27 Miller units). However MNF-HLPT (15 μM AI-2, 60 Miller units) elicits a response that is 2.5 times that produced in cells attached by chitosan-mag only (no AI-2, 23 Miller units), 2.2 times that produced by the native response of the cells (no AI-2, 27 Miller units) and 1.7 times that produced by

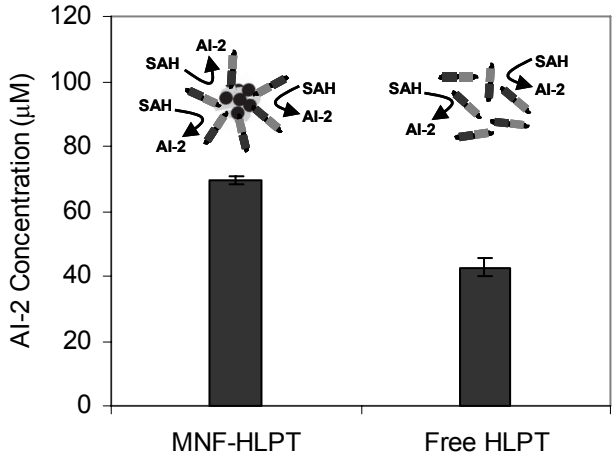

Figure 3-6. Comparing the activity of the magnetic nanofactories, MNF-HLPT, to equimolar amounts of free, unbound HLPT.

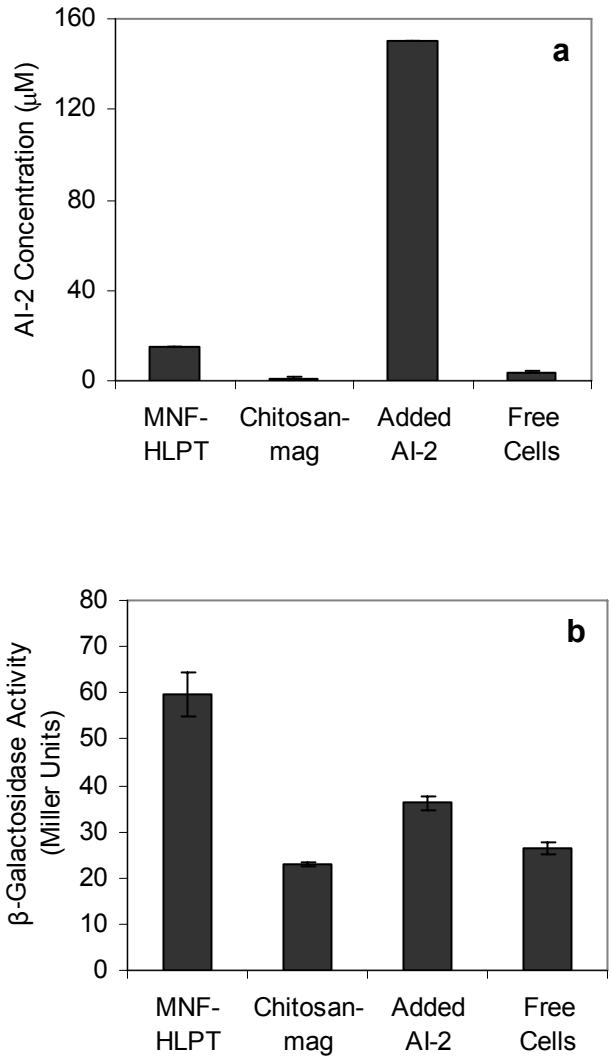

Figure 3-7. Altering AI-2-dependent β-galactosidase production in reporter *E. coli* LW7 pLW11 using magnetic nanofactories. Comparing the response produced by MNF-HLPT to that produced by cells attached to chitosan-mag only (chitosan-mag), by direct addition of 10 times the AI-2 concentration (added AI-2) and by unattached cells (free cells, native response). a. AI-2 delivered to the reporter cells by the various samples. b. AI-2-dependent β-galactosidase (Miller units) produced by the various samples.

direction addition of AI-2 to the cells (150 μM AI-2, 10 times the AI-2 delivered by MNF-HLPT, 36 Miller units).

Taken together, Figure 3-7 indicates that localized synthesis and delivery of AI-2 using MNF-HLPT results in altered (increased) AI-2-dependent response in targeted cells as compared to controls and that the response is higher than that produced by direct addition of 10 times the amount of AI-2 under the stated experimental conditions.

3.5 Discussion

Plasmid pHLPT expresses the AI-2 biosynthesis module HLPT (Figure 3-3) which was demonstrated to have higher activity than equimolar amounts of the constituent enzymes Pfs and LuxS over a wide range of reaction times and temperatures (Figures 3-4 and 3-5). We believe the reason for this is that the proximity of the two enzymes in the fusion protein decreases the path length for the diffusion of the reaction products of the Pfs reaction to the sites of the LuxS reaction. The catalytic turnover number of Pfs [127] has been shown to be higher than that of LuxS [128, 129] and hence over time, there will be accumulation of the Pfs reaction products (SRH and adenine) as the LuxS reaction becomes limiting. Also because diffusion is temperature-dependent [130], an increased temperature causes faster diffusion and consequently an accumulation of the Pfs reaction products if the LuxS reaction does proceed fast enough.

Evidence to support this assertion of an activity advantage due to proximity effects was provided by the fact that as synthesis times were increased, the ratio of the activity of the fusion protein to that of the constituent enzymes was found to decrease (from a ratio of 1.6 at 30 minutes to 1.2 at 4 hours). Also, as the synthesis temperature

was increased, the observed trends were similar (activity ratio decreasing from 4.9 at 4 ^{o}C to 1.6 at 37 ^{o}C). Calculation of the diffusion path length between the site of the Pfs reaction and that of the LuxS reaction (i.e. the proximity advantage) as well as quantification of the concentrations of the intermediate products of the reactions was not investigated. These parameters will be investigated in a more rigorous manner in a microfluidics device [131] where reaction temperatures and times can be precisely controlled.

A second advantage of the using HLPT is that the creation of the fusion does not cause any apparent loss in the intrinsic activities of the constituent enzymes. The enzymes were observed to remain stable over the investigated experimental time-scales; stability over longer time scales was not investigated.

MNF-HLPT was seen to have higher activity than the free, unbound HLPT. This indicates that the immobilization of HLPT onto chitosan-mag seems to either stabilize the fusion protein or inhibit the effects that cause a loss of enzyme activity. MNF-HLPT elicited a higher AI-2-dependent response in reporter *E. coli* LW7 pLW11 as compared to controls where no AI-2 was added (chitosan-mag and free cells). MNF-HLPT was also demonstrated to produce a higher response than the addition of 10 times the concentration of AI-2 directly to the cells. We believe that this is because the cells experience a localized high concentration of AI-2 when using MNF-HLPT which is more effective at eliciting a response than using a global high concentration via the direction addition of AI-2 to the cells.

3.6 Conclusions

We have demonstrated a multi-modular magnetic nanofactory for the localized synthesis and delivery of the 'universal' signal molecule AI-2 to targeted bacteria. The nanofactories comprised of an AI-2 biosynthesis module adsorbed onto a cell capture module with magnetic responsiveness (chitosan-mag). The AI-2 biosynthesis module, HLPT, expresses the enzymes Pfs and LuxS on a single fusion protein and was shown to be more active than Pfs and LuxS over a wide range of experimental conditions. The magnetic nanofactory, MNF-HLPT, was shown to be more active than the free enzyme and also shown to alter (increase) AI-2 specific cellular response in targeted cells due to a localized high concentration of AI-2.

We believe that this work is significant for the following reasons. The work demonstrates the expression of enzymes of a signaling pathway on a single, active fusion protein and its assembly on a magnetic nanoparticle in the form of a magnetic nanofactory. Creation of this fusion protein greatly aids in protein purification and has concomitant advantages with respect to enzymatic activity over a wide range of experimental conditions. Even though we do not currently know the exact surface concentrations of the signal molecule, the magnetic nanofactory provides a facile tool to locally (and more effectively) deliver the signal molecules to the target cells in a quantitative manner (on a global scale). Further experiments conducted on the intracellular targets of AI-2 in *E. coli* as well as other QS bacteria will help (quantitatively) elucidate the mechanisms of AI-2 based signaling in bacteria as well as test the universality of AI-2. The results of these studies will also enable us to create magnetic nanofactories that contain different synthesis modules, including those that may

intercept and interrupt QS signaling by degrading AI-2 thereby downregulating or 'switching off' AI-2 based responses.

3.7 Acknowledgements

The authors would like to acknowledge the help provided by Dr. Gregory E. Fernandes (Texas A & M University) in understanding chitosan-mag particle stability. Funding for this research was provided by the R. W. Deutsch Foundation and the National Science Foundation (EFRI-735987)

Chapter 4: Antibody Nanofactories: Probing Bacterial Communication by Localized Synthesis and Delivery of Autoinducer-2

4.1 Abstract

Biological nanofactories are bio-inspired and comprised of multiple functional modules. Biological nanofactories locally synthesize and deliver molecules-of-interest at the surface of cells they target, thereby altering their native response. Here we demonstrate antibody nanofactories as a method to alter the native quorum sensing response of bacterial cells via localized synthesis and delivery of the universal bacterial quorum sensing signaling molecule, autoinducer-2 (AI-2). Quorum sensing has been shown to play a role in intra- and inter-species bacterial communication, as well as in bacterial interaction with eukaryotes. The antibody nanofactory described here combines the exquisite targeting capabilities of an antibody with the AI-2 synthesis capabilities of a fusion protein. The fusion protein His-Protein G-LuxS-Pfs-Tyr, HGLPT, contains Protein G and the *E. coli* AI-2 biosynthetic enzymes Pfs and LuxS. Upon mixing of the targeting antibody with the fusion protein HGLPT, the antibody nanofactory self-assembles when HGLPT attaches to the Fc region of the antibody via Protein G. The nanofactories are shown to alter the native phenotype of targeted *Escherichia coli* and *Salmonella typhimurium* cells by locally synthesizing and delivering AI-2 at the surface of the targeted cells. Selective delivery of quorum sensing signals via antibody nanofactories is envisaged to play an important role in the creation of the next generation of antimicrobials based on altering (turning up or turning down) native quorum sensing based response.

4.2 Introduction

Biological nanofactories alter the native response of cells they target by locally synthesizing and delivering molecules-of-interest (signal molecules, growth factors or drugs) at the surface of the targeted cells [73, 74]. Biological nanofactories are bio-inspired in that the mechanism for synthesis and delivery of the molecule-of-interest is usually a natural biological synthesis pathway taken and reconstructed *in vitro*. Biological nanofactories comprise multiple functional modules and in their most basic form consist of two modules: a targeting module and a synthesis module. In this work, we demonstrate antibody nanofactories, bi-modular biological nanofactories, for the synthesis and delivery of the universal bacterial signaling molecule autoinducer-2 (AI-2).

Quorum sensing (QS) is a phenomenon by which bacteria exchange small chemical signals known as autoinducers and co-ordinate their activities in a population density dependent manner [44, 132, 133]. A wide range of bacterial phenomena such as bioluminescence [56, 57], biofilm formation [58, 59], virulence [46, 60], sporulation [61], swarming motility [62] etc are in part QS regulated. QS has been shown to play a role in both intra-species and inter-species bacterial communication [44, 45]. Emerging research also implicates QS a means for bacteria to interact directly with eukaryotes via their autoinducers [44]. Of the various classes of signaling autoinducers, AI-2 is particularly interesting as the AI-2 synthase has been found in over 70 bacterial species. Further, bacteria that do not possess their own AI-2 synthesis machinery have been observed to respond to AI-2 [70, 134]. Hence AI-2 has been referred to as the 'universal' bacterial signaling molecule [71]. While the mechanism for AI-2 synthesis, secretion, sensing and uptake has been described in some bacteria, little is known about the exact role of this

elaborate signaling mechanism. One step toward understanding this is to create a method to selectively deliver AI-2 to targeted bacteria and observe the effect of the same on their response (phenotype).

In this work, we create a method to selectively deliver AI-2 to targeted bacteria using antibody nanofactories (Figure 4-1a). An antibody nanofactory consists of a bacterium targeting module (an antibody) and a synthesis module (fusion protein His-Protein G-LuxS-Pfs-Tyr, HGLPT) that self assemble (Figure 4-1b). Fusion protein HGLPT expresses Protein G, the AI-2 biosynthesis enzymes S-adenosylhomocysteine nucleosidase, Pfs and S-riboysl homocysteinase, LuxS and a N-terminal hexahistidine tag and a C-terminal pentatyrosine tag (providing flexibility for covalent conjugation of the fusion protein to amine-groups). Protein G is derived from group C and G *Streptococcus* strains and binds to the Fc region of numerous immunogloblulins [135, 136]. Protein G in HGLPT facilitates binding of HGLPT to the Fc region of the targeting antibody. Enzymes Pfs and LuxS are derived from *Escherichia coli* where they are part of the activated methyl cycle and convert toxic metabolite S-adenosylhomocysteine (SAH) to 4,5-dihydroxy-2,3-pentanedione (DPD) which spontaneously converts to AI-2 [44, 66].

When HGLPT and the antibody are mixed in solution, HGLPT binds to the Fc region of the targeting antibody. The resulting self-assembled macromolecule consisting of proteins is called an antibody nanofactory and contains both modules: antibody and HGLPT. The antibody nanofactories (Ab-NF) are added to targeted cells and they bind to the targeted cell surface via the antibody. Upon addition of the substrate SAH, Ab-NF synthesizes AI-2 at the target cell surface. This locally synthesized AI-2 is sensed by the cell and taken up and produces an AI-2 dependent response which is measured.

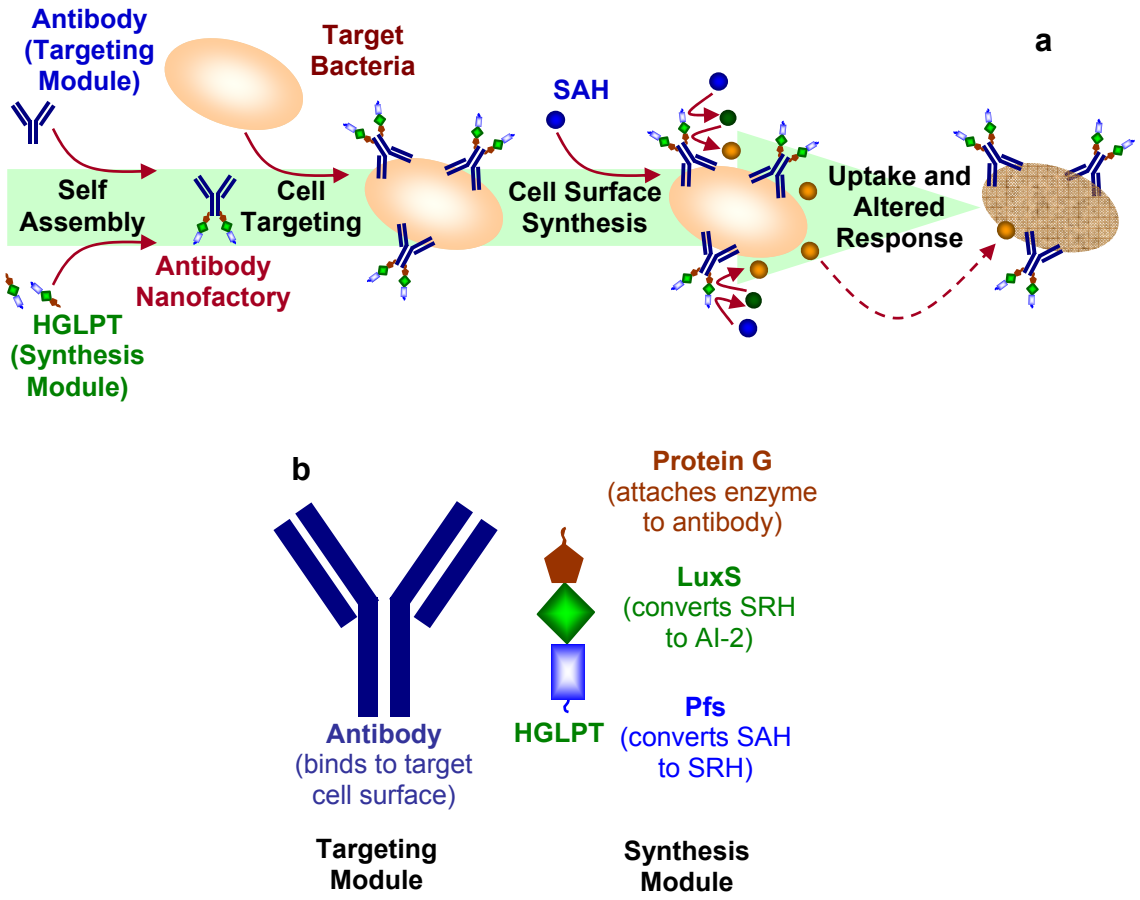

Figure 4-1. Scheme for the localized synthesis and delivery of autoinducer-2 to targeted bacteria using an antibody nanofactory (Ab-NF). a. Self assembly of Ab-NF, which consists of the antibody and fusion protein HGLPT and targeting of bacteria using Ab-NF. Addition of metabolite SAH results in cell surface synthesis and delivery of AI-2 by the Ab-NF. The cells uptake the localized AI-2 and produce an AI-2 dependent response. b. Components of an Ab-NF; antibody for targeting and fusion enzyme HGLPT that contains Protein G for attaching to the antibody and *E. coli* AI-2 synthesis enzymes Pfs and LuxS.

In this study, we demonstrate construction, expression and purification of the fusion protein HGLPT. Subsequently, we prepare Ab-NF and compare the activities of the nanofactory to HGLPT over a range of synthesis conditions. The ability of Ab-NF to bind the target cell is investigated using microscopy. Ab-NF is then added to cultures of *E. coli*, and the effect of localized synthesis and delivery on cellular response is measured (AI-2 dependent β-galactosidase production). Finally Ab-NF, which contains *E. coli* Pfs and LuxS, is added to cultures of *S. typhimurium*. The effect of this *E. coli* Ab-NF on AI-2 specific *S. typhimurium* response is measured (once again, AI-2 dependent β-galactosidase production).

The emergence of bacterial strains that are resistant to antibiotics, such as methicillin resistant *Staphylococcus aureus* [137, 138] has necessitated alternative approaches to combating bacterial resistance. While AI-2 has been found to increase QS response in gut bacteria such as *E. coli* and *S. typhimurium* [139, 140], it has also been found to decrease or delay QS response in pathogenic bacteria such as *Vibrio cholerae* [46, 141] and *Bacillus cereus* [122, 142]. Quorum sensing inhibition based on selective delivery of AI-2 to bacteria to terminate its QS response holds promise for the development of the next generation of antimicrobials. Such methods are also believed to apply less selective pressure on the organisms to develop resistance as they do not target processes vital to the organism's viability [71].

4.3 Materials and Methods

Chemicals

Isopropyl β-D-thiogalactopyranoside (IPTG), phosphate buffered saline tablets (10 mM phosphate buffer, 2.7 mM KCl and 137 mM NaCl, pH 7.4), S-(5'-deoxyadenosin-5')-L-homocysteine (SAH), chloroform, sodium dodecyl sulfate salt (SDS, >98.5 %), o-nitrophenyl-β-D-galactopyranoside (ONPG), 2-mercaptoethanol, imidazole, albumin from bovine serum (BSA) and 5,5'-Dithiobis (2-nitrobenzoic acid) (DTNB) were purchased from Sigma Aldrich. Ampicillin sodium salt, kanamycin, Tris, sodium carbonate (Na_2CO_3), dibasic sodium phosphate ($Na_2HPO_4.7H_2O$), monobasic sodium phosphate ($NaH_2PO_4.H_2O$), potassium chloride (KCl), magnesium sulfate ($MgSO_4.7H_2O$) and sodium acetate trihydrate ($CH_3COONa.3H_2O$) were purchased from Fisher Scientific. Texas Red-X succinimidyl esters, mixed isomers (excitation wavelength peak 595 nm and emission wavelength peak 615 nm) and Fluoreporter FITC (excitation wavelength peak 494 nm and emission wavelength peak 518 nm) protein labeling kit were purchased from Invitrogen.

Antibodies

Polyclonal rabbit anti *Escherichia coli* was purchased from AbD Serotec and polyclonal rabbit anti *Salmonella typhimurium* was purchased from Abcam.

Plasmid pHGLPT construction

Plasmid pTrcHis-G-LuxS-Pfs-Tyr (pHGLPT) expresses HGLPT, the fusion protein containing the AI-2 synthesis enzymes Pfs and LuxS (from *E. coli*) and Protein G (from

Streptococcus). To construct pHGLPT, the forward and reverse oligonucleotide primers listed in table 4-1 were used to amplify the Protein G gene (329 bp) from plasmid pET-E73-G3 [143]. The PCR reactions were carried out using AccuPrime Taq High Fidelity polymerase (Invitrogen). The 329 bp fragment containing Protein G was isolated and purified using the QIAquick gel extraction kit (Qiagen). The PCR fragment was digested using the restriction endonucleases, *Nco*I and *Nhe*I (New England Biolab, NEB). The purified fragment was inserted into the destination vector pHLPT [144], previously cut using *NcoI* and *Nhe*I, and ligated using the Quick ligation kit (NEB) generating the final plasmid pHGLPT. The plasmid integrity was verified by sequencing at the DNA core facility at the Center for Biosystems Research, University of Maryland Biotechnology Institute. Once the correct sequence was verified, pHGLPT transformed into the expression strain *E. coli* BL21 luxS$^-$ (a *luxS* knockout, table 4-1).

Bacterial strains and growth conditions

Table 4-1 lists the bacterial strains and plasmids used in this study. *E. coli* W3110, *E. coli* BL21 luxS- carrying plasmid pHGLPT, *E. coli* LW7 carrying plasmid pLW11 and *S. typhimurium* MET715 were all grown in Luria-Bertani (LB) medium at 37 ^oC with vigorous shaking (250 rpm) unless otherwise noted. The Luria-Bertani (LB) medium used for bacterial growth contains 5 g/L of yeast extract (Sigma), 10 g/L of Bacto tryptone (Difco) and 10 g/L NaCl (J. T. Baker). Antibiotic concentrations used for the different strains, unless otherwise noted, were 50 µg/mL ampicillin for *E. coli* BL21 luxS-, 100 µg/mL ampicillin for *E. coli* LW7 and 100 µg/mL kanamycin for *S. typhimurium* MET715.

Table 4-1. List of bacterial strains, plasmids and primers used in this study.

Strain, plasmid or primer	Relevant genotype and/or property	Reference
Escherichia coli strains		
W3110	Wild type	Laboratory stock
BL21 luxS$^-$	*F'* ompT hsdS_B *($r_B^-m_B^-$) gal dcm* Δ*luxS* :: Kan	Laboratory Stock
LW7	W3110 Δ*lacU160-tna2* Δ*luxS* :: Kan	Wang *et al.*[66]
Salmonella typhimurium strains		
MET715	*rpsl putRA ::* Kan-*lsr-lacZYA luxS* :: T-POP	Taga *et al.*[67]
Plasmids		
pLW11	*galK'-lacZYA* transcriptional fusion vector, containing *lsrACDBFG* promoter region, Amp^r	Wang *et al.*[66]
pET-E72-G32	pET derivative, expressing fusion protein E72G3	Tanaka *et al.*[143]
pHGLPT	pTrcHisC derivative, *Escherichia coli* W3110 *pfs*$^+$, *luxS*$^+$, *Streptococcus* Protein G$^+$, Amp^r	This study
Oligonucleotide primers		
Name	Sequence	Relevant property
C1 Seq 5'	5'- GGG CAC TCG ACC GGA A-3'	Upstream primer for cloning Protein G from pET-E72-G3, contains *Nco*I
C4-3'	5'- CCA CCA GTC ATG CTA GCC GGG TCC ATT TCC GT -3'	Downstream primer for cloning Protein G from pET-E72-G3, contains *Nhe*I

Expression, purification and analysis of HGLPT

E. coli BL21 luxS$^-$ pHGLPT was cultured at 37 ^oC and 250 rpm in LB medium supplemented with ampicillin at a concentration of 50 µg/mL. When the optical density (OD_{600}) of the cell culture was between 0.4 - 0.6, IPTG was added to induce over expression of HGLPT (final IPTG concentration used was 1 mM). After a 6 hr induction period at the same culture conditions, the cells were harvested by centrifugation at 12,000 xg for 15 minutes at 4 ^oC. The cells were stored at -20 ^oC or directly resuspended in PBS + 10 mM imidazole. The resuspended cells were lysed by sonication using Sonic Dismembrator 550 (Fisher Scientific). After sonication, the soluble cell extract was collected by centrifugation at 14,000 xg for 15 minutes at 4 ^oC, filtered using a 0.22 µm polyether sulfone, low protein binding filter (Millipore) and then loaded on a pre-equilibrated immobilized metal-ion affinity chromatography (IMAC) column (HiTrap Chelating HP, GE Healthcare Life Sciences). After washing with varying amounts of phosphate buffer, sodium chloride and imidazole (Wash 1: 20 mM PO_4^{3-}, 250 mM NaCl and 10 mM imidazole; Wash 2: 20 mM PO_4^{3-}, 250 mM NaCl and 50 mM imidazole), HGLPT was eluted with 20 mM PO_4^{3-}, 250 mM NaCl and 350 mM imidazole. The protein was desalted using an Amicon Ultra-15 centrifugal unit (NMWL 10,000, Millipore) and resuspended in 10 mM PO_4^{3-} buffer pH 6 and stored at -80 ^oC until use.

The sizing and analysis of HGLPT was performed using a LabChip® Protein 200 plus kit (Agilent Technologies). Briefly 1 µg each of purified HGLPT (molecular weight 57039 Daltons), the constituent enzymes Pfs (molecular weight 29716 Daltons) and LuxS (molecular weight 24778 Daltons), from lab stock, were loaded per well in the chip and

the assay was conducted according to the manufacturer's specifications (website: http://www.chem.agilent.com).

Antibody nanofactory (Ab-NF) preparation

Ab-NF was prepared by incubating HGLPT with an excess of the targeting antibody in phosphate buffer (molar ratio of HGLPT : antibody used was 1 : 4) to ensure that most HGLPT binds to the targeting antibody. The samples were incubated at room temperature for atleast one hour prior to use.

***In vitro* AI-2 synthesis and concentration estimation**

In vitro AI-2 was synthesized by incubating either HGLPT or Ab-NF (anti *E. coli* antibody) with the substrate SAH in phosphate buffer. The reactions were carried out using varying concentrations of HGLPT (0.1 μM, 0.2 μM or 0.5 μM), Ab-NF (0.1 μM HGLPT + 0.4 μM Ab, 0.2 μM HGLPT + 0.8 μM Ab or 0.5 μM HGLPT + 2 μM Ab) and SAH (100 or 200 μM) for either 1 hour or 2 hours at 37 ^{o}C. The effect of BSA on AI-2 production was investigated by the addition of an excess of BSA (8 μM). After reaction, the concentration of AI-2 generated was estimated by determining the concentration of homocysteine produced during the reaction. Homocysteine is a byproduct of the AI-2 synthesis reaction produced in stoichiometrically equal amounts to AI-2 . To estimate the concentration of homocysteine, the products of the AI-2 synthesis reaction were added to DTNB reagent (100 μM DTNB, 2.5 mM sodium acetate in 0.1 M Tris buffer, pH 8). The reaction was carried out at room temperature for at least 15 minutes. After the reaction, the absorbance at 412 nm (OD_{412}) was measured and the concentration of homocysteine

calculated using molar extinction coefficient (13600 M^{-1} cm^{-1}) of the reaction product 5-thio-2-nitrobenzoic acid (TNB) [126].

Fluorescence microscopy

HGLPT was labeled with Texas Red-X and the antibody rabbit anti *Escherichia coli* was labeled with FITC as per the manufacturer's specification (Invitrogen). Ab-NF using the fluorescently labeled HGLPT and antibody were prepared as described earlier. *E. coli* W3110 was grown under the culture conditions described previously (until an OD_{600} of 0.4). The cells were harvested and suspension of the cells in phosphate buffer was prepared. Ab-NF, containing 0.1 μM HGLPT, 0.4 μM anti *E. coli* and 8 μM BSA were added to the cells at room temperature for 30 minutes (protected from light). To separate unbound Ab-NF from the cells, the samples were spun in Centrisart I ultrafiltraton units (MWCO 300,000; Sartorius) which retains the cells and allows the Ab-NF to flow through. The retained cells were resuspended in phosphate buffer and observed under a fluorescence microscope using a 40X objective (Olympus BX60). As controls, cells were treated either with anti *E. coli* (+ BSA) only, HGLPT (+ BSA) only or left untreated. Images of the samples were taken using a Canon EOS D60 digital camera, a photo eyepiece 3.3X with either a Endow GFP longpass emission filter set (Chroma) for green fluorescence or a DsRed2 filter set (Chroma) for red fluorescence for an exposure time of 3 seconds.

Localized synthesis and delivery of AI-2 using antibody nanofactories

The target cells (*E. coli* LW7 pLW11 or *S. typhimurium* MET715) were pre-cultured overnight separately in LB medium at 37 ^{o}C and 250 rpm supplemented with the appropriate antibiotic (100 μg/mL ampicillin for *E. coli* LW7 and 100 μg/mL kanamycin for *S. typhimurium* MET715). The overnight cultures were diluted into fresh LB medium supplemented with antibiotic (60 μg/mL ampicillin for *E. coli* LW7 and 100 μg/mL kanamycin for *S. typhimurium* MET715) and the samples were grown at 30 ^{o}C for 4 hours at 250 rpm. After 4 hours, the cells were collected by centrifuging at 10,000 xg for 10 minutes and resuspended in 10mM phosphate buffer, pH 6. The cells were contacted with either Ab-NF (0.1 μM HGLPT, 0.4 μM anti *E. coli* for *E. coli* LW7 samples or 0.4 μM anti *S. typhimurium* for *S. typhimurium* samples and 8 μM BSA), HGLPT (0.1 μM HGLPT and 8 μM BSA) or left untreated for 30 minutes at room temperature. SAH (0.2 μM) was added to each sample and the samples were incubated at 37 ^{o}C for 2 hours to allow localized synthesis and delivery of *in vitro* AI-2 to the cells. After the stated time, the samples were centrifuged for 5 min at 14,000 rpm. The cell free supernatants were analyzed for their AI-2 concentration as described earlier and the cell pellets were analyzed to measure the AI-2 based response (β-galactosidase production). The AI-2 dependent specific β-galactosidase activity was measured as described in the literature [66].

4.4 Results

Expression, purification and analysis of HGLPT

Plasmid pHGLPT (Figure 4-2a) overexpresses HGLPT upon induction of the production strain *E. coli* BL21 luxS^{-}. HGLPT contains Protein G derived from *Streptococcus* and the AI-2 synthesis enzymes Pfs and LuxS from *E. coli*. The overexpressed protein is

purified and is analyzed for its size using LabChip®. Figure 4-2b shows the results of the protein assay run using 1 µg of purified HGLPT, Pfs and LuxS run separately. The gel shows bands at molecular weights of the enzyme that are in agreement with the molecular weights of the same theoretically predicted based on the amino acid sequences. HGLPT shows a band at 59.4 kDa (predicted 57.0 kDa), Pfs shows a band at 28.7 kDa (predicted 29.7 kDa) and LuxS shows a band at 23.1 kDa (predicted 24.8 kDa)

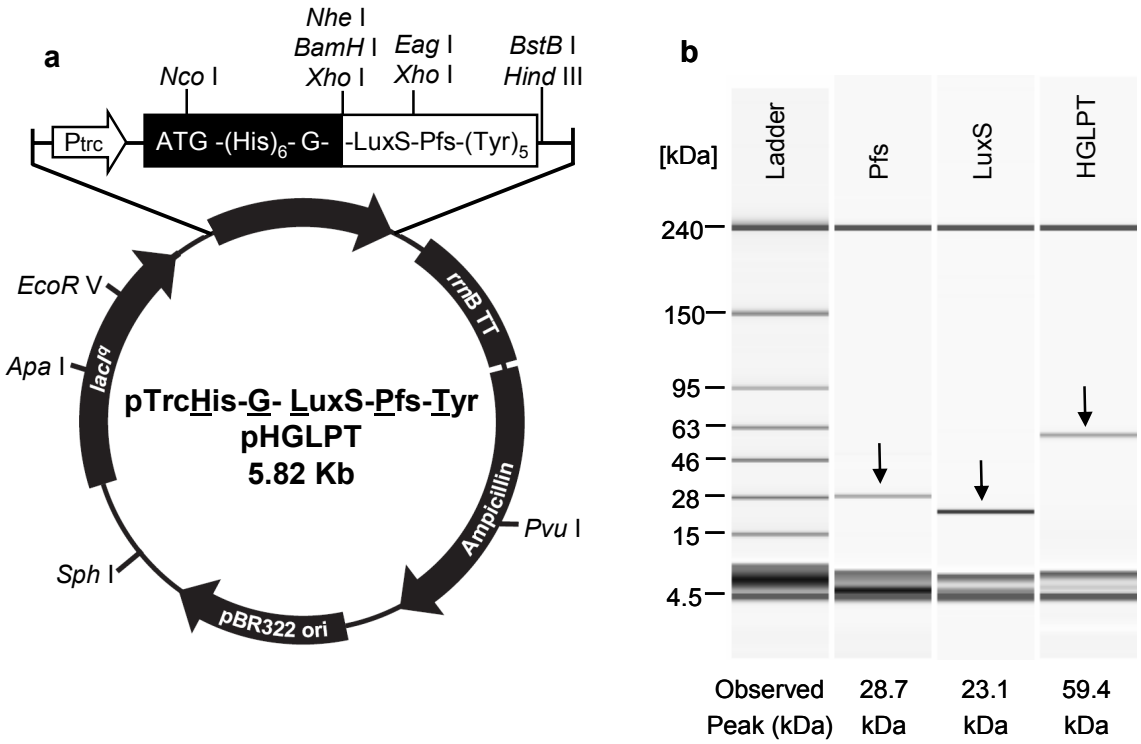

Figure 4-2. Construction of plasmid pHGLPT, expression and purification of HGLPT. a. Map of plasmid pHGLPT for expressing fusion protein HGLPT. b. Analysis of HGLPT using LabChip®. HGLPT predicted molecular weight based on primary amino acid sequence is 57039 Da, that of Pfs is 29716 Da and that of LuxS is 24778 Da.

Comparing activities of Ab-NF and HGLPT

Ab-NF of varying HGLPT concentrations (0.1, 0.2 and 0.5 μM, HGLPT:Ab molar ratio of 1:4) are prepared and the activities of Ab-NF and HGLPT are compared over a variety of reaction conditions. Figure 4-3a shows that as the concentration of HGLPT (from 0.1 – 0.5 μM) is increased, both in Ab-NF and in HGLPT samples, AI-2 production increases. Figure 4-3a also shows that AI-2 production increases with increased reaction times (from 1 hour to 2 hours). AI-2 production is higher in the HGLPT samples than in the Ab-NF samples over all investigated concentrations (0.1, 0.2 and 0.5 μM HGLPT) and reaction times (1 hour and 2 hours) in the absence of BSA, which is commonly added to mixtures of proteins to block non-specific binding of proteins. Upon addition of BSA (8 μM), AI-2 production in Ab-NF is found to increase and is higher than that of HGLPT for the concentration (0.1 μM HGLPT) and times (1 hour and 2 hours) investigated (Figure 4-3b). No significant effect of BSA on the AI-2 production in HGLPT samples is observed.

Cell targeting with Ab-NF

Ab-NF containing 0.1 μM HGLPT, 0.4 μM anti *E. coli* and 8 μM BSA is prepared using the Texas Red-X labeled HGLPT and FITC labeled anti *E. coli*. The fluorescently labeled Ab-NF is added to a suspension of wild type *E. coli* (W3110) cells in phosphate buffer for 30 minutes. The target cells are separated from the unbound Ab-NF and viewed under a fluorescence microscope. Figure 4-4 shows photographs of wild type *E. coli* (no color) contacted with either Ab-NF (green antibody, red HGLPT), Ab only (green), HGLPT (red) or left untreated (no color).

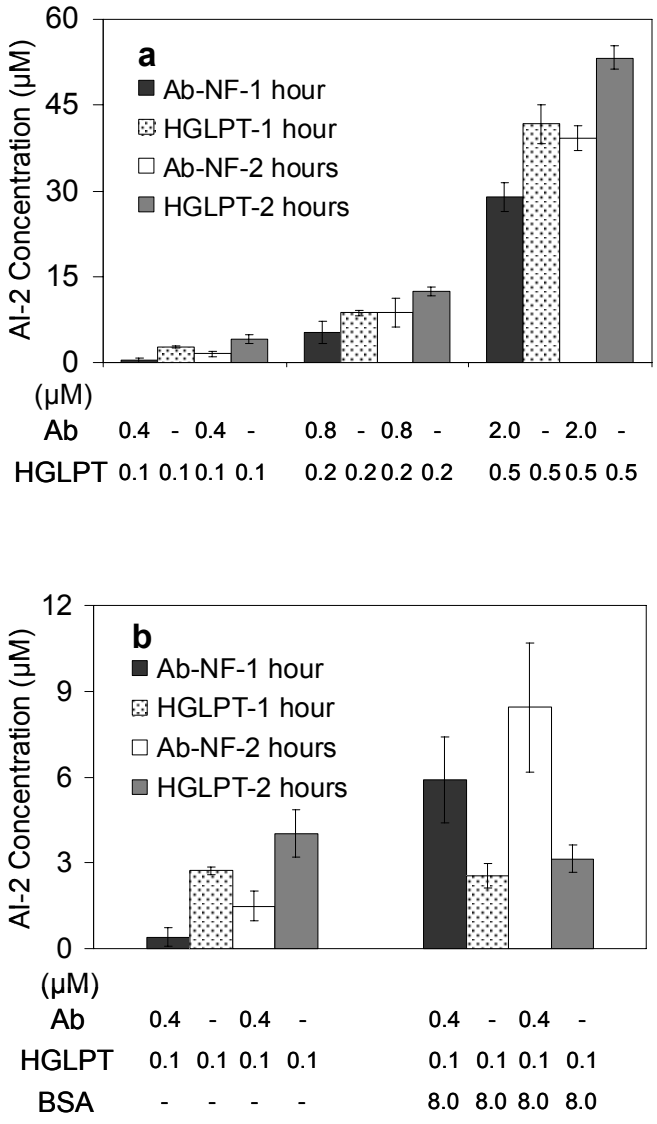

Figure 4-3. Comparing the AI-2 activity of HGLPT and Ab-NF containing equimolar amounts of HGLPT as function of a. concentration and synthesis time and b. BSA addition.

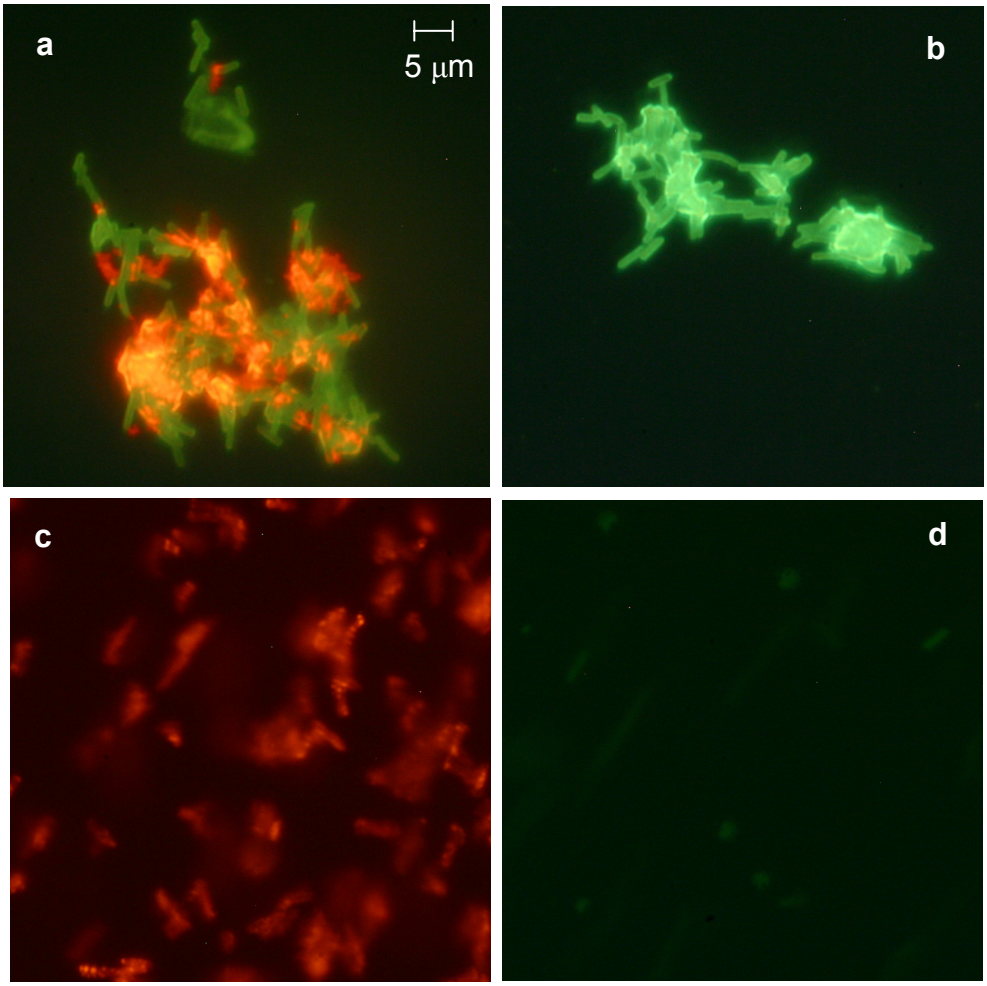

Figure 4-4. Fluorescence microscopy images of *E. coli* wild type cells targeted by Ab-NF, Ab only, HGLPT only or left untreated. a. Image of *E. coli* cells targeted by Ab-NF shows co-localization of both green fluorescence (FITC labeled anti *E. coli*) and red fluorescence (Texas Red-X labeled HGLPT) when viewed using the GFP longpass emission filter set. b. Image of *E. coli* cells targeted by Ab shows only green fluorescence using the GFP longpass emission filter set. c. Image of *E. coli* cells targeted by HGLPT shows red fluorescence under the DsRed2 filter set (very little green fluorescence observed). d. Image of *E. coli* cells left untreated shows low background levels of green fluorescence under the GFP filter set.

Cells contacted with Ab-NF show both green and red fluorescence (co-localization of the both green and red within the same region) when viewed using the GFP filter set (Figure 4-4a). Cells contacted with Ab only shows only green fluorescence (Figure 4-4b) while cells contacted with HGLPT showed very little fluorescence when viewed using the GFP filter set (data not shown) and red fluorescence when viewed under the DsRed filter set (Figure 4-4c). Untreated cells showed little to no fluorescence when view both using the GFP filter (Figure 4-4d) and DsRed filter (data not shown).

Effect of Ab-NF based localized synthesis and delivery of AI-2 on target cell response

The effect of Ab-NF based AI-2 synthesis and delivery is investigated using reporter strains *E. coli* LW7 pLW11 and *S. typhimurium* MET715. *E. coli* is a *luxS* and *lac* double mutant and hence cannot produce its own AI-2 and β-galactosidase (the product of the *lac* gene). *E. coli* LW7 pLW11 can produce β-galactosidase in response to added AI-2. *S. typhimurium* MET715 is a *luxS* mutant and hence cannot produce its own AI-2 (*S. typhimurium* does not produce β-galactosidase). *S. typhimurium* MET715 can also produce AI-2 dependent β-galactosidase.

E. coli LW7 pLW11 was grown and a suspension of the cells in buffer prepared as described in the methods section. Ab-NF, containing 0.1 μM HGLPT, 0.4 μM anti *E. coli* and 8 μM BSA, is added to the cells and allowed to contact for 30 minutes. Upon addition of SAH (0.2 mM), AI-2 is synthesized by Ab-NF at the *E. coli* cell surface. The cells take up the AI-2 and produce AI-2 dependent β-galactosidase. Figure 4-5a shows that the AI-2 delivered to the cells is higher in the cells targeted by Ab-NF (13.8 μM)

than in those targeted by HGLPT only (5 μM) or left untreated (3 μM). The resulting cellular response (specific β-galactosidase activity, Figure 4-5b) is significantly higher in Ab-NF targeted cells (180.8 Miller units) as compared to HGLPT targeted cells (25.3 Miller units) and untreated cells (22.1 Miller units).

S. typhimurium MET715 was grown and a suspension of the cells in buffer prepared as described in the methods section. Ab-NF, containing 0.1 μM HGLPT, 0.4 μM anti *S. typhimurium* and 8 μM BSA, is added to the cells and allowed to contact for 30 minutes. Here HGLPT, which contains the *E. coli* AI-2 synthesis enzymes, is added to *S. typhimurium* cells. When SAH (0.2 mM) is added, AI-2 is synthesized by Ab-NF at the *S. typhimurium* cell surface. The cells take up the AI-2 and produce AI-2 dependent β-galactosidase. Figure 4-6a shows that the AI-2 delivered to *S. typhimurium* is higher in the cells targeted by the *E. coli* Ab-NF (21 μM) than in those targeted by HGLPT only (7.9 μM) or left untreated (4.7 μM). The resulting cellular response (specific β-galactosidase activity, Figure 4-6b) is significantly higher in *S. typhimurium* cells targeted by *E. coli* antibody nanofactory (2042.5 Miller units) as compared to HGLPT targeted cells (663.7 Miller units) and untreated cells (403.7 Miller units).

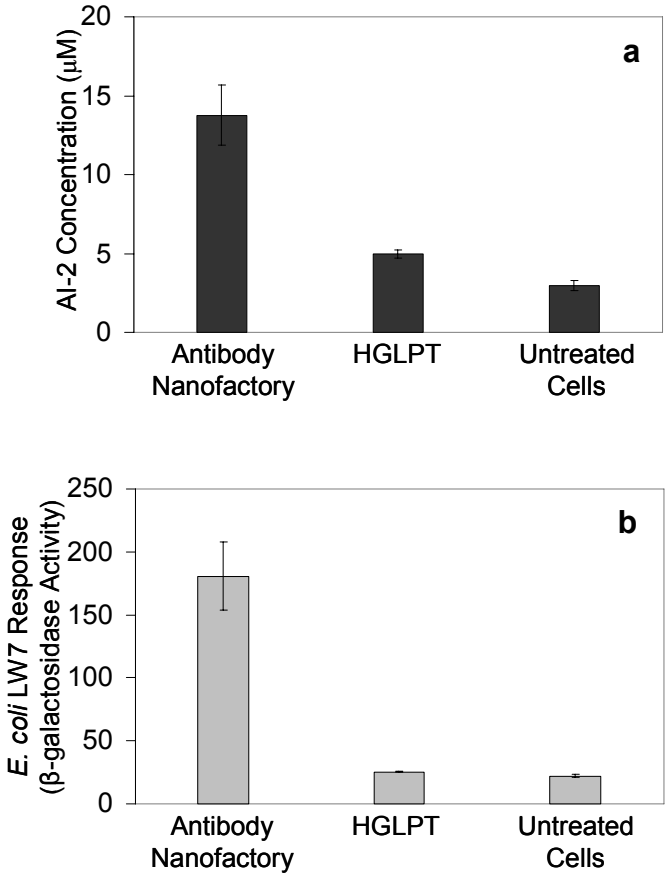

Figure 4-5. Effect of Ab-NF based localized synthesis and delivery of AI-2 on AI-2 specific β-galactosidase production in targeted *E. coli* LW7 pLW11 cells. a. AI-2 concentrations delivered to cells targeted by Ab-NF, HGLPT and untreated cells. b. AI-2 dependent specific β-galactosidase activity in cells targeted by Ab-NF, HGLPT and untreated cells.

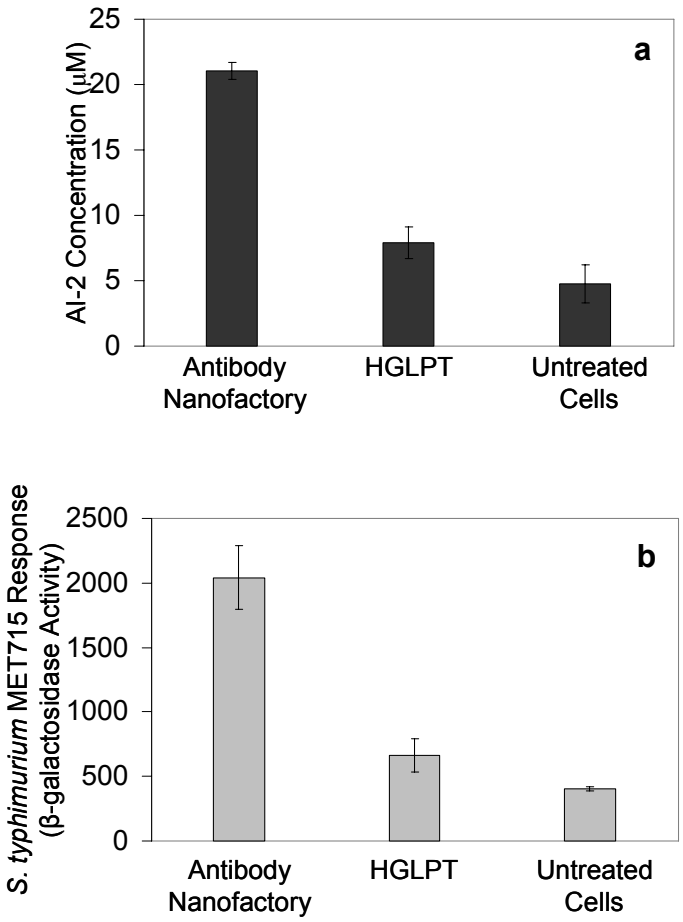

Figure 4-6. Effect of Ab-NF based localized synthesis and delivery of AI-2 on AI-2 specific β-galactosidase production in targeted *S. typhimurium* MET715 cells. a. AI-2 concentrations delivered to cells targeted by Ab-NF, HGLPT and untreated cells. b. AI-2 dependent specific β-galactosidase activity in cells targeted by Ab-NF, HGLPT and untreated cells.

4.5 Discussion

In this work, we have presented the concept of an antibody nanofactory for the localized synthesis and delivery of AI-2 to bacterial cells (Figure 4-1a). The nanofactories combine the specific targeting abilities of an antibody with the synthesis abilities of fusion protein HGLPT (Figure 4-1b). To express HGLPT, plasmid pHGLPT was constructed (Figure 4-2a). The purified protein was observed to have a molecular weight in agreement with that theoretically predicted by the primary amino acid sequence (Figure 4-2b).

Antibody nanofactories (Ab-NF) were formed by the self assembly of the targeting antibody (anti *E. coli* or anti *S. typhimurium*) and HGLPT via Protein G. The activity of Ab-NF was compared to that of HGLPT over a range of synthesis conditions. For syntheses carried out in buffer, in the absence of BSA, HGLPT was observed to produce more AI-2 than Ab-NF (Figure 4-3a). The addition of blocking agent BSA causes the activity of the Ab-NF to increase while that of HGLPT was not significantly altered (Figure 4-3b). We believe that the addition of BSA stabilizes the Ab-NF complex and causes the AI-2 productivity of the same to increase. We did not investigate the mechanism for Ab-NF stabilization in the presence of BSA in this work. Ab-NF was found to selectively target *E. coli* wild type cells (Figure 4-4a). Fluorescence microscopy showed co-localization of green fluorescence (FITC labeled anti *E. coli*) and red fluorescence (Texas Red-X labeled HGLPT) viewed under a GFP longpass emission filter. Similar co-localization was not observed in cells targeted with anti *E. coli* (Figure 4-4b), HGLPT (Figure 4-4c) and untreated (Figure 4-4d).

Targeting *E. coli* LW7 cells with Ab-NF resulted in increased AI-2 synthesis (13.8 μM, Figure 4-5a) and AI-2 specific β-galactosidase production (180.8 Miller units, Figure 4-5b) as compared to cells targeted with HGLPT (5 μM, 25.3 Miller units) and untreated cells (3 μM AI-2, 22.1 Miller units). The results indicate that the addition of antibody nanofactories significantly alter the natural progression of QS signaling in *E. coli*. Targeting *S. typhimurium* MET715 with Ab-NF also resulted in increased AI-2 production (21 μM, Figure 4-6a) and AI-2 specific β-galactosidase production (2042.5 Miller units, Figure 4-6b) as compared to cells targeted with HGLPT (7.9 μM AI-2, 663.7 Miller units) and untreated cells (4.7 μM AI-2, 403.7 Miller units). The results indicate that *S. typhimurium* responds to AI-2 synthesized by *E. coli* enzymes in an Ab-NF and alters the natural progression of its AI-2 based QS response.

We believe our work is significant for the following reasons. First, we have presented antibody nanofactories as a new technique for selectively delivering AI-2 to targeted bacteria. Ab-NF is bio-inspired, self-assembled and bi-modular and is capable of altering the natural QS response in bacteria. Selective delivery of AI-2 as a mechanism for tuning (turning up or down) bacterial response is particularly important in devising the next generation of antimicrobials based on altering QS based response. Finally, we believe that this technique of using antibody directed natural biosynthetic pathways in an antibody nanofactory can be used in other applications where the selective delivery of the product of the biosynthetic pathway 'fine-tunes' the response of the cells or tissue targeted.

4.6 Acknowledgment

The authors would like to thank Dr. Bonnie L. Bassler (Princeton University) for providing the *S. typhimurium* MET715 strain and Dr. Chen-Yu Tsao and Li Yang (University of Maryland) for the *E. coli* BL21 luxS$^-$ strain.

Chapter 5: Spatially-Selective Assembly and Manipulation of Quorum Sensing Bacteria in a BioMEMS Device using Antibody Nanofactories

5.1 Abstract

Biological microelectromechanical systems (bioMEMS) provide a unique platform to study and manipulate biological matter under the controlled conditions of MEMS devices. In this work, a method to assemble and manipulate quorum sensing (QS) bacteria in a spatially-selective manner in a bioMEMS device is demonstrated. QS is a phenomenon of bacterial communication via signaling autoinducers and has been shown to play a role in diverse, and sometimes undesirable, multicellular bacterial phenomena. The assembly technique involves construction of microchannels in a bioMEMS device consisting of patterned gold electrodes. The amine-group containing biopolymer chitosan is electrodeposited onto the negatively biased electrode. Antibody nanofactories comprising a fusion protein His-Protein G_3-LuxS-Pfs-Tyr (HG_3LPT) and a cell targeting antibody assembled together, are covalently conjugated onto the electrodeposited chitosan by activation of the C-terminal tyrosine tag (Tyr) of HG_3LPT using the enzyme tyrosinase. The assembled antibody nanofactories spatially capture targeted cells introduced into the microchannel. As proof-of-concept of manipulation of the QS response of bacteria captured spatially in a bioMEMS device, the nanofactories are demonstrated to locally synthesize and deliver the 'universal' bacterial signaling molecule autoinducer-2 to the targeted cells, thereby altering their native response. Prospects for uncovering the underlying mechanisms of QS signaling using this spatially-

selective method of capture and localized synthesis and delivery of signaling molecules via antibody nanofactories are envisioned.

5.2 Introduction

Biological microelectromechanical systems (bioMEMS) are a subset of microelectromechanical systems (MEMS) that involve the integration of biological matter or biological systems into MEMS [145-150]. In addition to providing the benefits of MEMS with respect to small device sizes, low reagent volumes, shorter reaction times and possibility for parallel processing, bioMEMS also provide a useful platform to study and manipulate the complexity of biological systems in the controlled environments of MEMS devices [146, 151-156].

The study of bacterial communication is becoming increasingly important as many bacterial phenomena such as biofilm formation, pathogenicity, bioluminescence etc are a consequence of co-ordinated bacterial response [46, 56-60]. Bacteria communicate with each other through the production, secretion, sensing and uptake of small signaling molecules called autoinducers in a process known as quorum sensing (QS) [43, 44, 132, 133]. QS has been implicated both in intra- as well as inter-species communication in bacteria [44, 45]. Understanding the specific effects of these signaling autoinducers on co-ordinated bacterial response holds the key to elucidating the fundamental mechanisms at play in the diverse and seemingly unrelated bacterial phenomena. BioMEMS provide unique opportunities to understand QS within their controlled environments.

In this work, a technique to spatially capture and manipulate QS bacteria within a test area of a microchannel in a bioMEMS device is demonstrated. Specifically, the QS

bacterium *Escherichia coli* will be spatially captured in the test area of the device and the response of the captured bacteria will be manipulated via locally synthesizing and delivering the signal molecule autoinducer-2 (AI-2). In *E. coli*, AI-2 is synthesized from its precursor S-adenosylhomocysteine (SAH) via a two step enzymatic reaction involving the enzymes, S-adenosylhomocysteine nucleosidase (Pfs) and S-ribosylhomocysteinase (LuxS) [44, 66]. AI-2 based signaling has been observed in *E. coli* as well as in at least 70 other bacterial species prompting AI-2 to be referred to as the universal bacterial signaling molecule [44, 71].

The technique demonstrated here involves creation of a bioMEMS device and using electrodeposited chitosan and antibody nanofactories to spatially capture and manipulate bacteria in the device (Figure 5-1). The bioMEMS device consists of microchannels (Figure 5-2a); each containing patterned gold electrodes (Figure 5-2b). The electrode that forms the test area of the bioMEMS device is functionalized with electrodeposited chitosan; an amine-group containing biopolymer with pH dependent solubility [157, 158]. When an electric current is imposed between two electrodes in the microchannel, chitosan electrodeposits from solution onto the negatively charged electrode on account of a high pH generated in the vicinity of the negative electrode [91, 92, 159, 160].

The antibody nanofactories are then assembled onto chitosan electrodeposited on the test area (negative electrode). Antibody nanofactories are a subset of biological nanofactories [73, 74, 144], which are comprised of multiple functional modules and manipulate the response of cells they target by locally synthesizing and delivering molecules-of-interest (signal molecules, drugs etc) at the surface of the targeted cells.

Antibody nanofactories presented here are self assembled and bi-modular, i.e. they consist of two functional modules: an AI-2 synthesis module and a bacteria targeting module.

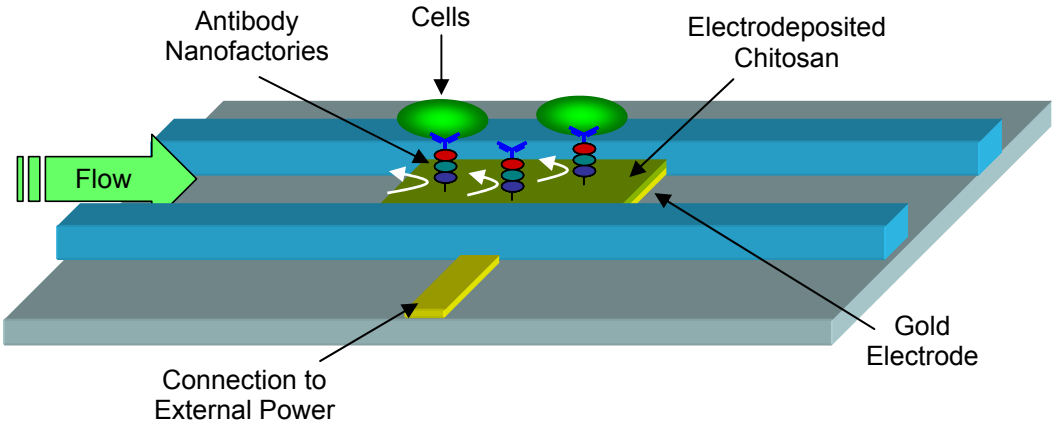

Figure 5-1. Scheme for spatially-selective assembly and manipulation of quorum sensing bacteria in a bioMEMS device using antibody nanofactories. The biopolymer chitosan is electrodeposited onto a patterned gold electrode in the microchannel of the bioMEMS device. Antibody nanofactories are assembled onto the chitosan, they capture targeted cells and alter their response by localized synthesis and delivery of AI-2.

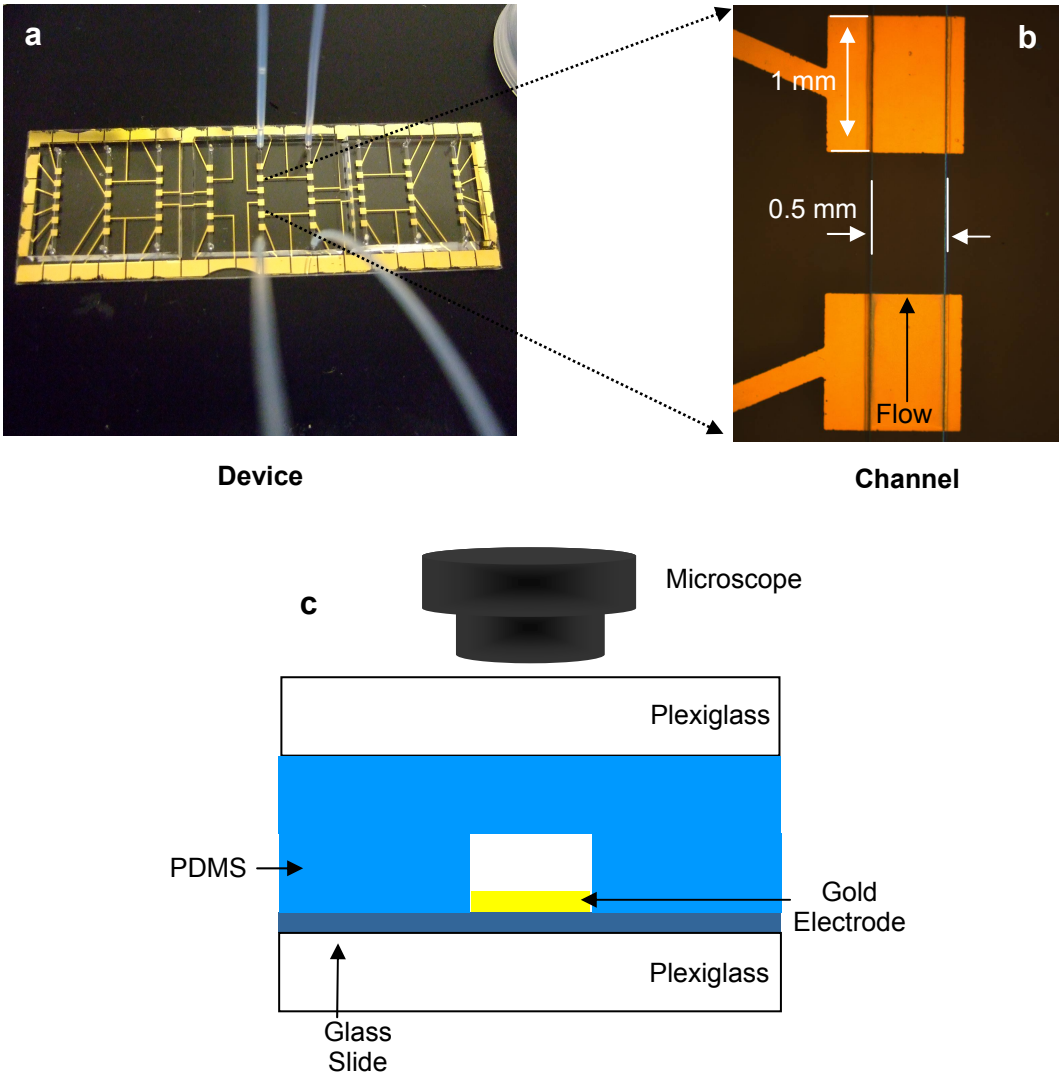

Figure 5-2. Perspectives of the bioMEMS device. a. Photograph of the bioMEMS device consisting of 9 microchannels each containing six patterned gold electrodes. b. Photograph of a microchannel showing the negative electrode (test area) and the positive electrode with dimensions. c. Cross section of the microchannel showing a glass slide containing an overlaid patterned gold electrode, flanked by PDMS sidewalls. These layers are sandwiched between two plexiglass slabs.

Fusion protein His-Protein G_3-LuxS-Pfs-Tyr (HG_3LPT, Figure 5-3a and b) which is the AI-2 synthesis module expresses the AI-2 synthesis enzymes Pfs and LuxS derived from *E. coli* and three Protein G units derived from group C and G *Streptococcus* [135, 136]. The bacteria targeting module is an antibody. Protein G binds to the Fc region of antibodies [135, 136]. Upon mixing of antibodies and HG_3LPT in solution, the antibody nanofactories self assemble when HG_3LPT binds to antibody at its Fc region (Figure 5-3c). The rationale for using 3 Protein G units is that it increases the amount of antibody bound by HG_3LPT [143]. HG_3LPT contains a tyrosine tag that consists of five tyrosine residues at its C-terminus. In the presence of the enzyme tyrosinase, the tyrosine residues are activated and they generate reactive o-quinones that are capable of reacting with available primary amines thus covalently conjugating tyrosines to amines [94, 104, 131].

The specific aims of this work is to create a plasmid (pHG_3LPT) to express fusion protein HG_3LPT, to spatially assemble the antibody nanofactories via tyrosinase on chitosan electrodeposited onto the negative electrode (test area) of the bioMEMS device, to spatially capture *E. coli* in the test area of the device and finally to demonstrate that localized synthesis and delivery of AI-2 to the captured cells can alter their native QS based response.

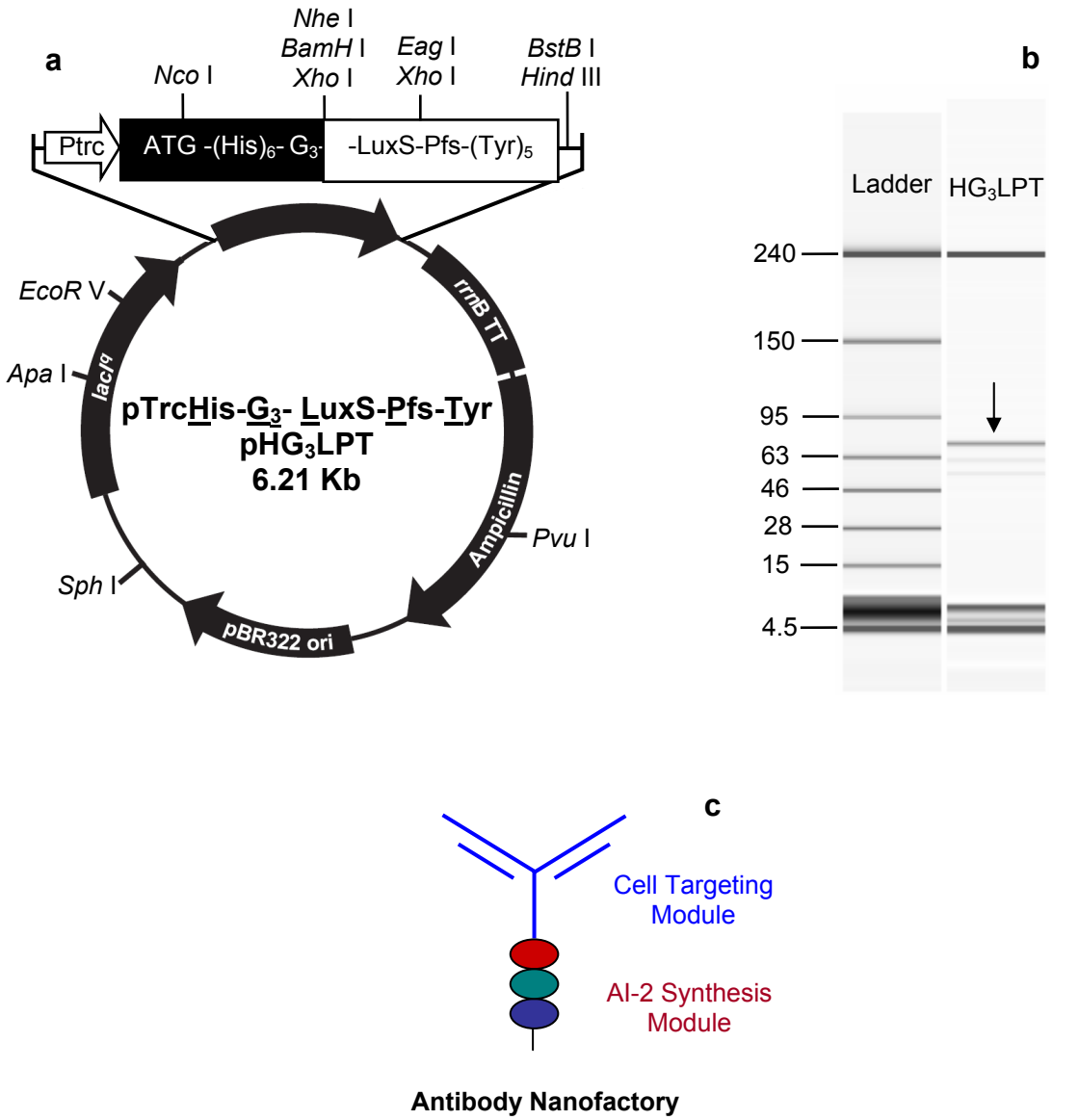

Figure 5-3. Construction of plasmid pHG$_3$LPT expressing fusion protein HG$_3$LPT and components of an antibody nanofactory. a. Plasmid map showing details of plasmid pHG$_3$LPT. b. Analysis of HG$_3$LPT using LabChip®. HG$_3$LPT predicted molecular weight based on primary amino acid sequence is 71463 Da. c. Schematic of an antibody nanofactory comprising a cell targeting module and an AI-2 synthesis module.

5.3 Materials and Methods

Chemicals

Chitosan (medium molecular weight, average molecular weight 300,000 g/mol), tyrosinase (from mushroom), phosphate buffered saline tablets (10 mM phosphate buffer, 2.7 mM KCl and 137 mM NaCl, pH 7.4), albumin from bovine serum (BSA), S-(5'-deoxyadenosin-5')-L-homocysteine (SAH) and 5,5'-Dithiobis (2-nitrobenzoic acid) (DTNB) were purchased from Sigma Aldrich. Ampicillin sodium salt, kanamycin, Tris, dibasic sodium phosphate ($Na_2HPO_4.7H_2O$), monobasic sodium phosphate ($NaH_2PO_4.H_2O$), sodium acetate trihydrate ($CH_3COONa.3H_2O$), sodium hydroxide and hydrochloric acid were purchased from Fisher Scientific. Fluoreporter FITC (excitation wavelength peak 494 nm and emission wavelength peak 518 nm) protein labeling kit was purchased from Invitrogen and non fat dry milk (blotter grade) was purchased from BioRad.

Antibodies

Polyclonal rabbit anti *Escherichia coli* was purchased from AbD Serotec and polyclonal rabbit anti *Salmonella typhimurium* was purchased from Abcam. FITC labeling of anti *Salmonella typhimurium* antibody was performed as per the manufacturer's specification (Invitrogen).

Plasmid pHG$_3$LPT construction

Plasmid pTrcHis-G$_3$-LuxS-Pfs-Tyr (pHG$_3$LPT) expresses HG$_3$LPT, the fusion protein containing the AI-2 synthesis enzymes Pfs and LuxS (from *E. coli*) and three repeats of

Protein G (from *Streptococcus*). To construct pHG$_3$LPT, the forward and reverse oligonucleotide primers listed in table 5-1 were used to amplify the G$_3$ sequence (617 bp) from plasmid pET-E73-G3 [143]. The PCR reactions were carried out using AccuPrime Taq High Fidelity polymerase (Invitrogen). The 617 bp fragment containing G$_3$ was isolated and purified using the QIAquick gel extraction kit (Qiagen) and inserted into pCR 2.1-TOPO (Invitrogen). The intermediate plasmid pCR-G$_3$ (TA) was transformed into the strain *E. coli* TOP10 (Invitrogen). The integrity of the intermediate construct was verified by sequencing the plasmid at the DNA core facility at the Center for Biosystems Research, University of Maryland Biotechnology Institute. The fragment containing G$_3$ was extracted by digesting pCR-G$_3$ (TA) using the restriction endonucleases, *Nco*I and *Nhe*I (New England Biolab, NEB). The gel purified fragment was inserted into the destination vector pHLPT [144], previously cut using *NcoI* and *Nhe*I, and ligated using the Quick ligation kit (NEB) generating the final plasmid pHG$_3$LPT (6.21 kb). The plasmid integrity was verified by sequencing at the DNA core facility at the Center for Biosystems Research, University of Maryland Biotechnology Institute. Once the correct sequence was verified, pHG$_3$LPT transformed into the expression strain *E. coli* BL21 luxS$^-$ (a *luxS* knockout, table 5-1).

Bacterial strains and growth conditions

Table 5-1 lists the bacterial strains and plasmids used in this study. All bacterial strains were grown in Luria-Bertani (LB) medium at 37 ^{o}C with vigorous shaking (250 rpm). The Luria-Bertani (LB) medium used for bacterial growth contains 5 g/L of yeast extract (Sigma), 10 g/L of Bacto tryptone (Difco) and 10 g/L NaCl (J. T. Baker).

Table 5-1. List of bacterial strains, plasmids and primers used in this study.

Strain, plasmid or primer	Relevant genotype and/or property	Reference
Escherichia coli strains		
W3110	Wild type	Laboratory stock
BL21	*F'* ompT hsdS$_B$ *($r_B^-m_B^-$) gal dcm*	Laboratory stock
BL21 luxS$^-$	*F'* ompT hsdS$_B$ *($r_B^-m_B^-$) gal dcm* Δ*luxS* :: Kan^r	Laboratory stock
MDAI2	W3110 Δ*luxS* :: Tc^r	
TOP10	*F- mcrA Δ(mrr-hsdRMS-mcrBC) φ80lacZΔM15 ΔlacX74 deoR nupG recA1 araD139 Δ(ara-leu)7697 galE15 galK16 rpsL(Str^R) endA1 λ$^-$*	Invitrogen
Plasmids		
pHLPT	pTrcHisC derivative, W3110 *pfs*$^+$, *luxS*$^+$, Amp^r	Fernandes and Bentley[144]
pET-E72-G3	pET derivative, expressing fustion protein E72G3	Tanaka *et al.*[143]
pCR-G$_3$ (TA)	pCR 2.1-TOPO derivative, G$_3^+$, Amp^r	This study
pHG$_3$LPT	pTrcHisC derivative, *Escherichia coli* W3110 *pfs*$^+$, *luxS*$^+$, *Streptococcus* Protein G$_3^+$, Amp^r	This study
pFZY1	*galK'-lacZYA* transcriptional fusion vector, Amp^r	Koop *et al.*[101]
pET200	Cloning vector containing T7 promoter, Amp^r	Invitrogen
pCT5	pFZY1 derivative, *lsr-t7RPol*$^+$, Amp^r	Laboratory stock
pCT6	pFZY1 derivative, containing *lsrR* and *lsrR* promoter fused with *t7RPol*$^+$, Amp^r	Laboratory stock
pEFGFP	pET200 derivative, *gfp*$^+$, Amp^r	Laboratory stock
pGFP	pTrcHisB derivative, *gfp*$^+$, Amp^r	Wu *et al.*[97]

Oligonucleotide primers		
Name	Sequence	Relevant property
C2-5'	5'- CCA TGG GGG GTT CTC ATC ATC ATC ATC ATC ATG TTA AGA TCC GCA TGA CA -3'	Upstream primer for cloning G$_3$ from pET-E72-G3, contains *Nco*I
C2-3'	5'- GCT AGC CAA GAT CTT CGG GTC CAT TTC CGT -3'	Downstream primer for cloning G$_3$ from pET-E72-G3, contains *Nhe*I

Antibiotic concentrations used for the different strains, was 100 µg/mL ampicillin for *E. coli* TOP10, 50 µg/mL ampicillin for *E. coli* BL21 luxS-, 50 µg/mL ampicillin and 20 µg/mL kanamycin for *E. coli* MDAI2 carrying plasmids pCT6 and pETGFP and *E. coli* W3110 carrying plasmids pCT5 and pETGFP.

Expression, purification and analysis of HG_3LPT

E. coli BL21 $luxS^-$ pHG_3LPT was cultured at 37 ^oC and 250 rpm in LB medium supplemented with ampicillin at a concentration of 50 µg/mL. When the optical density (OD_{600}) of the cell culture was between 0.4 - 0.6, IPTG was added to induce over expression of HG_3LPT (final IPTG concentration used was 1 mM). After a 6 hr induction period at the same culture conditions, the cells were harvested by centrifugation at 12,000 xg for 15 minutes at 4 ^oC. The cells were stored at -20 ^oC or directly resuspended in PBS + 10 mM imidazole. The resuspended cells were lysed by sonication using Sonic Dismembrator 550 (Fisher Scientific). After sonication, the soluble cell extract was collected by centrifugation at 14,000 xg for 15 minutes at 4 ^oC, filtered using a 0.22 µm polyether sulfone, low protein binding filter (Millipore) and then loaded on a pre-equilibrated immobilized metal-ion affinity chromatography (IMAC) column (HiTrap Chelating HP, GE Healthcare Life Sciences). After washing with varying amounts of phosphate buffer, sodium chloride and imidazole (Wash 1: 20 mM PO_4^{3-}, 250 mM NaCl and 10 mM imidazole; Wash 2: 20 mM PO_4^{3-}, 250 mM NaCl and 50 mM imidazole), HG_3LPT was eluted with 20 mM PO_4^{3-}, 250 mM NaCl and 350 mM imidazole. The protein was desalted using an Amicon Ultra-15 centrifugal unit (NMWL

10,000, Millipore) and resuspended in 10 mM PO_4^{3-} buffer pH 6 and stored at -80 ^oC until use.

The sizing and analysis of HG_3LPT was performed using a LabChip® Protein 200 plus kit (Agilent Technologies). Briefly 1 μg of purified HG_3LPT (molecular weight 71463 Daltons) was loaded in the chip and the assay was conducted according to the manufacturer's specifications (website: http://www.chem.agilent.com).

BioMEMS device fabrication

The bioMEMS device was fabricated as reported previously [131, 161]. Briefly, the device consists of 9 microchannels evenly distributed on a glass slide with six gold electrodes underneath each channel (Figure 5-2a). Each gold electrode is 1 mm x 1 mm and with an in-channel area of 0.5 mm x 1 mm (Figure 5-2b). The channel is 19 mm long and 150 μm high. The channel volume above each electrode is 0.075 microliters. The glass slide is placed over a layer of plexiglass (Figure 5-2c). The sidewalls of the channel consist of polydimethylsiloxane (PDMS), molded using soft lithographic techniques described in the literature [162, 163]. The device is sealed with a top layer of PDMS. Flow into and from the microchannel is through flexible polyethylene tubing.

Chitosan electrodeposition

A 0.5 % chitosan solution was prepared by adding chitosan flakes in de-ionized water, with HCl added dropwise to maintain pH ~2, and mixing overnight. The pH was then adjusted to pH 5 by the dropwise addition of 1 M NaOH. The resulting chitosan solution was then filtered and stored at 4 °C. To electrodeposit chitosan, the channel first was

prepared by rinsing with de-ionized water for atleast 10 minutes. The chitosan solution was introduced into the channel and electrodeposited onto the negatively biased electrode (the test area) by applying a constant current density of 3 A/m^2 for times ranging from 30 seconds to 2 minutes. After electrodeposition, the channel was rinsed with PBS to remove unbound chitosan.

Spatially-selective assembly of antibody nanofactories

The bioMEMS device containing chitosan electrodeposited onto test area (one out of the six electrodes in the channel) was prepared as described above. To prevent non-specific adsorption of proteins in the channel, a blocking solution containing 5 % non fat milk in PBS was introduced into the channel at a flow rate of 1 µL/min for 2 hours. After blocking, the channel was rinsed with PBS for 30 minutes at a flow rate of 5 µL/min. To attach HG_3LPT onto chitosan, a solution containing 1 µM HG_3LPT and 50 U/mL of the enzyme tyrosinase was introduced into the channel at a flow rate of 1 µL/min and allowed to react for a time period of 1 hour. The channel was rinsed with PBS for 30 minutes at 5 µL/min to remove unbound HG_3LPT. After rinsing, 1 µM FITC labeled anti *S. typhimurium* and 10 µM BSA was introduced at a flow rate of 1 µL/min for 1 hour. The channel was once again rinsed with PBS for 30 minutes at 5 µL/min to remove unbound antibody. The fluorescence of the test area and channel background was observed under fluorescence microscope (Carl Zeiss model 310) and a UV source (Zeiss HBO 100) using a FITC filter (Chroma, excitation wavelength 480 nm, excitation wavelength 535 nm) to investigate assembly of the antibody nanofactories in the channel. Photographs were taken using a digital camera (Carl Zeiss AxioCam MRc5) using 0.5 – 2

second exposure times. As a control, all the above steps were performed in another channel except the step involving the introduction of HG_3LPT and tyrosinase into the channel.

Spatial-selective capture of cells

E. coli carrying plasmid pGFP was cultured and induced to overexpress green fluorescent protein (GFP) using culture conditions as described before. The resultant fluorescent cells (on account of the overexpressed GFP) were collected by centrifuging at 10,000 xg for 5 minutes. An antibody nanofactory solution was prepared by mixing 1 μM HG_3LPT, 2 μM anti *Escherichia coli* and 50 U/mL tyrosinase at room temperature for alteast 1 hour. After the said period, the nanofactory solution was introduced into the channel containing electrodeposited chitosan, previously treated with the blocking solution, at a flow rate of 1 μL/min and allowed to react for 2 hours. After rinsing the channel with PBS for 30 min at 5 μL/min, a suspension of *E. coli* cells overexpressing GFP in PBS was introduced into the channel for 1 hour at 1 μL/min. The channel was rinsed with PBS for 30 min at 5 μL/min to remove the unbound cells. The fluorescence of the test area and channel background was observed under the fluorescence microscope under a Sapphire GFP/UV filter (Chroma, excitation wavelength 395 nm, emission wavelength 510 nm) to determine spatial capture of cells.

Synthesis of *in vitro* AI-2 by antibody nanofactories at the surface of the captured cells

E. coli MDAI-2 cells carrying plasmids pCT5 and pETGFP were spatially captured on the test area using the antibody nanofactories as described above. 1 mM SAH in 10 mM sodium phosphate buffer pH 6 was introduced into the channel at a flow rate of 0.11 µL/min for 16 hours. The nanofactories synthesized AI-2 in the vicinity of the cells. To estimate the amount of AI-2 delivered to the cells, the effluent from the channel was collected and analyzed for its homocysteine concentration. Homocysteine is a byproduct of the AI-2 synthesis reaction produced in stoichiometrically equal amounts to AI-2 [44]. To estimate the concentration of homocysteine, the collected effluent was added to DTNB reagent (100 µM DTNB, 2.5 mM sodium acetate in 0.1 M Tris buffer, pH 8). The reaction was carried out at room temperature for at least 15 minutes. After the reaction, the absorbance at 412 nm (OD_{412}) was measured and the concentration of homocysteine (equal to the amount of AI-2 delivered to the cells) calculated using molar extinction coefficient (13600 M^{-1} cm^{-1}) of the reaction product 5-thio-2-nitrobenzoic acid (TNB) of the reaction of homocysteine with DTNB [126]. As control, all of the above steps were performed in a control channel except for the introduction of the nanofactory into the channel.

Altering response of captured cells by localized synthesis and delivery of AI-2 by the antibody nanofactories

E. coli W3110 cells carrying plasmids pCT6 and pETGFP were spatially captured on the test area using the antibody nanofactories as described above. These cells produce their own AI-2 and carry plasmids that produce GFP in response to AI-2. AI-2 was synthesized at the surface of the captured cells by introducing 1 mM SAH dissolved in

LB medium for 12 hours at a flow rate of 0.11 μL/min. To monitor the response of the cells, the AI-2 based fluorescence (GFP expression) of the cells was observed as a function of time. In the control experiment, all the above steps were repeated in a control channel replacing HG_3LPT by HG_3T, a fusion protein that does not contain AI-2 synthesis enzymes Pfs and LuxS.

5.4 Results

Expression, purification and analysis of HG_3LPT

Plasmid pHG_3LPT (Figure 5-3a) overexpresses HG_3LPT upon induction of the production strain *E. coli* BL21 $luxS^-$. HG_3LPT contains 3 repeats (G_3) of Protein G derived from *Streptococcus* and the AI-2 synthesis enzymes Pfs and LuxS from *E. coli* (Figure 5-3c). The overexpressed protein is purified and is analyzed for its size using LabChip®. Figure 5-3b shows the results of the protein assay run using 1 μg of purified HG_3LPT. The assay shows a band at a molecular weight of 74.1 kDa, which is in agreement with the molecular weight predicted theoretically (71.463 kDa) based on the primary amino acid sequence of HG_3LPT.

Spatially-selective assembly of antibody nanofactories

1 μM HG_3LPT and 50 U/mL of the enzyme tyrosinase is introduced into the channel containing chitosan deposited on the test area. After the reaction and subsequent introduction of FITC labeled anti *S. typhimurium* in the channel, antibody nanofactories assemble spatially on the test area. Figure 5-4 shows photographs of the test areas of the experimental and control channels (no HG_3LPT and tyrosinase) after assembly of the

nanofactories and the fluorescence image analysis of the electrode areas. The average fluorescence observed in the test area of the experimental channel is 45.6 arbitrary units while that in the control channel is 14.1 arbitrary units. The intensity ratio of the observed fluorescence of the test areas in the experimental and control channel is 3.2:1.

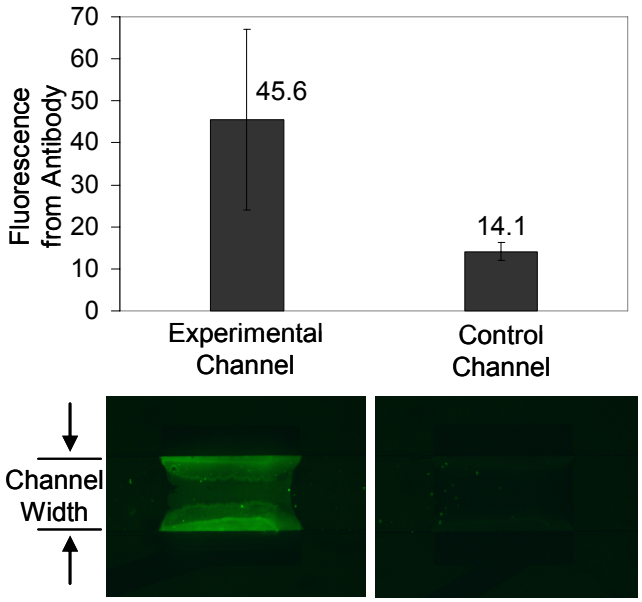

Figure 5-4. Spatial assembly of antibody nanofactories in the test area of a microfluidics channel. Photographs of the test area in an experimental channel and control channel (without HG3LPT and tyrosinase) and image analysis of the test areas.

Spatial-selective capture of cells

The antibody nanofactories spatially assembled onto the test area of the experimental channel captures fluorescent cells (*E. coli* cells that have overexpressed GFP) introduced into the channel. Figure 5-5a shows a photograph of the test area after cell capture and figure 5-5b shows the image analysis of the measured fluorescence. The average fluorescence observed in the test area is 133.6 arbitrary units while that in the channel background is 61.4 arbitrary units. The intensity ratio of the observed fluorescence of the test area to that observed in the channel background is 2.2:1.

Synthesis of *in vitro* AI-2 by antibody nanofactories at the surface of the captured cells

Antibody nanofactories synthesize AI-2 at the surface of *E. coli* MDAI2 cells captured in the test area of the experimental channel upon addition of SAH. Figure 5-6a shows the concentration of homocysteine, and hence AI-2, detected in the effluent from the channel. As seen in Figure 5-6a, the AI-2 concentration detected in the experimental channel is found to be 17.1 μM while that in the control channel (no antibody nanofactories) is 4.6 μM.

Altering response of captured cells by localized synthesis and delivery of AI-2 by the antibody nanofactories

E. coli W3110 carries plasmids pCT6 and pETGFP. The cells produce their own AI-2 as well as GFP in response to AI-2 (on account of plasmids pCT6 and pETGFP). The cells are spatially captured in the experimental channel test area via antibody nanofactories

while in the control channel test area; they are captured by antibodies attached to tyrosine tagged protein G (G_3T). Upon addition of SAH, the antibody nanofactories locally synthesize and deliver AI-2 to the surface of the captured cells in the test area of the experimental channel. The control channel does not have the Pfs and LuxS and hence there is no synthesis of *in vitro* AI-2 there. Since *E. coli* W3110 can produce its own AI-2 and consequently AI-2 dependent GFP, the measured fluorescence of the test area in the control channel is the native response of the captured cells while that in the experimental channel is the altered response on account of the AI-2 produced by the antibody nanofactories. Figure 5-6b shows the observed average fluorescence of the test areas in the experimental and control channels as a function of time since the introduction of the substrate SAH in LB medium into the channels. The observed fluorescence is found to increase in both the experimental (from 28.6 arbitrary units at 40 min to 30.0 arbitrary units at 2 hours and 40.9 arbitrary units at 11 hours) and control channels (from 23.9 arbitrary units at 40 min to 24.5 arbitrary units at 2 hours and 32.3 arbitrary units at 11 hours) as time progresses. The fluorescence in the experimental channel is observed to be higher than that observed in the control channel at all times investigated.

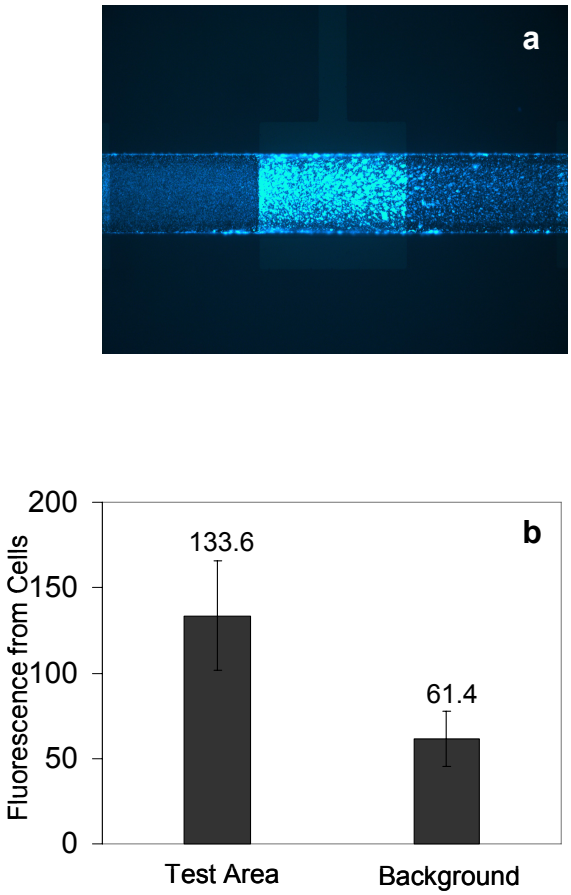

Figure 5-5. Spatially-selective capture of targeted *E. coli* cells that produce GFP in a test area using antibody nanofactories. a. Photograph of the test area in the microchannel. b. Image analysis of the test area and background in the microchannel.

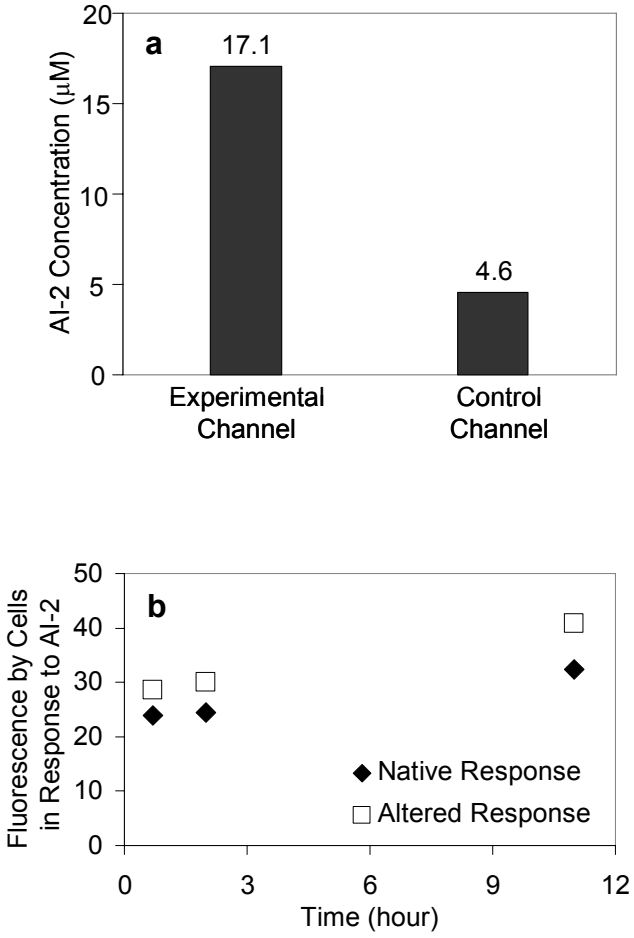

Figure 5-6. Effect of localized synthesis and delivery of AI-2 to targeted cells in a test area on cellular response. a. AI-2 concentrations synthesized in the experimental channel (containing antibody nanofactories) and in the control channel (without antibody nanofactories. b. AI-2 dependent cellular response (GFP production) in cells captured in the control channel (native response, without AI-2) and in the experimental channel (altered response, with AI-2).

5.5 Discussion

In this work, we have presented a technique for the spatial capture and manipulation of quorum sensing bacteria (*E. coli*) in a test area of a bioMEMS device using electrodeposited chitosan and antibody nanofactories (Figure 5-1). Chitosan is electrodeposited onto the test area (negatively biased electrode) on account of the high pH generated in the vicinity of the electrode. The antibody nanofactories consist of targeting module, anti *Escherichia coli*, and the AI-2 synthesis module, fusion protein HG_3LPT (Figure 5-3c) that self assemble when mixed in solution. Plasmid pHG_3LPT (Figure 5-3a) overexpresses HG_3LPT upon induction. The molecular weight of the purified HG_3LPT was found to be in agreement with that theoretically predicted based on its amino acid sequence (Figure 5-3b).

The antibody nanofactories were spatially deposited onto the test area of the microchannel upon activation using the enzyme tyrosinase (Figure 5-4). Tyrosinase activates the C-terminal pentatyrosine residues of HG_3LPT generating reactive o-quinones which react with the primary amine-groups of chitosan electrodeposited on the test area. Spatial assembly of the nanofactories in the test area requires the presence of all the necessary components: electrodeposited chitosan, targeting antibody, fusion protein HG_3LPT and activating enzyme tyrosinase. The spatial assembly of the nanofactories, monitored by measuring the fluorescence of the FITC labeled antibody in the test area, was found to be higher when all components were simultaneously present (experimental channel, 45.6 arbitrary units) than when tyrosinase and HG_3LPT was absent (control channel, 14.6 arbitrary units).

The antibody nanofactories facilitated spatial assembly of targeted fluorescent *E. coli* cells in the test area via the targeting antibody (Figure 5-5). The capture of cells, monitored by measuring the fluorescence produced by the cells, was found to be higher in the test area (133.6 arbitrary units, Figure 5-5b) than in the channel background (61.4 arbitrary units).

Upon addition of substrate SAH, the antibody nanofactories synthesize AI-2 and deliver it in the vicinity of the capture *E. coli* cells (Figure 5-6a). The AI-2 concentration synthesized in the experimental channel (containing HG_3LPT, 17.1 μM) was found to be higher than that observed in the control channel (no HG_3LPT, 4.6 μM) indicating that the assembled nanofactories retain their activity even after capture of the targeted cells in the test area. In a proof-of-concept study, the localized synthesis and delivery of AI-2 via the nanofactories to targeted cells in the test area resulted in altering the native AI-2 based response (GFP production) of the cells (Figure 5-6b). Use of the nanofactories resulted in increased AI-2 dependent GFP production (altered response) over all the times investigated as compared to controls (native response) indicating that the captured cells are capable of being manipulated using this technique.

The presented work is significant for the following reasons. First, a technique to spatially capture cells and biosynthetic pathway enzymes in a given test area of a microchannel is demonstrated. The captured enzymes and cells retain their activity in the test area over the times investigated (12 hours). Finally, the native response of the captured cells in the test area was demonstrated to be altered via localized synthesis and delivery using antibody nanofactories. While only a modest increase in the native response (AI-2 based GFP production) of the captured cells was observed in this work

(Figure 5-6b), future studies conducted with optimized reaction conditions in the device should address this current limitation. This will create a versatile platform to study QS based response, such as biofilm formation and cell attachment phenotypes, for various bacteria (by changing the targeting antibody) in a controllable manner within the bioMEMS device.

Chapter 6: General Conclusions

6.1 Results Summary

In this dissertation, a biological nanofactory approach to targeted delivery was presented. The biological nanofactories, comprising multiple functional modules, effected targeted delivery by localized synthesis and delivery of the 'universal' quorum sensing signaling molecule autoinducer-2 at the surface of targeted bacteria.

In chapter 2, the concept of a magnetic nanofactory was presented. The magnetic nanofactories comprised enzymes of the AI-2 biosynthesis pathway, Pfs and LuxS, attached separately to chitosan functionalized magnetic nanoparticles (chitosan-mag) by activation of their terminal tyrosine pro-tags. The magnetic nanofactories, shown to be able to capture cells and synthesize AI-2, were added to cultures of *E. coli* cells at various times along the growth of the bacteria. The localized synthesis and delivery of AI-2 was found to alter the natural response of the targeted cells over all the times investigated. The magnetic nanofactories were also demonstrated to elicit a higher AI-2 dependent response in targeted cells than that caused by direct addition of an equivalent amount of free enzymes in solution.

In chapter 3, the design of the AI-2 synthesis module was improved by the creation of a fusion protein HLPT that co-expressed both Pfs and LuxS. The updated module was shown to have higher AI-2 activity than equimolar amounts of the constituent enzymes added separately over a wide range of reaction conditions investigated. The synthesis module was assembled onto chitosan-mag nanoparticles via

adsorption and the resulting nanofactory was found to increase AI-2 dependent response in targeted cells as compared to the control (direct addition of AI-2).

In chapter 4, the concept of an antibody nanofactory was presented. The antibody nanofactories were self-assembled and made up of two functional modules: AI-2 synthesis module (fusion enzyme HGLPT) and cell targeting module (anti bacteria antibody). The antibody nanofactories self-assembled when the Protein G of HGLPT bound to the Fc region of the targeting antibody. The antibody nanofactories were found to effectively target bacteria and shown to produce AI-2. The localized synthesis and delivery of AI-2 via the antibody nanofactories was found to significantly alter the native response of both targeted *E. coli* and *S. typhimurium* (using the *E. coli* enzymes).

In chapter 5, quorum sensing bacteria were spatially immobilized and manipulated in a bioMEMS device. The immobilization technique involved creation of a patterned microdevice, electrodeposition of the chitosan onto the test area, assembly of the antibody nanofactory (fusion protein HG_3LPT and targeting antibody) onto the test area by activation of the C-terminal tyrosine pro-tag of HG_3LPT by tyrosinase. The technique was demonstrated to facilitate spatially-selective capture of targeted *E. coli* bacteria on a test area of the bioMEMS device. Manipulation of the captured bacteria by localized synthesis and delivery of AI-2 via the antibody nanofactories co-localized in the test area was shown to alter the native response of the captured cells.

6.2 Broader Impact of the Work

The work presented in this dissertation provides a fundamentally different way of approaching targeted delivery. The results demonstrate that targeted delivery via

localized synthesis and delivery of signaling autoinducers are successful in altering the natural response of targeted bacteria. In theory, this mode of delivery can be adapted to biological systems that are different and potentially more complex than the bacterial systems investigated here. For example, in contemporary literature there is a considerable interest in creating methods that draw inspiration from the human body's ability to self-medicate or self-heal. In such approaches, molecular machinery is envisioned to be introduced into the body at a target site where it utilizes raw materials in the vicinity of the target site and converts it to a therapeutic compound or a (useful) substance required there. While the biological nanofactories presented here are not currently capable of using pre-existing raw materials, they could potentially be adapted to do the same by careful design.

6.3 Future Directions

The results presented in this dissertation involve monitoring the AI-2 dependent production of model reporter proteins (β-galactosidase and green fluorescent protein) in mutant bacteria as indicative of cellular response. The above studies can be adapted to study the response of wild type bacteria such as *Escherichia coli* W3110 and *Salmonella typhimurium* LT2. In these studies, instead of monitoring a reporter protein production, one may study the effect of the localized synthesis and delivery of AI-2 on native gene expression such as AI-2 uptake and signal processing genes and other downstream genes as well as on phenotypic expression such as increased/decreased biofilm formation or increased/decreased toxin secretion.

The magnetic nanofactories can be used for the spatial capture of cells in a bioMEMS device. In these studies, the magnetic nanofactories will be added to cell cultures (e.g. *E. coli* or *S. typhimurium*) where they bind to the surface of the targeted cells. In the presence of an external magnetic field, the nanofactories can be recovered along with the targeted cells. The magnetic nanofactories along with the bound cells can be introduced into a microfluidics channel of a bioMEMS device. Application of a magnetic field within a test area of the channel will enable immobilization of the magnetic nanofactories as well as bound cells within that test area. The bound cells can be subjected to treatment within the test area. After treatment, the cells can be released by removing the magnetic field.

By changing the targeting antibody, bacteria other than *E. coli* and *S. typhimurium* can be targeted. These studies would be particularly useful in studying the AI-2 based response of bacteria such as *Vibrio cholerae* and *Bacillus cereus*. AI-2 has been shown to decrease virulence in *V. cholerae* [46] and reduce biofilm formation in *B. cereus* [122]. In addition, the antibody nanofactories can be used to probe the AI-2 based response of bacteria not investigated thus far in the literature.

Another important study would be to demonstrate selective targeting and manipulation using antibody nanofactories of a single type of bacterium within a mixed culture of bacteria. In these studies, the antibody nanofactories would target only one type of bacterium within the mixed culture and manipulate its response while leaving the other bacteria unaltered. This would be particularly useful in situations that typically involve different types of bacteria such as oral bacteria, bacteria of the gut and biofilms involving different bacterial species. These studies can be extended to co-cultures

involving eukaryotic cell lines such as Caco-2 epithelial cells and bacteria such as *E. coli* and *V. cholerae* so as to investigate the effect of the biological nanofactories on the ability of the these bacteria to adhere to the Caco-2 cells. Such studies are important in the creation of an *in vitro* model of bacterial colonization and adhesion in the human gut.

Finally, in addition to the two types of biological nanofactories describe here, alternative nanofactories that add modules to or combine modules of the nanofactories described here can be devised for specific end applications. For e.g. instead of the addition of substrate SAH externally, a storage module in the form a vesicle or capsule containing SAH can be added to the biological nanofactory so as to provide the raw material (by release from the storage module) for conversion by the enzymes of the nanofactory at the targeted site.

References

1. Pollock, S.; Dwek, R. A.; Burton, D. R.; Zitzmann, N., N-Butyldeoxynojirimycin is a broadly effective anti-HIV therapy significantly enhanced by targeted liposome delivery. *Aids* **2008,** 22, (15), 1961-9.

2. Wan, L.; Pooyan, S.; Hu, P.; Leibowitz, M. J.; Stein, S.; Sinko, P. J., Peritoneal macrophage uptake, pharmacokinetics and biodistribution of macrophage-targeted PEG-fMLF (N-formyl-methionyl-leucyl-phenylalanine) nanocarriers for improving HIV drug delivery. *Pharm Res* **2007,** 24, (11), 2110-9.

3. Juillerat-Jeanneret, L., The targeted delivery of cancer drugs across the blood-brain barrier: chemical modifications of drugs or drug-nanoparticles? *Drug Discov Today* **2008**.

4. Torchilin, V., Antibody-modified liposomes for cancer chemotherapy. *Expert Opin Drug Deliv* **2008,** 5, (9), 1003-25.

5. Barnett, B. P.; Arepally, A.; Karmarkar, P. V.; Qian, D.; Gilson, W. D.; Walczak, P.; Howland, V.; Lawler, L.; Lauzon, C.; Stuber, M.; Kraitchman, D. L.; Bulte, J. W., Magnetic resonance-guided, real-time targeted delivery and imaging of magnetocapsules immunoprotecting pancreatic islet cells. *Nat Med* **2007,** 13, (8), 986-91.

6. Morishita, M.; Tanaka, T.; Shida, T.; Takayama, K., Usefulness of colon targeted DHA and EPA as novel diabetes medications that promote intrinsic GLP-1 secretion. *J Control Release* **2008**.

7. Durcan, N.; Murphy, C.; Cryan, S. A., Inhalable siRNA: potential as a therapeutic agent in the lungs. *Mol Pharm* **2008,** 5, (4), 559-66.

8. Kleinstreuer, C.; Zhang, Z.; Donohue, J. F., Targeted drug-aerosol delivery in the human respiratory system. *Annu Rev Biomed Eng* **2008,** 10, 195-220.

9. Fumoto, S.; Nishi, J.; Nakamura, J.; Nishida, K., Gene therapy for gastric diseases. *Curr Gene Ther* **2008,** 8, (3), 187-200.

10. Simone, E.; Ding, B. S.; Muzykantov, V., Targeted delivery of therapeutics to endothelium. *Cell Tissue Res* **2008**.

11. Dimitrova, M.; Affolter, C.; Meyer, F.; Nguyen, I.; Richard, D. G.; Schuster, C.; Bartenschlager, R.; Voegel, J. C.; Ogier, J.; Baumert, T. F., Sustained delivery of siRNAs targeting viral infection by cell-degradable multilayered polyelectrolyte films. *Proc Natl Acad Sci U S A* **2008,** 105, (42), 16320-5.

12. Suzuki, K.; Mitsui, K.; Aizawa, E.; Hasegawa, K.; Kawase, E.; Yamagishi, T.; Shimizu, Y.; Suemori, H.; Nakatsuji, N.; Mitani, K., Highly efficient transient gene expression and gene targeting in primate embryonic stem cells with helper-dependent adenoviral vectors. *Proc Natl Acad Sci U S A* **2008,** 105, (37), 13781-6.

13. Mahmoudi, M.; Simchi, A.; Imani, M.; Milani, A. S.; Stroeve, P., Optimal Design and Characterization of Superparamagnetic Iron Oxide Nanoparticles Coated with Polyvinyl Alcohol for Targeted Delivery and Imaging. *J Phys Chem B* **2008**.

14. Sofou, S.; Sgouros, G., Antibody-targeted liposomes in cancer therapy and imaging. *Expert Opin Drug Deliv* **2008,** 5, (2), 189-204.

15. Delehanty, J. B.; Mattoussi, H.; Medintz, I. L., Delivering quantum dots into cells: strategies, progress and remaining issues. *Anal Bioanal Chem* **2008**.

16. Weng, K. C.; Noble, C. O.; Papahadjopoulos-Sternberg, B.; Chen, F. F.; Drummond, D. C.; Kirpotin, D. B.; Wang, D.; Hom, Y. K.; Hann, B.; Park, J. W., Targeted tumor cell internalization and imaging of multifunctional quantum dot-conjugated immunoliposomes in vitro and in vivo. *Nano Lett* **2008,** 8, (9), 2851-7.

17. Liqun Wang, R.; McLaughlin, T.; Cossette, T.; Tang, Q.; Foust, K.; Campbell-Thompson, M.; Martino, A.; Cruz, P.; Loiler, S.; Mueller, C.; Flotte, T. R., Recombinant AAV Serotype and Capsid Mutant Comparison for Pulmonary Gene Transfer of alpha-1-Antitrypsin Using Invasive and Noninvasive Delivery. *Mol Ther* **2008**.

18. Schaffer, D. V.; Koerber, J. T.; Lim, K. I., Molecular engineering of viral gene delivery vehicles. *Annu Rev Biomed Eng* **2008,** 10, 169-94.

19. Murphy, E. A.; Majeti, B. K.; Barnes, L. A.; Makale, M.; Weis, S. M.; Lutu-Fuga, K.; Wrasidlo, W.; Cheresh, D. A., Nanoparticle-mediated drug delivery to tumor

vasculature suppresses metastasis. *Proc Natl Acad Sci U S A* **2008,** 105, (27), 9343-8.

20. Tasciotti, E.; Liu, X.; Bhavane, R.; Plant, K.; Leonard, A. D.; Price, B. K.; Cheng, M. M.; Decuzzi, P.; Tour, J. M.; Robertson, F.; Ferrari, M., Mesoporous silicon particles as a multistage delivery system for imaging and therapeutic applications. *Nat Nanotechnol* **2008,** 3, (3), 151-7.

21. Joshi, A.; Punyani, S.; Bale, S. S.; Yang, H.; Borca-Tasciuc, T.; Kane, R. S., Nanotube-assisted protein deactivation. *Nat Nanotechnol* **2008,** 3, (1), 41-5.

22. Liu, Z.; Chen, K.; Davis, C.; Sherlock, S.; Cao, Q.; Chen, X.; Dai, H., Drug delivery with carbon nanotubes for in vivo cancer treatment. *Cancer Res* **2008,** 68, (16), 6652-60.

23. Boddapati, S. V.; D'Souza, G. G.; Erdogan, S.; Torchilin, V. P.; Weissig, V., Organelle-targeted nanocarriers: specific delivery of liposomal ceramide to mitochondria enhances its cytotoxicity in vitro and in vivo. *Nano Lett* **2008,** 8, (8), 2559-63.

24. Meers, P.; Neville, M.; Malinin, V.; Scotto, A. W.; Sardaryan, G.; Kurumunda, R.; Mackinson, C.; James, G.; Fisher, S.; Perkins, W. R., Biofilm penetration, triggered release and in vivo activity of inhaled liposomal amikacin in chronic Pseudomonas aeruginosa lung infections. *J Antimicrob Chemother* **2008,** 61, (4), 859-68.

25. Li, C.; Wallace, S., Polymer-drug conjugates: recent development in clinical oncology. *Adv Drug Deliv Rev* **2008,** 60, (8), 886-98.

26. Xiong, X. B.; Uludag, H.; Lavasanifar, A., Biodegradable amphiphilic poly(ethylene oxide)-block-polyesters with grafted polyamines as supramolecular nanocarriers for efficient siRNA delivery. *Biomaterials* **2009,** 30, (2), 242-53.

27. Barkin, R. L., Extended-release Tramadol (ULTRAM ER): a pharmacotherapeutic, pharmacokinetic, and pharmacodynamic focus on effectiveness and safety in patients with chronic/persistent pain. *Am J Ther* **2008,** 15, (2), 157-66.

28. Bendas, E. R.; Tadros, M. I., Enhanced transdermal delivery of salbutamol sulfate via ethosomes. *AAPS PharmSciTech* **2007,** 8, (4), E107.

29. Chappell, J. C.; Song, J.; Burke, C. W.; Klibanov, A. L.; Price, R. J., Targeted delivery of nanoparticles bearing fibroblast growth factor-2 by ultrasonic microbubble destruction for therapeutic arteriogenesis. *Small* **2008,** 4, (10), 1769-77.

30. Niu, X.; Feng, Q.; Wang, M.; Guo, X.; Zheng, Q., Preparation and characterization of chitosan microspheres for controlled release of synthetic oligopeptide derived from BMP-2. *J Microencapsul* **2008**, 1-9.

31. Boehm, A. L.; Sen, M.; Seethala, R.; Gooding, W. E.; Freilino, M.; Wong, S. M.; Wang, S.; Johnson, D. E.; Grandis, J. R., Combined targeting of epidermal growth factor receptor, signal transducer and activator of transcription-3, and Bcl-X(L) enhances antitumor effects in squamous cell carcinoma of the head and neck. *Mol Pharmacol* **2008,** 73, (6), 1632-42.

32. Zhao, W.; Han, Q.; Lin, H.; Sun, W.; Gao, Y.; Zhao, Y.; Wang, B.; Wang, X.; Chen, B.; Xiao, Z.; Dai, J., Human Basic Fibroblast Growth Factor Fused with Kringle4 Peptide Binds to a Fibrin Scaffold and Enhances Angiogenesis. *Tissue Eng Part A* **2008**.

33. Lammers, T.; Hennink, W. E.; Storm, G., Tumour-targeted nanomedicines: principles and practice. *Br J Cancer* **2008,** 99, (3), 392-7.

34. Singh, A.; Nie, H.; Ghosn, B.; Qin, H.; Kwak, L. W.; Roy, K., Efficient Modulation of T-cell Response by Dual-mode, Single-carrier Delivery of Cytokine-targeted siRNA and DNA Vaccine to Antigen-presenting Cells. *Mol Ther* **2008**.

35. Cao, N.; Feng, S. S., Doxorubicin conjugated to D-alpha-tocopheryl polyethylene glycol 1000 succinate (TPGS): conjugation chemistry, characterization, in vitro and in vivo evaluation. *Biomaterials* **2008,** 29, (28), 3856-65.

36. Moon, S. J.; Govindan, S. V.; Cardillo, T. M.; D'Souza, C. A.; Hansen, H. J.; Goldenberg, D. M., Antibody Conjugates of 7-Ethyl-10-hydroxycamptothecin (SN-38) for Targeted Cancer Chemotherapy. *J Med Chem* **2008**.

37. Katragadda, S.; Gunda, S.; Hariharan, S.; Mitra, A. K., Ocular pharmacokinetics of acyclovir amino acid ester prodrugs in the anterior chamber: evaluation of their utility in treating ocular HSV infections. *Int J Pharm* **2008,** 359, (1-2), 15-24.

38. Palanki, M. S.; Akiyama, H.; Campochiaro, P.; Cao, J.; Chow, C. P.; Dellamary, L.; Doukas, J.; Fine, R.; Gritzen, C.; Hood, J. D.; Hu, S.; Kachi, S.; Kang, X.; Klebansky, B.; Kousba, A.; Lohse, D.; Mak, C. C.; Martin, M.; McPherson, A.; Pathak, V. P.; Renick, J.; Soll, R.; Umeda, N.; Yee, S.; Yokoi, K.; Zeng, B.; Zhu, H.; Noronha, G., Development of prodrug 4-chloro-3-(5-methyl-3-{[4-(2-pyrrolidin-1-ylethoxy)phenyl]amino}-1,2,4-be nzotriazin-7-yl)phenyl benzoate (TG100801): a topically administered therapeutic candidate in clinical trials for the treatment of age-related macular degeneration. *J Med Chem* **2008,** 51, (6), 1546-59.

39. Cooper, D. R.; Marrel, C.; Testa, B.; van de Waterbeemd, H.; Quinn, N.; Jenner, P.; Marsden, C. D., L-Dopa methyl ester--a candidate for chronic systemic delivery of L-Dopa in Parkinson's disease. *Clin Neuropharmacol* **1984,** 7, (1), 89-98.

40. Khor, S. P.; Hsu, A., The pharmacokinetics and pharmacodynamics of levodopa in the treatment of Parkinson's disease. *Curr Clin Pharmacol* **2007,** 2, (3), 234-43.

41. Mishra, S.; Karmodiya, K.; Parasuraman, P.; Surolia, A.; Surolia, N., Design, synthesis, and application of novel triclosan prodrugs as potential antimalarial and antibacterial agents. *Bioorg Med Chem* **2008,** 16, (10), 5536-46.

42. Vaara, M.; Fox, J.; Loidl, G.; Siikanen, O.; Apajalahti, J.; Hansen, F.; Frimodt-Moller, N.; Nagai, J.; Takano, M.; Vaara, T., Novel polymyxin derivatives carrying only three positive charges are effective antibacterial agents. *Antimicrob Agents Chemother* **2008,** 52, (9), 3229-36.

43. Fuqua, W. C.; Winans, S. C.; Greenberg, E. P., Quorum sensing in bacteria: the LuxR-LuxI family of cell density-responsive transcriptional regulators. *J Bacteriol* **1994,** 176, (2), 269-75.

44. Lowery, C. A.; Dickerson, T. J.; Janda, K. D., Interspecies and interkingdom communication mediated by bacterial quorum sensing. *Chem Soc Rev* **2008,** 37, (7), 1337-46.

45. Waters, C. M.; Bassler, B. L., Quorum sensing: cell-to-cell communication in bacteria. *Annu Rev Cell Dev Biol* **2005,** 21, 319-46.

46. Higgins, D. A.; Pomianek, M. E.; Kraml, C. M.; Taylor, R. K.; Semmelhack, M. F.; Bassler, B. L., The major Vibrio cholerae autoinducer and its role in virulence factor production. *Nature* **2007,** 450, (7171), 883-6.

47. Waters, C. M.; Lu, W.; Rabinowitz, J. D.; Bassler, B. L., Quorum sensing controls biofilm formation in Vibrio cholerae through modulation of cyclic di-GMP levels and repression of vpsT. *J Bacteriol* **2008,** 190, (7), 2527-36.

48. Skindersoe, M. E.; Alhede, M.; Phipps, R.; Yang, L.; Jensen, P. O.; Rasmussen, T. B.; Bjarnsholt, T.; Tolker-Nielsen, T.; Hoiby, N.; Givskov, M., Effects of antibiotics on quorum sensing in Pseudomonas aeruginosa. *Antimicrob Agents Chemother* **2008,** 52, (10), 3648-63.

49. Wagner, V. E.; Iglewski, B. H., P. aeruginosa Biofilms in CF Infection. *Clin Rev Allergy Immunol* **2008,** 35, (3), 124-34.

50. Rychlik, I.; Barrow, P. A., Salmonella stress management and its relevance to behaviour during intestinal colonisation and infection. *FEMS Microbiol Rev* **2005,** 29, (5), 1021-40.

51. Xavier, K. B.; Bassler, B. L., Interference with AI-2-mediated bacterial cell-cell communication. *Nature* **2005,** 437, (7059), 750-3.

52. Rickard, A. H.; Palmer, R. J., Jr.; Blehert, D. S.; Campagna, S. R.; Semmelhack, M. F.; Egland, P. G.; Bassler, B. L.; Kolenbrander, P. E., Autoinducer 2: a concentration-dependent signal for mutualistic bacterial biofilm growth. *Mol Microbiol* **2006,** 60, (6), 1446-56.

53. Danhorn, T.; Fuqua, C., Biofilm formation by plant-associated bacteria. *Annu Rev Microbiol* **2007,** 61, 401-22.

54. Belas, R.; Mileham, A.; Cohn, D.; Hilman, M.; Simon, M.; Silverman, M., Bacterial bioluminescence: isolation and expression of the luciferase genes from Vibrio harveyi. *Science* **1982,** 218, (4574), 791-3.

55. Nealson, K. H.; Hastings, J. W., Bacterial bioluminescence: its control and ecological significance. *Microbiol Rev* **1979,** 43, (4), 496-518.

56. Chen, X.; Schauder, S.; Potier, N.; Van Dorsselaer, A.; Pelczer, I.; Bassler, B. L.; Hughson, F. M., Structural identification of a bacterial quorum-sensing signal containing boron. *Nature* **2002,** 415, (6871), 545-549.

57. Waters, C. M.; Bassler, B. L., The Vibrio harveyi quorum-sensing system uses shared regulatory components to discriminate between multiple autoinducers. *Genes & Development* **2006,** 20, (19), 2754-2767.

58. Hardie, K. R.; Heurlier, K., Establishing bacterial communities by 'word of mouth': LuxS and autoinducer 2 in biofilm development. *Nat Rev Microbiol* **2008,** 6, (8), 635-43.

59. Irie, Y.; Parsek, M. R., Quorum sensing and microbial biofilms. *Curr Top Microbiol Immunol* **2008,** 322, 67-84.

60. Le Berre, R.; Nguyen, S.; Nowak, E.; Kipnis, E.; Pierre, M.; Ader, F.; Courcol, R.; Guery, B. P.; Faure, K., Quorum-sensing activity and related virulence factor expression in clinically pathogenic isolates of Pseudomonas aeruginosa. *Clin Microbiol Infect* **2008,** 14, (4), 337-43.

61. DeLisa, M. P.; Bentley, W. E., Bacterial autoinduction: looking outside the cell for new metabolic engineering targets. *Microb Cell Fact* **2002,** 1, (1), 5.

62. Williamson, N. R.; Fineran, P. C.; Ogawa, W.; Woodley, L. R.; Salmond, G. P., Integrated regulation involving quorum sensing, a two-component system, a GGDEF/EAL domain protein and a post-transcriptional regulator controls swarming and RhlA-dependent surfactant biosynthesis in Serratia. *Environ Microbiol* **2008,** 10, (5), 1202-17.

63. Davies, D., Understanding biofilm resistance to antibacterial agents. *Nat Rev Drug Discov* **2003,** 2, (2), 114-22.

64. Characklis, W. G., *Biofilms*. John Wiley & Sons, Inc.: New York, 1990; p 523-584.

65. Little, B. J.; Wagner, P. A.; Characklis, W. G., *Microbial corrosion*. John Wiley & Sons, Inc.: New York, 1990; p 635-670.

66. Wang, L.; Hashimoto, Y.; Tsao, C. Y.; Valdes, J. J.; Bentley, W. E., Cyclic AMP (cAMP) and cAMP receptor protein influence both synthesis and uptake of extracellular autoinducer 2 in Escherichia coli. *J Bacteriol* **2005,** 187, (6), 2066-76.

67. Taga, M. E.; Miller, S. T.; Bassler, B. L., Lsr-mediated transport and processing of AI-2 in Salmonella typhimurium. *Mol Microbiol* **2003,** 50, (4), 1411-27.

68. Sela, S.; Frank, S.; Belausov, E.; Pinto, R., A Mutation in the luxS gene influences Listeria monocytogenes biofilm formation. *Appl Environ Microbiol* **2006,** 72, (8), 5653-8.

69. Jones, M. B.; Blaser, M. J., Detection of a luxS-signaling molecule in Bacillus anthracis. *Infect Immun* **2003,** 71, (7), 3914-9.

70. Duan, K.; Dammel, C.; Stein, J.; Rabin, H.; Surette, M. G., Modulation of Pseudomonas aeruginosa gene expression by host microflora through interspecies communication. *Mol Microbiol* **2003,** 50, (5), 1477-91.

71. Vendeville, A.; Winzer, K.; Heurlier, K.; Tang, C. M.; Hardie, K. R., Making 'sense' of metabolism: autoinducer-2, LuxS and pathogenic bacteria. *Nat Rev Microbiol* **2005,** 3, (5), 383-96.

72. Miller, S. T.; Xavier, K. B.; Campagna, S. R.; Taga, M. E.; Semmelhack, M. F.; Bassler, B. L.; Hughson, F. M., Salmonella typhimurium recognizes a chemically distinct form of the bacterial quorum-sensing signal AI-2. *Mol Cell* **2004,** 15, (5), 677-87.

73. Fernandes, R.; Tsao, C. Y.; Hashimoto, Y.; Wang, L.; Wood, T. K.; Payne, G. F.; Bentley, W. E., Magnetic nanofactories: Localized synthesis and delivery of quorum-sensing signaling molecule autoinducer-2 to bacterial cell surfaces. *Metabolic Engineering* **2007,** 9, (2), 228-239.

74. Leduc, P. R.; Wong, M. S.; Ferreira, P. M.; Groff, R. E.; Haslinger, K.; Koonce, M. P.; Lee, W. Y.; Love, J. C.; McCammon, J. A.; Monteiro-Riviere, N. A.; Rotello, V. M.; Rubloff, G. W.; Westervelt, R.; Yoda, M., Towards an in vivo biologically inspired nanofactory. *Nature Nanotechnology* **2007,** 2, (1), 3-7.

75. Shiner, E. K.; Rumbaugh, K. P.; Williams, S. C., Inter-kingdom signaling: deciphering the language of acyl homoserine lactones. *FEMS Microbiol Rev* **2005,** 29, (5), 935-47.

76. Truckses, D. M.; Bloomekatz, J. E.; Thorner, J., The RA domain of Ste50 adaptor protein is required for delivery of Ste11 to the plasma membrane in the filamentous growth signaling pathway of the yeast Saccharomyces cerevisiae. *Mol Cell Biol* **2006,** 26, (3), 912-28.

77. Wang, B.; Li, S.; Southern, P. J.; Cleary, P. P., Streptococcal modulation of cellular invasion via TGF-beta1 signaling. *Proc Natl Acad Sci U S A* **2006,** 103, (7), 2380-5.

78. Yang, S.; Lopez, C. R.; Zechiedrich, E. L., Quorum sensing and multidrug transporters in Escherichia coli. *Proc Natl Acad Sci U S A* **2006**.

79. Geer, D. J.; Swartz, D. D.; Andreadis, S. T., Biomimetic delivery of keratinocyte growth factor upon cellular demand for accelerated wound healing in vitro and in vivo. *Am J Pathol* **2005,** 167, (6), 1575-86.

80. Shansky, J.; Creswick, B.; Lee, P.; Wang, X.; Vandenburgh, H., Paracrine release of insulin-like growth factor 1 from a bioengineered tissue stimulates skeletal muscle growth in vitro. *Tissue Eng* **2006,** 12, (7), 1833-41.

81. Wei, G.; Jin, Q.; Giannobile, W. V.; Ma, P. X., Nano-fibrous scaffold for controlled delivery of recombinant human PDGF-BB. *J Control Release* **2006,** 112, (1), 103-10.

82. Taylor, L.; Jones, L.; Tuszynski, M. H.; Blesch, A., Neurotrophin-3 gradients established by lentiviral gene delivery promote short-distance axonal bridging beyond cellular grafts in the injured spinal cord. *J Neurosci* **2006,** 26, (38), 9713-21.

83. Holland, T. A.; Bodde, E. W.; Cuijpers, V. M.; Baggett, L. S.; Tabata, Y.; Mikos, A. G.; Jansen, J. A., Degradable hydrogel scaffolds for in vivo delivery of single and dual growth factors in cartilage repair. *Osteoarthritis Cartilage* **2006**.

84. Lee, J. P.; Jalili, R. B.; Tredget, E. E.; Demare, J. R.; Ghahary, A., Antifibrogenic effects of liposome-encapsulated IFN-alpha2b cream on skin wounds in a fibrotic rabbit ear model. *J Interferon Cytokine Res* **2005,** 25, (10), 627-31.

85. Chung, Y. I.; Tae, G.; Hong Yuk, S., A facile method to prepare heparin-functionalized nanoparticles for controlled release of growth factors. *Biomaterials* **2006,** 27, (12), 2621-6.

86. Gonzalez Barrios, A. F.; Zuo, R.; Hashimoto, Y.; Yang, L.; Bentley, W. E.; Wood, T. K., Autoinducer 2 controls biofilm formation in Escherichia coli through a novel motility quorum-sensing regulator (MqsR, B3022). *J Bacteriol* **2006,** 188, (1), 305-16.

87. Henke, J. M.; Bassler, B. L., Bacterial social engagements. *Trends Cell Biol* **2004,** 14, (11), 648-56.

88. Winzer, K.; Hardie, K. R.; Williams, P., Bacterial cell-to-cell communication: sorry, can't talk now - gone to lunch! *Curr Opin Microbiol* **2002,** 5, (2), 216-22.

89. Honda, H.; Kawabe, A.; Shinkai, A.; Kobayashi, T., Development of chitosan-conjugated magnetite for magnetic cell separation. *Journal of Fermentation and Bioengineering* **1998,** 86, (2), 191-196.

90. Honda, H.; Kawabe, A.; Skinkai, M.; Kobayashi, T., Recovery of recombinant Escherichia coli by chitosan-conjugated magnetite. *Biochemical Engineering Journal* **1999,** 3, (2), 157-160.

91. Fernandes, R.; Wu, L. Q.; Chen, T. H.; Yi, H. M.; Rubloff, G. W.; Ghodssi, R.; Bentley, W. E.; Payne, G. F., Electrochemically induced deposition of a polysaccharide hydrogel onto a patterned surface. *Langmuir* **2003,** 19, (10), 4058-4062.

92. Wu, L. Q.; Gadre, A. P.; Yi, H. M.; Kastantin, M. J.; Rubloff, G. W.; Bentley, W. E.; Payne, G. F.; Ghodssi, R., Voltage-dependent assembly of the polysaccharide chitosan onto an electrode surface. *Langmuir* **2002,** 18, (22), 8620-8625.

93. Chen, T. H.; Embree, H. D.; Wu, L. Q.; Payne, G. F., In vitro protein-polysaccharide conjugation: Tyrosinase-catalyzed conjugation of gelatin and chitosan. *Biopolymers* **2002,** 64, (6), 292-302.

94. Chen, T. H.; Small, D. A.; Wu, L. Q.; Rubloff, G. W.; Ghodssi, R.; Vazquez-Duhalt, R.; Bentley, W. E.; Payne, G. F., Nature-inspired creation of protein-polysaccharide conjugate and its subsequent assembly onto a patterned surface. *Langmuir* **2003,** 19, (22), 9382-9386.

95. Chen, T. H.; Vazquez-Duhalt, R.; Wu, C. F.; Bentley, W. E.; Payne, G. F., Combinatorial screening for enzyme-mediated coupling. Tyrosinase-catalyzed coupling to create protein-chitosan conjugates. *Biomacromolecules* **2001,** 2, (2), 456-462.

96. Bassler, B. L.; Wright, M.; Silverman, M. R., Multiple signalling systems controlling expression of luminescence in Vibrio harveyi: sequence and function of genes encoding a second sensory pathway. *Mol Microbiol* **1994,** 13, (2), 273-86.

97. Wu, C. F.; Cha, H. J.; Rao, G.; Valdes, J. J.; Bentley, W. E., A green fluorescent protein fusion strategy for monitoring the expression, cellular location, and separation of biologically active organophosphorus hydrolase. *Appl Microbiol Biotechnol* **2000,** 54, (1), 78-83.

98. Connell, N.; Han, Z.; Moreno, F.; Kolter, R., An E. coli promoter induced by the cessation of growth. *Mol Microbiol* **1987,** 1, (2), 195-201.

99. Cadieux, N.; Bradbeer, C.; Reeger-Schneider, E.; Koster, W.; Mohanty, A. K.; Wiener, M. C.; Kadner, R. J., Identification of the periplasmic cobalamin-binding protein BtuF of Escherichia coli. *J Bacteriol* **2002,** 184, (3), 706-17.

100. Bassler, B. L.; Wright, M.; Showalter, R. E.; Silverman, M. R., Intercellular signalling in Vibrio harveyi: sequence and function of genes regulating expression of luminescence. *Mol Microbiol* **1993,** 9, (4), 773-86.

101. Koop, A. H.; Hartley, M. E.; Bourgeois, S., A low-copy-number vector utilizing beta-galactosidase for the analysis of gene control elements. *Gene* **1987,** 52, (2-3), 245-56.

102. Miller, J., *Experiments in molecular genetics*. Cold Spring Harbor Laboratory Press: Cold Spring Harbor, 1972.

103. Fernandes, R.; Yi, H. M.; Wu, L. Q.; Rubloff, G. W.; Ghodssi, R.; Bentley, W. E.; Payne, G. F., Thermo-biolithography: A technique for patterning nucleic acids and proteins. *Langmuir* **2004,** 20, (3), 906-913.

104. Lewandowski, A. T.; Small, D. A.; Chen, T. H.; Payne, G. F.; Bentley, W. E., Tyrosine-based "activatable pro-tag": Enzyme-catalyzed protein capture and release. *Biotechnology And Bioengineering* **2006,** 93, (6), 1207-1215.

105. Lee, J. E.; Cornell, K. A.; Riscoe, M. K.; Howell, P. L., Structure of Escherichia coli 5'-methylthioadenosine/ S-adenosylhomocysteine nucleosidase inhibitor complexes provide insight into the conformational changes required for substrate binding and catalysis. *J Biol Chem* **2003,** 278, (10), 8761-70.

106. Lewis, H. A.; Furlong, E. B.; Laubert, B.; Eroshkina, G. A.; Batiyenko, Y.; Adams, J. M.; Bergseid, M. G.; Marsh, C. D.; Peat, T. S.; Sanderson, W. E.; Sauder, J. M.; Buchanan, S. G., A structural genomics approach to the study of quorum sensing: crystal structures of three LuxS orthologs. *Structure* **2001,** 9, (6), 527-37.

107. Surette, M. G.; Bassler, B. L., Quorum sensing in Escherichia coli and Salmonella typhimurium. *Proc Natl Acad Sci U S A* **1998,** 95, (12), 7046-50.

108. Agarwal, A.; Mallapragada, S. K., Synthetic sustained gene delivery systems. *Current Topics in Medicinal Chemistry* **2008,** 8, (4), 311-330.

109. Peer, D.; Karp, J. M.; Hong, S.; FaroKHzad, O. C.; Margalit, R.; Langer, R., Nanocarriers as an emerging platform for cancer therapy. *Nature Nanotechnology* **2007,** 2, (12), 751-760.

110. Tessmar, J. K.; Gopferich, A. M., Matrices and scaffolds for protein delivery in tissue engineering. *Advanced Drug Delivery Reviews* **2007,** 59, (4-5), 274-291.

111. Bagshawe, K. D., Antibody-directed enzyme prodrug therapy (ADEPT) for cancer. *Expert Review of Anticancer Therapy* **2006,** 6, (10), 1421-1431.

112. Lai, L. S.; Xu, Z. H.; Zhou, J. H.; Lee, K. D.; Amidon, G. L., Molecular basis of prodrug activation by human valacyclovirase, an alpha-amino acid ester hydrolase. *Journal of Biological Chemistry* **2008,** 283, (14), 9318-9327.

113. Bassler, B. L.; Losick, R., Bacterially speaking. *Cell* **2006,** 125, (2), 237-246.

114. March, J. C.; Bentley, W. E., Quorum sensing and bacterial cross-talk in biotechnology. *Curr Opin Biotechnol* **2004,** 15, (5), 495-502.

115. Williams, P.; Winzer, K.; Chan, W. C.; Camara, M., Look who's talking: communication and quorum sensing in the bacterial world. *Philosophical Transactions of the Royal Society B-Biological Sciences* **2007,** 362, (1483), 1119-1134.

116. Rarnbow-Larsen, A. A.; Rajashekara, G.; Petersen, E.; Splitter, G., Putative quorum-sensing regulator BlxR of Brucella melitensis regulates virulence factors including the type IV secretion system and flagella. *Journal of Bacteriology* **2008,** 190, (9), 3274-3282.

117. Syvitski, R. T.; Tian, X. L.; Sampara, K.; Salman, A.; Lee, S. F.; Jakeman, D. L.; Li, Y. H., Structure-activity analysis of quorum-sensing signaling peptides from Streptococcus mutans. *Journal of Bacteriology* **2007,** 189, (4), 1441-1450.

118. Yoon, Y.; Sofos, I. N., Autoinducer-2 activity of gram-negative foodborne pathogenic bacteria and its influence on biofilm formation. *Journal of Food Science* **2008,** 73, (3), M140-M147.

119. Li, J.; Attila, C.; Wang, L.; Wood, T. K.; Valdes, J. J.; Bentley, W. E., Quorum sensing in Escherichia coli is signaled by AI-2/LsrR: Effects on small RNA and Biofilm architecture. *Journal of Bacteriology* **2007,** 189, (16), 6011-6020.

120. Rader, B. A.; Campagna, S. R.; Semmelhack, M. F.; Bassler, B. L.; Guillemin, K., The quorum-sensing molecule autoinducer 2 regulates motility and flagellar morphogenesis in Helicobacter pylori. *Journal of Bacteriology* **2007,** 189, (17), 6109-6117.

121. Widmer, K. W.; Jesudhasan, P. R.; Dowd, S. E.; Pillai, S. D., Differential expression of virulence-related genes in a Salmonella enterica serotype typhimurium luxS mutant in response to autoinducer AI-2 and poultry meat-derived AI-2 inhibitor. *Foodborne Pathogens and Disease* **2007,** 4, (1), 5-15.

122. Auger, S.; Krin, E.; Aymerich, S.; Gohar, M., Autoinducer 2 affects biofilm formation by Bacillus cereus. *Applied and Environmental Microbiology* **2006,** 72, (1), 937-941.

123. Sztajer, H.; Lemme, A.; Vilchez, R.; Schulz, S.; Geffers, R.; Yip, C. Y. Y.; Levesque, C. M.; Cvitkovitch, D. G.; Wagner-Dobler, I., Autoinducer-2-regulated genes in Streptococcus mutans UA159 and global metabolic effect of the luxS mutation. *Journal of Bacteriology* **2008,** 190, (1), 401-415.

124. Peters, N. K.; Dixon, D. M.; Holland, S. M.; Fauci, A. S., The research agenda of the National Institute of Allergy and Infectious Diseases for antimicrobial resistance. *J Infect Dis* **2008,** 197, (8), 1087-93.

125. Schauder, S.; Shokat, K.; Surette, M. G.; Bassler, B. L., The LuxS family of bacterial autoinducers: biosynthesis of a novel quorum-sensing signal molecule. *Molecular Microbiology* **2001,** 41, (2), 463-476.

126. Janatova, J.; Fuller, J. K.; Hunter, M. J., Heterogeneity of Bovine Albumin with Respect to Sulfhydryl and Dimer Content. *Journal of Biological Chemistry* **1968,** 243, (13), 3612-&.

127. Gutierrez, J. A.; Luo, M.; Singh, V.; Li, L.; Brown, R. L.; Norris, G. E.; Evans, G. B.; Furneaux, R. H.; Tyler, P. C.; Painter, G. F.; Lenz, D. H.; Schramm, V. L., Picomolar inhibitors as transition-state probes of 5 '-methylthioadenosine nucleosidases. *Acs Chemical Biology* **2007,** 2, (11), 725-734.

128. Zhu, J.; Knottenbelt, S.; Kirk, M. L.; Pei, D. H., Catalytic mechanism of S-ribosylhomocysteinase: Ionization state of active-site residues. *Biochemistry* **2006,** 45, (40), 12195-12203.

129. Zhu, J.; Patel, R.; Pei, D., Catalytic mechanism of S-ribosylhomocysteinase (LuxS): Stereochemical course and kinetic isotope effect of proton transfer reactions. *Biochemistry* **2004,** 43, (31), 10166-10172.

130. Leshansky, A. M.; Morris, J. F.; Brady, J. F., Collective diffusion in sheared colloidal suspensions. *Journal of Fluid Mechanics* **2008,** 597, 305-341.

131. Luo, X. L.; Lewandowski, A. T.; Yi, H. M.; Payne, G. F.; Ghodssi, R.; Bentley, W. E.; Rubloff, G. W., Programmable assembly of a metabolic pathway enzyme in a pre-packaged reusable bioMEMS device. *Lab on a Chip* **2008,** 8, (3), 420-430.

132. Camilli, A.; Bassler, B. L., Bacterial small-molecule signaling pathways. *Science* **2006,** 311, (5764), 1113-6.

133. Jayaraman, A.; Wood, T. K., Bacterial quorum sensing: signals, circuits, and implications for biofilms and disease. *Annu Rev Biomed Eng* **2008,** 10, 145-67.

134. Keller, L.; Surette, M. G., Communication in bacteria: an ecological and evolutionary perspective. *Nat Rev Microbiol* **2006,** 4, (4), 249-58.

135. Bjorck, L.; Kronvall, G., Purification and some properties of streptococcal protein G, a novel IgG-binding reagent. *J Immunol* **1984,** 133, (2), 969-74.

136. Sjobring, U.; Bjorck, L.; Kastern, W., Streptococcal protein G. Gene structure and protein binding properties. *J Biol Chem* **1991,** 266, (1), 399-405.

137. Diep, B. A.; Otto, M., The role of virulence determinants in community-associated MRSA pathogenesis. *Trends Microbiol* **2008,** 16, (8), 361-9.

138. Navarro, M. B.; Huttner, B.; Harbarth, S., Methicillin-resistant Staphylococcus aureus control in the 21st century: beyond the acute care hospital. *Curr Opin Infect Dis* **2008,** 21, (4), 372-9.

139. Taga, M. E.; Semmelhack, J. L.; Bassler, B. L., The LuxS-dependent autoinducer AI-2 controls the expression of an ABC transporter that functions in AI-2 uptake in Salmonella typhimurium. *Mol Microbiol* **2001,** 42, (3), 777-93.

140. Xavier, K. B.; Bassler, B. L., Regulation of uptake and processing of the quorum-sensing autoinducer AI-2 in Escherichia coli. *J Bacteriol* **2005,** 187, (1), 238-48.

141. Duan, F.; March, J. C., Interrupting Vibrio cholerae infection of human epithelial cells with engineered commensal bacterial signaling. *Biotechnol Bioeng* **2008,** 101, (1), 128-34.

142. Frezza, M.; Soulere, L.; Balestrino, D.; Gohar, M.; Deshayes, C.; Queneau, Y.; Forestier, C.; Doutheau, A., Ac2-DPD, the bis-(O)-acetylated derivative of 4,5-dihydroxy-2,3-pentanedione (DPD) is a convenient stable precursor of bacterial quorum sensing autoinducer AI-2. *Bioorg Med Chem Lett* **2007,** 17, (5), 1428-31.

143. Tanaka, G.; Funabashi, H.; Mie, M.; Kobatake, E., Fabrication of an antibody microwell array with self-adhering antibody binding protein. *Anal Biochem* **2006,** 350, (2), 298-303.

144. Fernandes, R.; Bentley, W. E., AI-2 biosynthesis module in a magnetic nanofactory alters bacterial response via localized synthesis and delivery. *Biotechnol Bioeng*, In Press.

145. Bashir, R., BioMEMS: state-of-the-art in detection, opportunities and prospects. *Advanced Drug Delivery Reviews* **2004,** 56, (11), 1565-1586.

146. Beebe, D. J.; Mensing, G. A.; Walker, G. M., Physics and applications of microfluidics in biology. *Annual Review Of Biomedical Engineering* **2002,** 4, 261-286.

147. Grayson, A. C. R.; Shawgo, R. S.; Johnson, A. M.; Flynn, N. T.; Li, Y. W.; Cima, M. J.; Langer, R., A BioMEMS review: MEMS technology for physiologically integrated devices. *Proceedings Of The Ieee* **2004,** 92, (1), 6-21.

148. Min, J.; Kim, J. H.; Kim, S., Microfluidic device for bio analytical systems. *Biotechnology And Bioprocess Engineering* **2004,** 9, (2), 100-106.

149. Polla, D. L.; Erdman, A. G.; Robbins, W. P.; Markus, D. T.; Diaz-Diaz, J.; Rizq, R.; Nam, Y.; Brickner, H. T.; Wang, A.; Krulevitch, P., Microdevices in medicine. *Annual Review Of Biomedical Engineering* **2000,** 2, 551-576.

150. Shawgo, R. S.; Grayson, A. C. R.; Li, Y. W.; Cima, M. J., BioMEMS for drug delivery. *Current Opinion In Solid State & Materials Science* **2002,** 6, (4), 329-334.

151. Atencia, J.; Beebe, D. J., Controlled microfluidic interfaces. *Nature* **2005,** 437, (7059), 648-655.

152. Bilitewski, U.; Genrich, M.; Kadow, S.; Mersal, G., Biochemical analysis with microfluidic systems. *Analytical And Bioanalytical Chemistry* **2003,** 377, (3), 556-569.

153. Hong, J. W.; Quake, S. R., Integrated nanoliter systems. *Nature Biotechnology* **2003,** 21, (10), 1179-1183.

154. Hong, J. W.; Studer, V.; Hang, G.; Anderson, W. F.; Quake, S. R., A nanoliter-scale nucleic acid processor with parallel architecture. *Nature Biotechnology* **2004,** 22, (4), 435-439.

155. Ottesen, E. A.; Hong, J. W.; Quake, S. R.; Leadbetter, J. R., Microfluidic digital PCR enables multigene analysis of individual environmental bacteria. *Science* **2006,** 314, (5804), 1464-1467.

156. Shim, J.; Bersano-Begey, T. F.; Zhu, X. Y.; Tkaczyk, A. H.; Linderman, J. J.; Takayama, S., Micro- and nanotechnologies for studying cellular function. *Current Topics In Medicinal Chemistry* **2003,** 3, (6), 687-703.

157. Mourya, V. K.; Inamdar, N. N., Chitosan-modifications and applications: Opportunities galore. *Reactive & Functional Polymers* **2008,** 68, (6), 1013-1051.

158. Vinsova, J.; Vavrikova, E., Recent advances in drugs and prodrugs design of chitosan. *Current Pharmaceutical Design* **2008,** 14, (13), 1311-1326.

159. Park, J. J.; Luo, X. L.; Yi, H. M.; Valentine, T. M.; Payne, G. F.; Bentley, W. E.; Ghodssi, R.; Rubloff, G. W., Chitosan-mediated in situ biomolecule assembly in completely packaged microfluidic devices. *Lab On A Chip* **2006,** 6, (10), 1315-1321.

160. Wu, L. Q.; Yi, H. M.; Li, S.; Rubloff, G. W.; Bentley, W. E.; Ghodssi, R.; Payne, G. F., Spatially selective deposition of a reactive polysaccharide layer onto a patterned template. *Langmuir* **2003,** 19, (3), 519-524.

161. Luo, X.; Berlin, D. L.; Buckhout-White, S.; Bentley, W. E.; Payne, G. F.; Ghodssi, R.; Rubloff, G. W., Design optimization for bioMEMS studies of enzyme-controlled metabolic pathways. *Biomedical Microdevices* **2008,** 10, (6), 899-908.

162. McDonald, J. C.; Duffy, D. C.; Anderson, J. R.; Chiu, D. T.; Wu, H. K.; Schueller, O. J. A.; Whitesides, G. M., Fabrication of microfluidic systems in poly(dimethylsiloxane). *Electrophoresis* **2000,** 21, (1), 27-40.

163. McDonald, J. C.; Whitesides, G. M., Poly(dimethylsiloxane) as a material for fabricating microfluidic devices. *Accounts Of Chemical Research* **2002,** 35, (7), 491-499.